MPC BASED TORQUE ALLOCATION STRATEGY TO ENHANCE THE PERFORMANCE OF A REGENERATIVE BRAKING SYSTEM CONSIDERING HALF SHAFT VIBRATION

by

Bhushan Shirish Naik

A thesis submitted in partial fulfillment
of the requirements for the degree of
Master of Science in Engineering
(Automotive Systems Engineering)
in the University of Michigan-Dearborn
2016

Master's Thesis Committee:
Professor Taehyun Shim, Chair
Assistant Professor Stanley Baek
Associate Professor HongTae Kang

Acknowledgements

Foremost, I would like to thank my advisor Dr. Taehyun Shim for his views, recommendations and guidance for this work. I would also like to thank the Department of Interdisciplinary Programs, for allowing me to pursue my research in this field. It was an honor being a part of it. I would also like to thank the members of thesis committee Dr. Baek and Dr. Kang, for their time to review my research.

I would like to thank Mr. Chinmay Patil (Graduate Student, University of Michigan – Dearborn) for his technical and software recommendations regarding this work.

Lastly, I would like to thank my parents Mr Shirish Naik and Mrs. Prabha Naik, for supporting me throughout my research and my life in general.

Table of Contents

List of Tables

List of Figures

List of Appendices

Abstract

A regenerative brake system is widely used in the automotive industry mainly due to its ability for energy recovery. Since an electric motor used in the regenerative brake has a faster torque response compared to that of the hydraulic system, it can be applicable for various applications in the area of active safety systems, especially brake control applications. However, due to its actuation limitations, it cannot be independently used for all braking scenarios, and require to be used in combination with the conventional hydraulic brakes. In this work, a multi-objective brake torque allocation method using model predictive control is proposed. The proposed strategy has two objectives: bandwidth based torque allocation, and reduction in drive shaft vibrations. In order to show the effectiveness of the proposed control strategy, a simulation model with a single wheel and a five phase anti-lock brake system has been developed. This simulation study is then extended with a full vehicle model in Carsim software. The simulation results show that vehicle stopping distance and drive shaft vibrations are reduced by using the proposed control strategy

Chapter 1: Introduction

1.1 ELECTRIC VEHICLES AND HYBRID ELECTRIC VEHICLES.

Due to the increasing environmental pollution and depleting energy resources, the automotive industry is continuously developing means of alternate vehicle propulsion systems, such as traction motors. During the last decade, there has been an increased research and development in the fields of Electric Vehicles (EV's) and Hybrid electric Vehicles (HEV's). This paradigm shift is mainly because of the better fuel efficiency and lower emissions, of EVs and HEVs, as compared to the conventional internal combustion engine (ICE) driven vehicle. As compared to conventional ICE-driven vehicles, EVs and HEVs offer several advantages:

1. Reduced fuel consumption, and the fuel economy can be further optimized by using traction motors in combination with ICE, in HEVs.
2. Reduced Emissions.
3. The ICE size in HEVs can be smaller, due to the presence of electric motors, as an additional actuator for propulsion.
4. Increased controllability due to the presence of an additional actuator.
5. Regenerative Braking: recovering the kinetic energy during braking, thus further increasing the mileage for city driving.

The above mentioned advantages mainly depend on the powertrain configuration of the EV/HEV. The powertrain configuration depends on the position of the electric motor in the powertrain. In general, the various powertrain configurations, depending on the position of the electric motor is indicated in Figure 1.1.The configuration indicated in Figure 1.1 are: (a) direct central motor, (b) central motor with transmission, (c) On-board motor with/without gearbox and (d) in wheel motors (IWMs). Configurations (a) and (b)

are more common in HEVs, while configurations (c) and (d) are generally found in EVs. The electric motors in in-wheel motor driven EVs are located very close to the wheel, and hence are bigger in size. In IWM EVs, the mass of the electric motor is added to the unsprung mass of the vehicle, which greatly affects the suspension properties of the EV. To overcome this problem, configuration (c) is used in literature, where the motors are a part of the sprung mass of the vehicle.

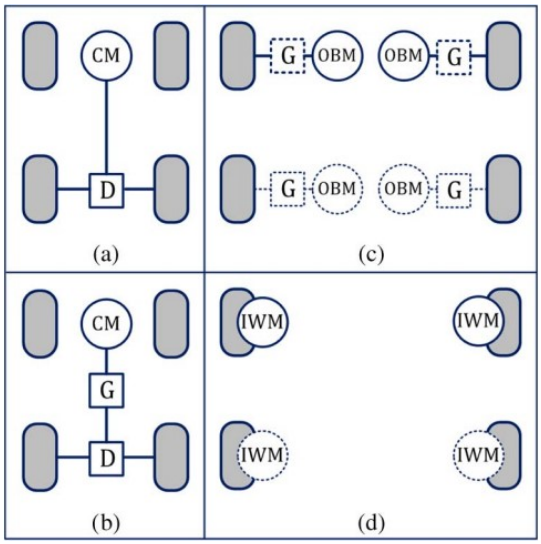

Figure 1.1: Various Powertrain configurations for regenerative brake systems [60]

1.1.1 Regenerative Braking

Regenerative braking is one of the most promising characteristics of an electric motor. It is an energy recovery mechanism, in which the vehicle is slowed down by converting the kinetic energy of the vehicle into a form which can be either used immediately or stored until needed (battery). In other words, in certain conditions, it can apply positive as well as negative torques, thus converting the kinetic energy during braking into electric energy, which can be stored in an energy storage device. As indicated in Figure 1.1, the flow of energy during vehicle acceleration is from the battery, to the traction motor and ultimately to the wheels. During braking, the traction motor now acts as a generator, which generates power, and hence the power flow is from the wheels to the motor (generator) and then to the battery. Hence the regenerative brake system consists of the electric motor as well as the battery and inverter.

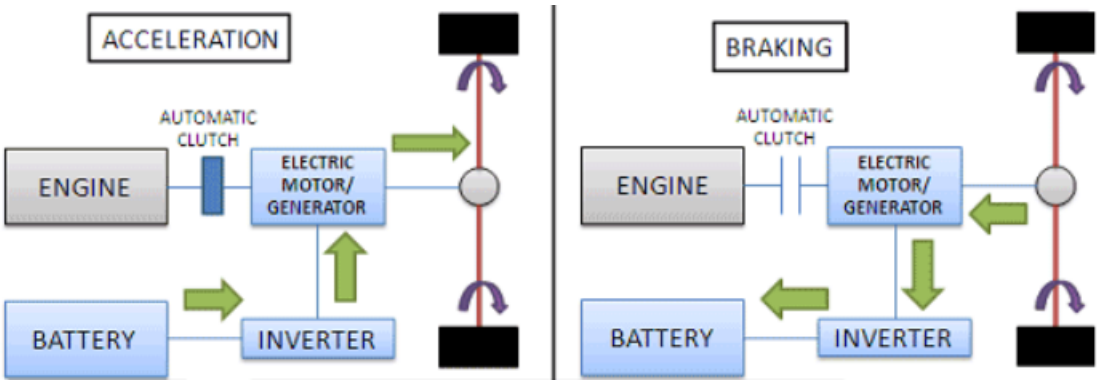

Figure 1.2: Power-flow during acceleration (left) and regenerative braking (right), in an HEV

The torque speed characteristics of electric motors is shown in Figure 1.3. It is the same for the positive as well as the negative torques. The maximum motor torque is available up to a certain motor speed (kick point 2), which is referred to as the base speed. After this speed, is the constant power curve, here the torque is limited by the maximum rated motor power. This is referred to as the flux-weakening region of the plot. The maximum rated motor speed is indicated by "kick point 1" in Figure 1.3.

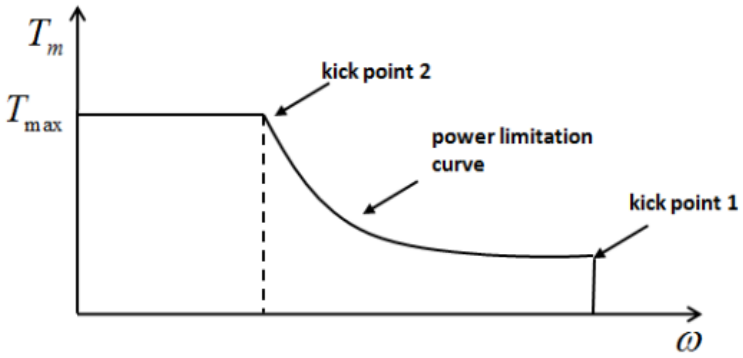

Figure 1.3 Torque speed characteristics of electric motors [56]

This implies that the maximum motor torque, is not available throughout the speed range of the motor. The significance of Figure 1.3, is that it indicates the various parameters, which affect the performance of the motor. These parameters are specified by the motor manufacturers.

A conventional vehicle with an internal combustion engine has hydraulic brakes as the only source of negative torque at the wheel. The main advantage of a conventional hydraulic brake is that of applying a high amount of braking torque on the wheels and its high reliability as compared to regenerative brakes. However, hydraulic brakes has slow dynamics, i.e. the reaction time of the hydraulic brakes is high. On the other hand, regenerative brakes depend on a

number of factors in which the most important being the state of charge (SoC) of the battery. If the battery is fully charged, the motor cannot regenerate energy and hence cannot apply a reverse torque. Also the maximum limits of the motor torque are much less as compared to the hydraulic brakes. However major advantage of regenerative brakes is its fast dynamics and low reaction time as compared to the hydraulic brakes. Hence applying regenerative brakes have dual advantage [1]: Firstly, the brake torque can be applicable faster, this results in an additional redundant actuator, adding a degree of freedom to the control system, and secondly, a major part of the kinetic energy is recovered, which would otherwise be lost in the form of heat by hydraulic brakes. Thus over the last decade, researchers are trying to develop control strategies to 'blend' regenerative and friction brake torques, so that the total brake force will consist of both, the regenerative part as well as the friction part.

The magnitude and bandwidth of regenerative brake torque applied at the wheel is largely affected by the powertrain configuration of the vehicle under consideration as previously indicated in Figure 1.1. It can also be observed from Figure 1.1 that in configurations (a), (b), and (c), the torque from the electric motor is applied on the wheel via a half-shaft/drive-shaft, while in the case of IWM EVs, the shaft dynamics are negligible. This implies that in (a), (b), and (c), the electric torque at the wheel is delayed due to shaft/transmission dynamics. Hence the magnitude and frequency of the regenerative brake torque applied on the wheel will depend on the presence of: (i) gearbox (value of gear ratio) and (ii) shaft/transmission dynamics.

1.1.2 Anti-lock brake system

Anti-lock Brake System (ABS) originated from the air plane industry, mainly used in the landing gear of air planes. It was then introduced in the automotive industry in the 1980s, by Bosch, and today, almost all new vehicles are equipped with ABS modules. The motivation behind implementing ABS in vehicles is twofold: firstly to minimize the stopping distance, and secondly to maintain the steerability (directional stability) of the vehicle in the event of emergency brake application. This can be scientifically explained with the help of Figure 1.4.

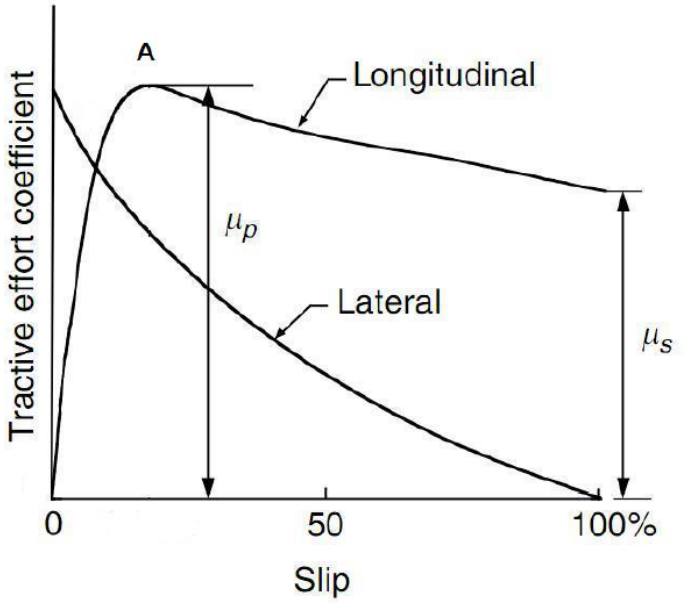

Figure 1.4: Slip – Tractive coefficient curve [71]

Figure 1.4 indicates the relation between tractive coefficient and normalized longitudinal wheel slip. Tractive effort coefficient signifies the amount of tractive force possible at the wheel. The longitudinal tractive coefficient curve indicates tractive effort in the longitudinal (straight line) direction, whereas the lateral tractive coefficient indicates the tractive effort in the lateral direction (required for steering the vehicle). The longitudinal slip is the difference between the vehicle speed and the wheel speed, normalized by the vehicle speed. Zero slip indicates that the wheel and vehicle is travelling at the same speed, while 100 % slip indicates that the wheel is "locked up" and the vehicle speed is non-zero, and the wheel speed in zero. It can be observed from Figure 1.4, that the tractive effort in the longitudinal direction is maximum (μ_p) for a particular slip value. The lateral slip however is maximum at 0 slip, but is zero at 100% slip, implying no steerability when the wheel is locked up. Hence in order to optimize the stopping distance and steerability at the same time, it is important to maintain the slip at around the value corresponding to μ_p. This is the objective of ABS. Hence as the wheel slip is sensed, ABS is activated, and the slip is maintained at around the optimal value by modulating the brake pressure. In reference to this research, it is important to know that the output signal of the ABS is in the form of brake torque/brake pressure modulations. This logic is explained in detail in Chapter 3.

1.2 LITERATURE REVIEW

As indicated in the previous discussions, the regenerative brakes cannot be used independently due to its limitations, and hence needs to be used in a combination with the hydraulic brakes. The presence of Anti-lock Braking Systems (ABS) and Electronic Stability Program (ESP) in modern vehicles further challenges the integration of the blending brake torque control strategies between hydraulic- and regenerative brakes with these control systems. This is mainly due to the fact that in the case of emergency maneuvers, the demanded torques variation will be high in order to restore the stability of the system and hence the efficiency of the brake torque blending control will depend on the robustness and the reliability of the blending control strategy.

Due to the reduced reliability, and limited maximum torque of regenerative brakes, most of the researchers in literature have developed combined control strategies in which the regenerative brakes are applied for low to medium braking [15 - 26]. The authors have seldom used regenerative brakes in cases where the braking intensity is high, i.e. in emergency braking situations where control systems like anti-lock brake system (ABS) is activated. This is mainly due to the ABS and emergency braking being critical situations, and the actuators involved in such a scenario need to be highly reliable. One of the counter-arguments for this problem is that the performance of the ABS in the emergency braking situations can be enhanced by using regenerative brakes [1, 50]. This is because of the electric motor being the faster actuator will result in faster and more accurate modulation of the brake torque at the wheel. This will further result in a shorter stopping distance. This improvement in stopping distance and more accurate slip control will vastly depend on the configuration of the vehicle powertrain, as indicated in section 1.1. The research of ABS/ESP for in-wheel motors is widely investigated in various research articles [2, 3, 4, 15, 16, 62]. However, there are not many studies for the effect of half shaft dynamics in combined braking control during ABS/ESP application in the literatures [1, 27, 46, 47]..

A majority of research on combined hydraulic and regenerative braking is based on light braking situations (0.3g to 0.5 g deceleration). A large number of these published works have incorporated rule based algorithms [21, 23, 24, 25, 26, 64, 65] to distribute the torque between hydraulic brake and regenerative brakes. The control objective for these algorithms is: maximum energy recovery [64], good pedal feel [66], and braking comfort [65]. In Ref [63] has used genetic

algorithm based optimization to maximize the recovered energy. These strategies ramp the regenerative torque to zero in the event of ABS/ESP activation.

The use of combined braking torques during an emergency braking situation is seldom investigated. Combined braking torque implies allocating the controlled braking torque between the hydraulic brakes and regenerative brake. In general, this control allocation problem during ABS can be addressed in two ways [50] as shown in Figure 1.5

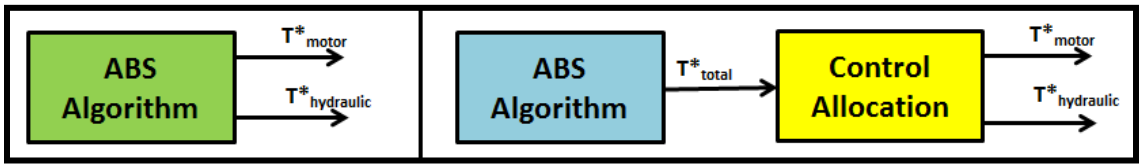

Figure 1.5: Different ways of incorporating regenerative braking system with ABS control logic [50]

Firstly one can design an ABS, with the torque allocation task done by the ABS itself (referred to as Hybrid ABS [1, 50]), and secondly, the ABS and the control allocation task can be completely decoupled. Hybrid ABS control strategies have been rarely explored in literature [60], but these strategies have not been sufficiently explained, as most of the manufacturers are unwilling to reveal the details of these algorithms [60]. However, the case of decoupled ABS and torque allocation, have been explored in a number of publications [1, 2, 3, 50]. One of the major advantages of such an approach is that one can use a pre-existing ABS controller and design the control allocation module only. In this work, the decoupled ABS and Control allocation approach is used, as one can independently design the ABS and the control allocation module.

In the case combined braking at the wheel in an EV/HEV, the addition of regenerative brakes adds an extra actuator to achieve the same function i.e. braking the vehicle. Hence there is one redundant actuator at each of the driven wheels. This aspect can be further used in our system in a number of different ways depending on the control objectives. The problem of actuator redundancy is solved by using the concept of control allocation. This procedure is popular in the area of aeronautics, where the number of actuators in an aircraft is more than the number degrees of freedom of the motion of the aircraft [6, 7, 8, 11, 13]. With reference to our case, i.e. longitudinal emergency braking, this concept can also be adopted.

The control allocation (CA) approach is an extensively used approach in the literature [1–3, 6, 7, 10] to address the problem of actuator redundancy, and it is a widely researched topic in the

aerospace industry [6, 7, 13]. Based on this approach for over actuated systems, the total control effort can be achieved by different actuators in many different ways, depending on the control objectives. In this work, we intend to apply a bandwidth based control allocation, where the faster actuator (Electric Motor) is allocated the high-frequency part of the control signal, and the slower actuator (hydraulic brake) is allocated the low frequency part [7].

The bandwidth-based control allocation approach is addressed in a number of different ways in the literature. In [56], an ad-hoc strategy with a frequency filter is used for splitting the torque between regenerative and hydraulic brakes, but it requires extensive tuning. A rule-based state machine is incorporated in [1], in order to have a dynamics split between the hydraulic and regenerative torques. Dynamic Control Allocation (DCA) approach is used in [3] and [50] offer better results by using a two-step optimization problem, thus acting as a dynamic frequency filter [3]. Model predictive control allocation is used in [2], to combine regenerative brakes and hydraulic brakes during ABS activation. However, in [2], the authors compared the DCA and MPCA strategies for an in-wheel motor-driven vehicle during an ABS maneuver and concluded that the MPCA technique is superior to the DCA technique. There exist works on application of dynamic control allocation and model predictive control allocation [2, 6, 7, 13], but their application to regenerative brakes during an emergency maneuver (ABS activation) is barely studied[2,3] because in most applications, regenerative braking is switched off or ramped to zero in the event of an emergency braking condition.

The topic of active vibration damping in EVs/HEVs is widely investigated during the last decade, with one of the earliest works published in [46, 47], where the authors have designed a direct torque compensation method, using a non-linear observer to estimate the torque in the gear, and hence generate a damping torque for the motor. In [1,50], the authors have designed an active damping controller using pole placement, where the on-board motor configuration system is described as a linear parameter varying (LPV) system, with the tire modeled as a linear damper, and a function of vehicle velocity. In [27], the effects of half shaft dynamics on ABS/TCS control systems is investigated, and a simple feedback controller, with extended Kalman filter is used to control the vibrations. More recently, model predictive control is widely being used for active vibration damping purposes [30-45]. In [45], MPC is used in conventional vehicles to damp the vibrations in drive shafts, during tip in/ tip out maneuvers, using engine

torque. A more general and non-automotive application of MPC-based vibration damping in electric drives, consisting of a two/three inertia systems connected by a flexible shaft is widely explored in [31, 37 to 44].

1.3 PROBLEM DEFINITION

From a thorough literature review, and the previous discussions, it can be concluded that the effect of half-shaft dynamics has not been explicitly included in the control allocation problem, but has been dealt with separately. Hence in this work, the author proposes a modified Model Predictive Control Allocation strategy, which explicitly includes the effect of half-shaft dynamics, and attempts to reduce the drivetrain vibrations by adjusting the MPC cost function.

1.4 CONTRIBUTIONS

The specific contributions of this thesis are:

1. Developed a multi-objective Model Predictive Control based control allocation strategy to allocate the brake torque between the regenerative brakes and hydraulic brakes, with modified plant model and cost function.

2. Simulated the proposed strategy with Carsim and a quarter car model, for the combined braking case, during emergency braking.

1.5 CONCLUSION

This chapter firstly describes the introduction and background of the various vehicle technologies used in this work, i.e. regenerative braking and ABS. Then, a thorough literature review is conducted, which help us understand the recent trend in the research in this area. Using the results of the literature review, the problem is defined, and the contributions of this thesis are specified. The rest of this thesis is organized as follows: chapter 2 describes the simulation model developed for this this study, chapter 3 describes the various control strategies used in

this work, chapter 4 presents and discusses the simulation results, and chapter 5 discusses the conclusion along with the possible future works.

Chapter 2: Development of HEV System

2.1 POWERTRAIN CONFIGURATION

As discussed in the previous chapter, the brake torque allocation control between the regenerative brakes and the hydraulic brakes greatly depend on the configuration of the powertrain of the EV/HEV. The powertrain configuration of the vehicle used in this work is shown in Figure 2.1

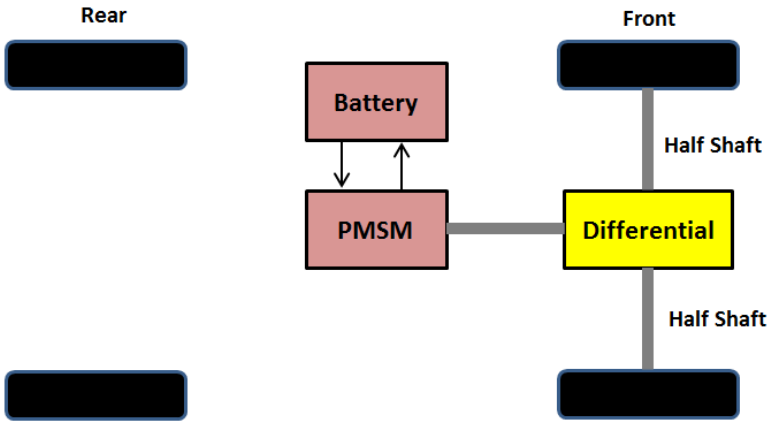

Figure 2.1: Power train Configuration of the vehicle used in this study

As indicated in Figure 2.1, the electric motor is connected to the wheels via a differential and two half shafts on each side. This research work assumes that the engine is disconnected via a clutch during braking, so that engine torque can be neglected during simulation. Also, the differential is assumed to be an open-differential, as braking along a straight line without steering is considered here. This work can be easily extended for the case of in-board motors, where an individual motor is connected to each wheel via a half shaft.

2.2 SIMULATION MODEL CONFIGURATION

The simulation configuration developed for this research work is shown in Figure 2.2. It consists of a driver input block, a five-phase ABS module, Model Predictive Control Allocator, hydraulic actuator (front and rear), PMSM motor (front only) and a Vehicle dynamics module.

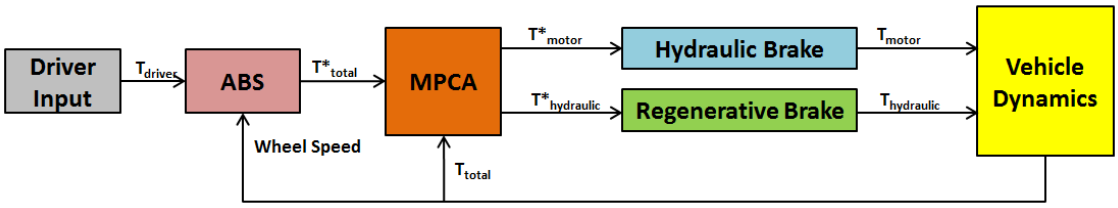

Figure 2.2: Simulation model configuration

The following section describes the modelling aspect of each of these sub-systems, i.e. the driver input module, the hydraulic brake, regenerative brake and the vehicle dynamics module.

2.3 DRIVER INPUT: BRAKE PEDAL

During a braking maneuver, the driver has two possible means of input: brake pedal and steering wheel. In this work, since we have only considered for the cases of straight line braking, the steering input from the driver is assumed to be zero. There are two ways of defining driver input: one can define it either in Carsim itself or in Simulink. In this work, the driver brake pedal input is defined in Simulink, for the sake simplicity. A typical brake pedal system (not by-wire) is shown in Figure 2.3.

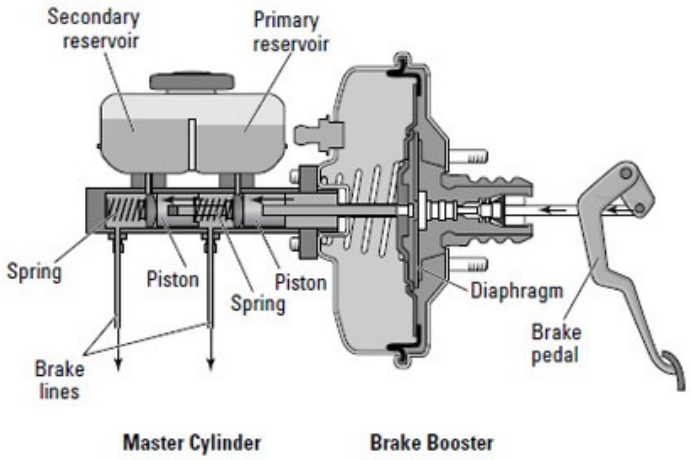

Figure 2.3: A typical brake pedal layout in a conventional vehicle. [71]

The input from the brake pedal first goes to the brake booster, where it is amplified, and then is sent to the Master cylinder. From the master cylinder, it goes to the wheel cylinders, via the Hydraulic modulator (for ABS). The arrows labeled at the brake lines lead the brake fluid to the hydraulic modulator unit. In this work, the brake pedal input is normalized [58, 72], i.e. it ranges from 0 to 100% pedal travel. The normalized pedal travel is then related to the master cylinder pressure by fitting experimentally obtained data [72]. The following is the equation used.

$$P_{MC} = \begin{matrix} 0 \; for \; 0 \; \leq x_{pt} \; \leq 0.1 \\ -11.98\, x_{pt}^2 + 118.65\, x_{pt} - 18.67 \; for \; 0.1 < x_{pt} \leq 1 \end{matrix} \quad (2.s1)$$

where P_{MC} is the master cylinder pressure and x_{pt} is the normalized pedal travel.

The master cylinder pressure is then applied at the wheel by the relation:

$$T_{HB} = K_{b(f,r)}.P_{MC} \quad (2.2)$$

where T_{HB} is the hydraulic brake torque, and $K_{b(f,r)}$ is the brake gain, which is different for the front and the rear brakes. The parameter $K_{b(f,r)}$ is assumed to be constant throughout this simulation study. In actual practice, this will depend on the age of the brakes, and also the brake disk temperature. This parameter is adapted from the Carsim software. The response of Master cylinder pressure vs. normalized pedal travel is indicated in Figure 2.4.

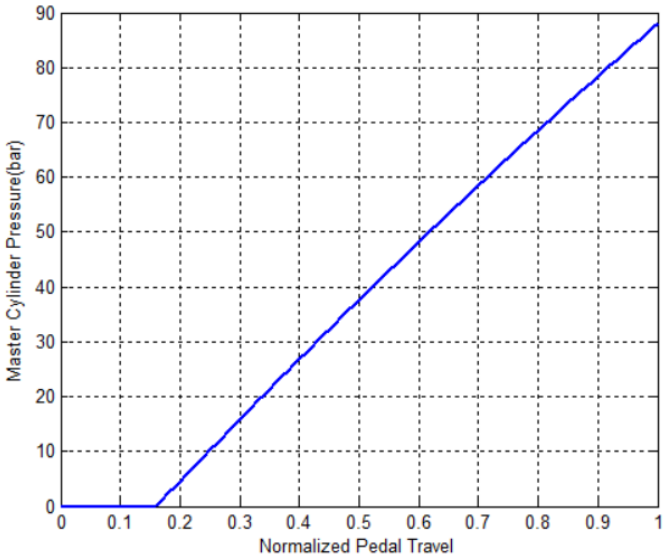

Figure 2.4: Master Cylinder Pressure vs. Normalized Pedal travel

2.4 HYDRAULIC BRAKE

The hydraulic brake torque defined in equation (2.2), is not sufficient to completely capture the behavior of a hydraulic brake, as the equation has no dynamics. The hydraulic brake is described as a non-linear second order actuator model, with actuator and rate limits embedded. A similar second order model was used in [54], and is described by the following equation:

$$\dot{T}_{act}(t) = \max\left(min\left(\omega_c^2 \int_0^t \left(T_{ref}(s-\Delta t) - T_{act}(s)\right) ds - 2\xi\omega_c T_{act}(t), \dot{T}_{bmax}\right), \dot{T}_{bmin}\right) \tag{2.3}$$

In the above equation ω_c is the cut-off frequency, ξ is the damping ratio, Δt is the pure time delay, T_{ref} is the reference torque, T_{act} is the actual torque, and $\dot{T}_{bmax}, \dot{T}_{bmin}$ are the actuator rate limits respectively. The dynamic equation (2.3) can be explained by applying a step input for T_{ref}, and analyzing T_{act}, as indicated in Figure 2.5.

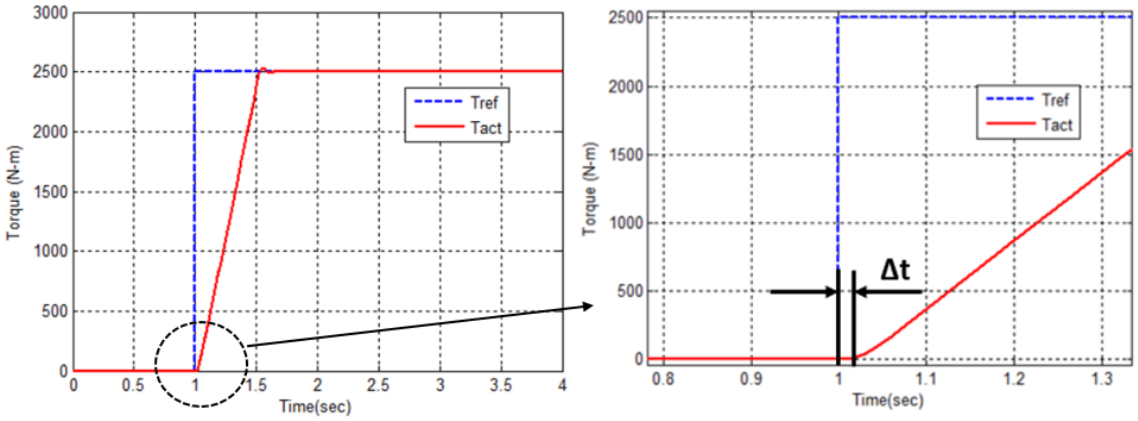

Figure 2.5: Step response of the Hydraulic brake model.

It can be observed from Figure 2.6, that the rate of increase of the torque, is limited by the maximum and minimum limits of the actuator. This model sufficiently captures the dynamic behavior of a hydraulic brake.

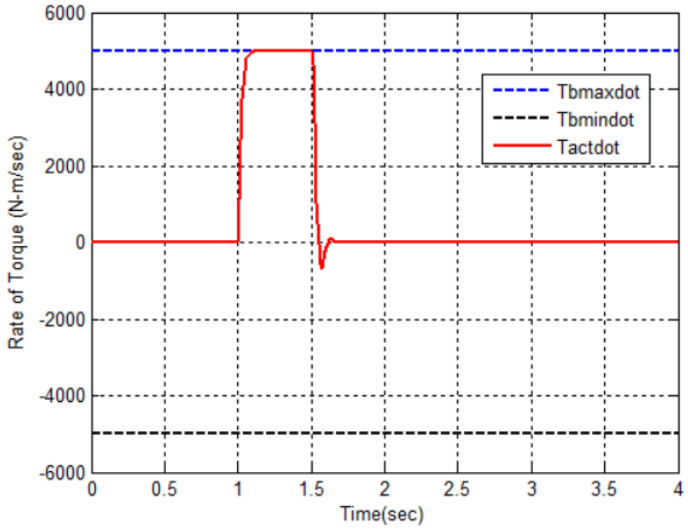

Figure 2.6: Rate of Brake Torque response, for Step input.

2.5 REGENERATIVE BRAKE SYSTEM

The regenerative brake system used in this work consists of a permanent magnet synchronous motor and a simple battery model. These sub-systems are described in detail in the following sections.

2.5.1 PMSM

In this research, a Permanent Magnet Synchronous Motor (PMSM) is used for the purpose of regenerative braking and the modelling and control is adopted from [58]. The PMSM model incorporated in this work is the popular d-q model [58, 59]. The equations defining the electric part of the model are:

$$\frac{d}{dt}(i_q) = (\, v_q - Ri_q - p\omega_r(L_d i_d + \lambda_f))/L_q \tag{2.4}$$

$$\frac{d}{dt}(i_d) = (v_d - Ri_d + p\omega_r L_q i_q)/L_d \tag{2.5}$$

The equations defining the mechanical part are:

$$T_e = 1.5\, p\{\lambda_f i_q + (L_d - L_q) i_q i_d\} \tag{2.6}$$

$$\frac{d}{dt}\omega_r = \frac{1}{J}(T_e - F\omega_r - T_m) \tag{2.7}$$

Here, i_q, i_d are the q and d-axis currents; v_q, v_d are the q and d-axis voltages; L_q, L_d are the q and d-axis inductances; R is the stator resistance, p is the number of pole pairs, ω_r is the motor velocity, λ_f is the flux, T_e is the electric torque, J is the motor inertia, F is the damping coefficient and T_m is the load torque.

2.5.2 Battery model

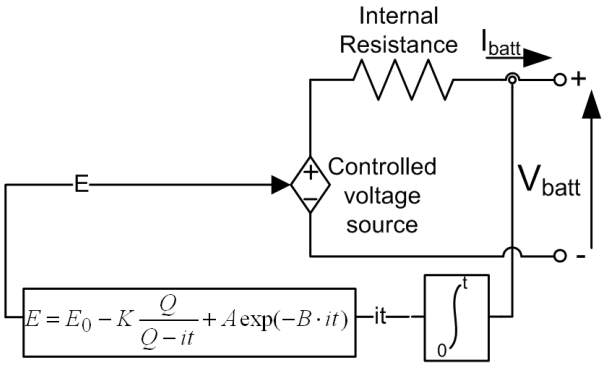

Figure 2.7: Nonlinear battery model from [57]

A non-linear empirical battery model similar to [57] is used in this work. It is assumed that the battery has the same characteristics for charging and discharging cycles. The governing differential equations for the battery model are as follows:

$$i = \frac{dq}{dt} \tag{2.16}$$

$$E = E_o - K\frac{Q}{Q_{initial} - q} + A_i e^{-B_i(Q - Q_{initial} + q)} \tag{2.17}$$

$$V_{batt} = E - R_b.i \tag{2.18}$$

This is the model for a single battery cell, which will have to be arranged in the form of a battery pack.

2.6 VEHICLE DYNAMICS

In this work, two different vehicle dynamic models are considered for simulation. Firstly a simple single wheel model with non-linear tire is used, and the simulation is then extended for a non-linear full vehicle dynamics model in Carsim.

2.6.1 Single wheel model

A single-corner model is used in this work, in which the drive shaft dynamics is added to a single-wheel dynamics by adding a motor inertia and a flexible driveshaft, as shown in Figure 2.8 .The driveshaft dynamics is represented by a torsional spring and damper, as indicated in Figure 2.9.

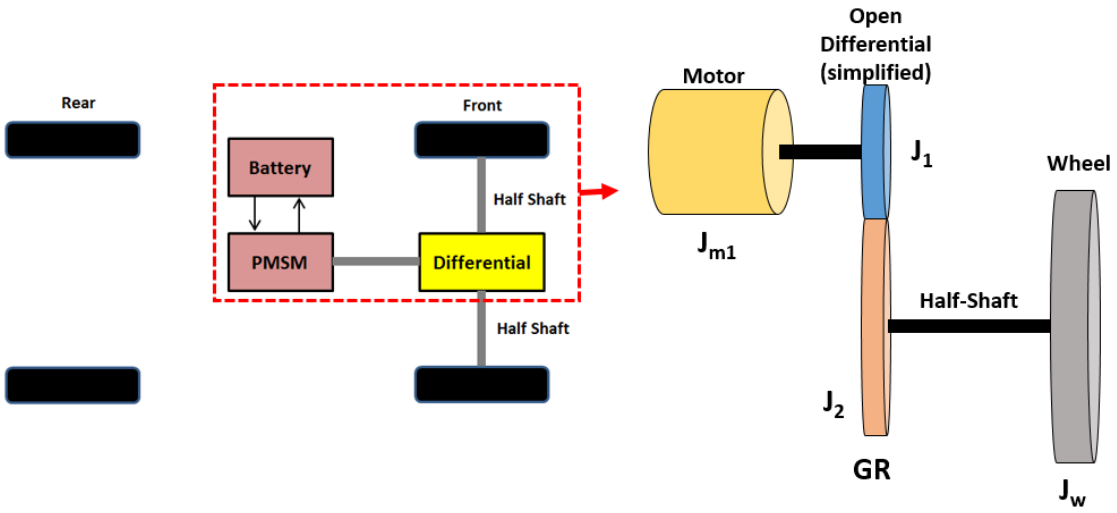

Figure 2.8: Single wheel representation of the Vehicle model.

In Figure 2.8, the motor inertia J_{m1} is reflected at the end of the half-shaft using the equivalence of kinetic energy as follows:

$$\frac{1}{2}.J_{eq}\omega_{eq}^2 = \sum \frac{1}{2} J_i \omega_i^2 \tag{2.19}$$

$$J_{eq} = J_m = (J_{m1} + J_1)\frac{\omega_1^2}{\omega_{halfshaft}^2} + J_2 \frac{\omega_{halfshaft}^2}{\omega_{halfshaft}^2} \tag{2.20}$$

$$J_m = (J_{m1} + J_1)(G.R.)^2 + J_2 \tag{2.21}$$

Hence as indicated in equation 2.21, the equivalent motor inertia is calculated at the half shaft. In the analysis in equations 2.19 to 2.21, it is assumed that the differential gears and the shaft connecting the motor to the differential are rigid and the gears do not contain any backlash, in order to simplify the analysis. This equivalent inertia is hence used for all further analysis in this work.

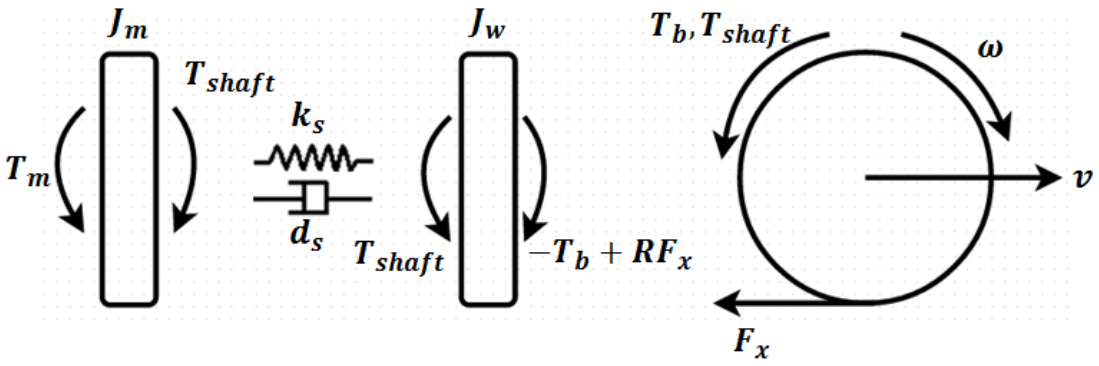

Figure 2.9: Single wheel model with drive shaft dynamics

The equations of motion for a wheel, motor, and shaft are as follows:

$$J_w \ddot{\theta}_w = -T_b + R\,F_x - T_{shaft} \tag{2.22}$$

$$J_m \ddot{\theta}_m = -T_m + T_{shaft} \tag{2.23}$$

$$T_{shaft} = k_s(\theta_w - \theta_m) + d_s\left(\dot{\theta}_w - \dot{\theta}_m\right) \tag{2.24}$$

The longitudinal motion of a single-corner model is described by:

$$m\,\dot{v} = -F_x \tag{2.25}$$

$$F_x = \mu(\lambda).F_z \tag{2.26}$$

For longitudinal maneuvers, F_x depends solely on λ and F_z. The longitudinal slip λ is defined as:

$$\lambda = \frac{v - R\,\omega}{v} \tag{2.27}$$

The function μ is approximated from the tire data available from Carsim software for different road surfaces.

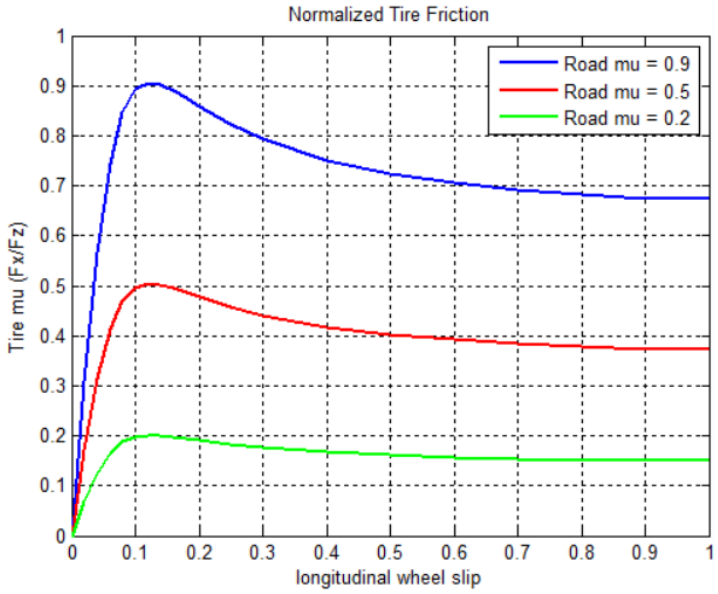

Figure 2.10: Tire friction (Normalized Tire Force) coefficient vs. slip plot

2.6.2 Carsim

Carsim is a commercial software widely used in the automotive industry. In this work, a B-class hatchback model from Carsim has been used. The tire data is similar to the one used in the previous section. The brake torques, along with their actuation dynamics and transportation delays are specified in Simulink itself.

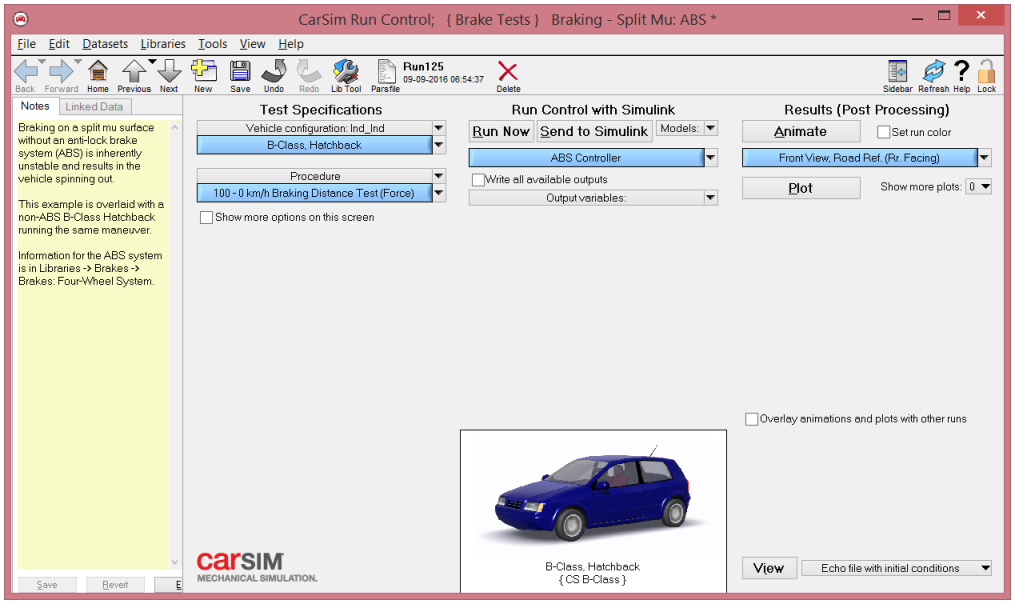

Figure 2.11: Carsim interface screenshot.

The tire model used in this work is a default tire model from Carsim software. The details of this tire model and data are provided in Figure 2.11.

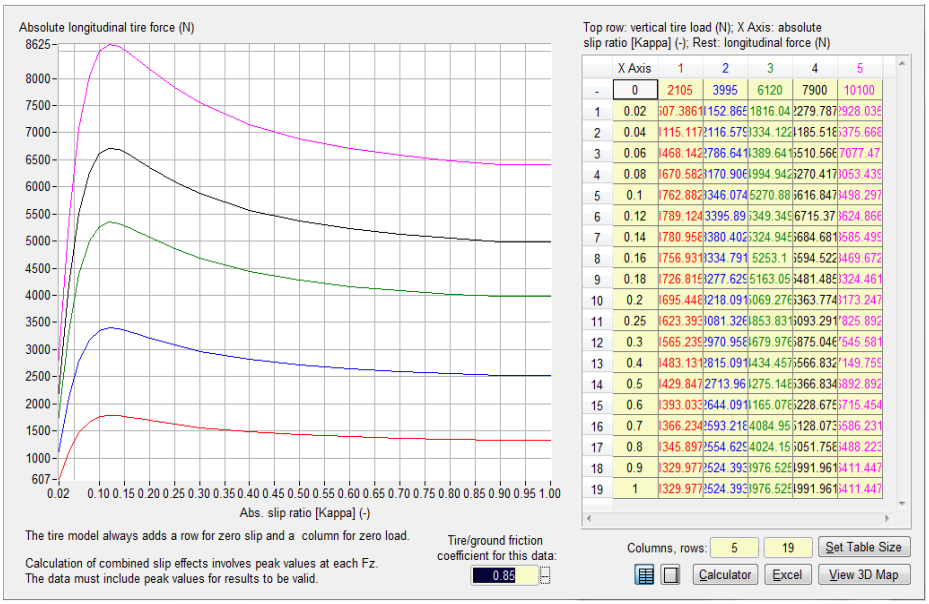

Figure 2.12: Tire F_x dataset in Carsim software, showing the tire model data, used in this research

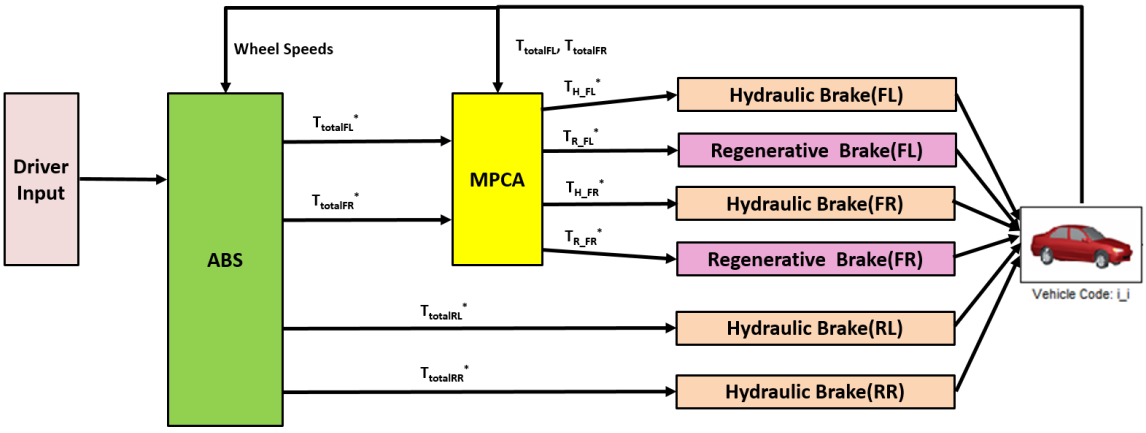

Figure 2.13: Carsim Co-simulation schematic

Figure 2.13 explains the simulation schematic used for the Carsim co-simulation. The ABS control, MPCA, Hydraulic (section 2.4) and regenerative brakes (section 2.5), and Driver input model (section 2.3) are the same as the one used in the Single wheel model. However, in this case, there is one ABS for each wheel, and hence individual brake torques are applied to the respective wheels. There is one hydraulic brake model for each wheel, and as the vehicle is a

front wheel drive vehicle, the Regenerative brake models are only present at the front wheels. The actual Simulink representation of Figure 2.13 is indicated in Appendix A2

2.7: CONCLUSION

This chapter describes the simulation model used in this work. The models for the brake pedal, hydraulic brake, PMSM motor, battery, single wheel model and Carsim, are thoroughly described as per their governing differential equations.

Chapter 3: Controller development

This section describes the development of the control strategies used in this work. In the simulation model, there are a total of 3 controllers: the ABS module, the MPCA block and PMSM control. This chapter firstly describes the MPCA strategy, which is the highlight and major contribution of this research, and then describes the ABS module and the decoupled PI control of the PMSM, which are adopted from literature.

3.1 MODEL PREDICTIVE CONTROL ALLOCATION

The braking system of an HEV/EV can be classified as an over-actuated system, i.e. at the driven wheels, there are more actuators than degrees of freedom [1, 2, 3, 50]. The brake torque required to decelerate the wheel can be achieved by the hydraulic brake as well as the regenerative brake. This results in actuator redundancy, and hence the system is over-actuated. In general the control hierarchy of over-actuated motion control systems can be said to have 3 levels [7], where the upper level consists of high-level motion control, a middle level control allocation, and a lower level actuator control. This concept can be extrapolated for the HEV/EV brake system as well, where the high level motion control is the ABS module (or ESC), the middle level control allocation is the MPCA module, and the lower level control is actuator control (Hydraulic and PMSM). A typical Control allocation scheme for over-actuated systems is shown in Figure 3.1

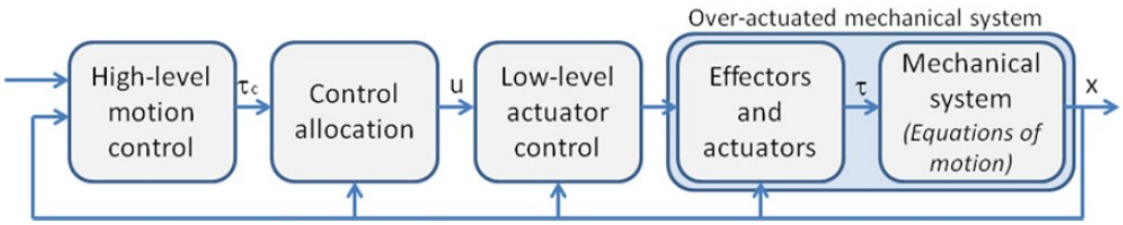

Figure 3.1: A typical Control allocation structure [7]

It consists of a high-level control law, a middle level control allocation module and a low level actuator control [7]. Control allocation allows the designer to incorporate modularity in the control development process, i.e. the high-level control task can be designed independent of the middle and low level controls. This implies that the high level control law (ABS module) and the control allocation task are decoupled and are hence independent. This further implies that an existing ABS algorithm can be used in this research, as it is independent of the control allocation task. One of the major advantages of using control allocation for over-actuated systems, is that the actuator redundancy can be used to achieve secondary objectives in the optimization process, such as maximizing the efficiency or prioritizing the use of one particular actuator [1, 2, 3, 50].

As discussed before, the brake system of an HEV/EV can be classified as an over-actuated system, where the hydraulic brakes have a higher actuation capability in terms of magnitude, but are slower in response, as compared to regenerative brakes. Regenerative brake, on the other hand, is faster and more accurate, but the regenerative brake torque is not available, when the battery is fully charged [1, 50]. Hence, it is desirable to optimize the use of both the actuators, in order to have a good braking performance.

The problem of control allocation is addressed in a number of ways in literature, with methods such as: redistributed pseudo-inverse [7], daisy-chaining [7], direct control allocation [7], quadratic programming using active set methods [8, 11], dynamic control allocation [3, 8, 11], and model predictive control allocation [2, 6, 7, 13]. MPCA is an optimization based control strategy, which uses the actuator models to predict the input and output states of the system, and handles the actuation saturation as well as the actuator rate saturation [2, 7].

3.1.1 Model Predictive Control (MPC)

Model Predictive Control is an advanced control technique, which uses iterative, finite-horizon optimization of the plant model[2, 6, 7, 67]. In simple words, it minimizes the tracking error between

the predicted future responses of the system, and the desired responses. In this work, MPC is used to accomplish the allocation task for 2 major reasons: optimization based allocation of actuators, and inclusion of actuator dynamic model, and rate constraint. Other methods like dynamic control allocation[3, 8, 9] also uses optimization, but does not include the dynamic model of the actuator. Also, the results of MPCA being superior to dynamic control allocation are already published in literature [2].

In general, there are two important aspects of MPC: firstly the plant model, which is used to predict the future trajectories, and secondly the control law defined by the cost function and its associated constraints. In general, for a dynamic system defined in the state space format as follows:

$$x_{k+1} = A.x_k + B.u_k \tag{3.1}$$
$$y_k = C.x_k + D.u_k$$

where, A is the state matrix, B is the input matrix, C is the output matrix, D is the feedthrough matrix, x is the state vector, u is the input vector, y is the output vector and subscript 'k' represents current instant of time. Equation (3.1) is referred to as the plant model of MPC. The control law is defined by a cost function as follows:

$$\min_u J = \sum_{k=1}^{N_p} \left|\left|y_{ref}(k+1) - y(k+1)\right|\right|_{Q_y}^2 + \sum_{k=1}^{N_c-1} \left|\left|u(k+1)\right|\right|_{Q_u}^2 + \sum_{k=1}^{N_c-1} \left|\left|\Delta u(k+1)\right|\right|_{Q_{\Delta u}}^2 \tag{3.2}$$

Subject to

Input Constraint: $u_{min} \le u(k) \le u_{max}$

Input Rate Constraint: $\Delta u_{min} \le \Delta u(k) \le \Delta u_{max}$

Output constraint(If applicable): $y_{min} \le y(k) \le y_{max}$

Here, y_{ref} is the reference trajectory, y is the actual output trajectory, u is the actuator input, Δu is the actuator rate, N_p is the prediction horizon, N_c is the control horizon, and $Q_{y,\ u,\ \Delta u}$ is the weighting matrix, and subscript "max" and "min" indicate the maximum and minimum limits respectively. The general concept of MPC is indicated in Figure 3.2. In MPC, the future trajectory of the plant is predicted at each sampling instant based on the dynamic plant model in

equation (3.1). In Figure 3.2, the "Reference Trajectory" and "Predicted Output" is predicted for (k, k+1, k+2, …….. k+N). In this Figure N refers to the Prediction Horizon N_p.

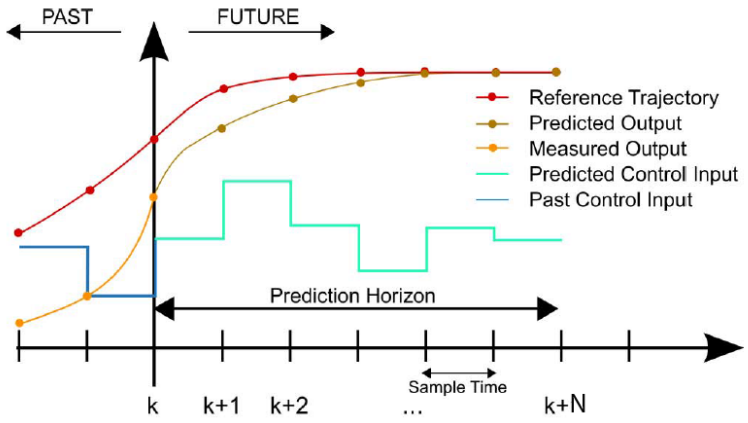

Figure 3.2: Model Predictive Control Concept [68]

Similarly the "Predicted Control input" is predicted for (k, k+1, k+2, ……, k+N), until the Control Horizon N_c. In the case depicted in the diagram, $N=N_p=N_c$, but in reality considering practical computational capabilities, N_p is always set greater than N_c. As per the cost function in equation (3.2), the difference between the Reference and Predicted output is then minimized over the prediction horizon at each time instant, and similarly the control input ant the control input rate is computed for each instant over the control horizon. However, only the control at the next instant is applied. This process is subject to the actuator and actuator rate constraints, as well as the output constraints. The mathematical formulation of the aforementioned method is explained in the next section.

3.1.2 MPC Formulation

In this section, the basic formulation of the MPC problem in mathematical form is discussed. Let us consider a continuous dynamic and non-linear system, whose states are defined by the vector x(t), and the actuator input is defined by the vector u(t), while the system output is defined by y(t):

$$\dot{x}(t) = f(x(t), u(t), w(t)) \tag{3.3}$$

$$y(t) = g(x(t)) \tag{3.4}$$

Here, w(t) is the system noise. In this work, the effect of system noise is neglected.

Using Taylor Series expansion to linearize the dynamic system defined in equation (3.3) we get:

$$\dot{x}(t) \approx f(x_0, u_0, w_0) + A_j(x - x_0) + B_j(u - u_0) \tag{3.5}$$

Here A_j and B_j are referred to as Jacobian Matrices and are mathematically defined as:

$$A_j = \frac{\partial \dot{x}}{\partial x} \; and \; B_j = \frac{\partial \dot{x}}{\partial u} \tag{3.6}$$

The approximation in equation (3.5) is then converted by difference method of sample time T_s, and sample step 'k'

$$\frac{\Delta x_{k+1}}{T_s} = f(x_0, u_o, w_0) + A_j(x_k - x_0) + B_j(u_k - u_o) \tag{3.7}$$

Where Δx_{k+1} is the difference in the state variable over the sample instant k, is defined as:

$$\Delta x_{k+1} = x_{k+1} - x_k \tag{3.8}$$

On substituting equation (3.8) in (3.7), we get:

$$x_{k+1} = x_k + T_s.f(x_0, u_o, w_0) + T_s.A_j(x_k - x_0) + T_s.B_j(u_k - u_o) \tag{3.9}$$

Similarly, equation (3.9) can be used to compute $\Delta x_k = x_k - x_{k-1}$, by shifting the equation (3.8) back by 1 time step:

$$x_k = x_{k-1} + T_s.f(x_0, u_o, w_0) + T_s.A_j(x_{k-1} - x_0) + T_s.B_j(u_{k-1} - u_o) \tag{3.10}$$

Now, in order to eliminate the initial condition term, the equation (3.10) is subtracted from (3.9) to get:

$$x_{k+1} - x_k = x_k - x_{k-1} + T_s.A_j(x_k - x_{k-1}) + T_s.B_j(u_k - u_{k-1}) \tag{3.11}$$

$$\Delta x_{k+1} = \Delta x_k\left(1 + T_s A_j\right) + T_s \,.B_j.\Delta u_k \tag{3.12}$$

Defining, $A = (1+T_s.A_j)$ and $B = (T_s.B_j)$

$$\Delta x_{k+1} = A.\Delta x_k + B.\Delta u_k \tag{3.13}$$

$$x_{k+1} = x_k + A.\Delta x_k + B.\Delta u_k \tag{3.14}$$

Equation (3.14) indicates that the state vector at sample k+1, is a function of the state vector at sample k, Jacobian matrices over the sample k, change in state over sample k, and the change in control input over sample k. This equation primarily describes the "Prediction" aspect of Model predictive control, where the state at instant k+1 is defined as a function of the parameters at the

instant k and k-1. Similarly, the prediction over a prediction horizon N_p and control horizon N_c can be mathematically described as:

$$x(k+1) = x(k) + \sum_{i=1}^{N_p} A^i \Delta x(k) + \sum_{i=0}^{N_p-1} A^i B \Delta u(k) + \sum_{i=0}^{N_p-2} A^i B(k+1)\Delta u(k+1) + \cdots + \sum_{i=0}^{N_p-N_c+1} A^i B(N_c-1)\Delta u(k+N_p) \quad (3.15)$$

Equation (3.15) is valid for the assumption that $N_p > N_c > 0$. Similarly, the prediction output vector y(t) from equation (3.4) can be expressed as (similar to and adopted from [67, 68]):

$$y(k+1) = C.x(k+1) \quad (3.16)$$

$$Y = G\Delta x(k) + F.\Delta U \quad (3.17)$$

Where,

$$Y = \begin{bmatrix} y(k+1) - y(k) \\ y(k+2) - y(k) \\ y(k+3) - y(k) \\ y(k+4) - y(k) \\ \cdots \\ y(k+N_p) - y(k) \end{bmatrix} \quad G = \begin{bmatrix} CA \\ CA + CA^2 \\ CA + CA^2 + CA^3 \\ CA + CA^2 + CA^3 + CA^4 \\ \cdots \\ \sum_{i=1}^{N_p} CA^i \end{bmatrix}$$

$$\Delta U = \begin{bmatrix} u(k+1) - u(k) \\ u(k+2) - u(k+1) \\ u(k+3) - u(k+2) \\ u(k+4) - u(k+3) \\ \cdots \\ u(k+N_c) - u(k+N_c-1) \end{bmatrix} \quad (3.18)$$

$$F = \begin{bmatrix} CB & 0 & 0 & \cdots & 0 \\ CB + CAB & CB & 0 & \cdots & 0 \\ CB + CAB + CA^2B & CB + CAB & CB & \cdots & 0 \\ \cdots & \cdots & \cdots & \cdots & \cdots \\ \sum_{i=0}^{N_p} CA^iB & \sum_{i=0}^{N_p-1} CA^iB & \sum_{i=0}^{N_p-2} CA^iB & \cdots & \sum_{i=0}^{N_p-N_c} CA^iB \end{bmatrix}$$

Hence equation (3.17) can be used to compute the output vector Y in terms of state vector variation Δx(k) and input vector ΔU. Equations (3.15) and (3.17) lay the basic foundation for

developing a Model Predictive Controller, as these equations are used for predicting the future output vectors, Input vectors, and state vectors.

The prediction in MPC is only as accurate as the plant model used, and in almost all applications, the plant has to be simplified/linearized in order to avoid controller implementation difficulty. Hence in order to account for this mismatch and more importantly, to track the output error, the next step in MPC, is to define a cost function. In general, the cost function has 3 weighted errors: Error in predicted and desired output vector, desired control input vector, and the change in control input vector. The output error is minimized over the prediction horizon N_p, while the predicted control input, and the change in control input is minimized over the control horizon.

$$\min_{u} J = \sum_{k=1}^{N_p} \left|\left|y_{ref}(k+1) - y(k+1)\right|\right|_{Q_y}^2 + \sum_{k=1}^{N_c-1} \left|\left|u(k+1)\right|\right|_{Q_u}^2 + \sum_{k=1}^{N_c-1} \left|\left|\Delta u(k+1)\right|\right|_{Q_{\Delta u}}^2 \tag{3.19}$$

Hence the goal here is to minimize the cost function J, which is subject to the following constraints:

$$\begin{aligned} \text{Input Constraint:} \quad & u_{min} \le u(k) \le u_{max} \\ \text{Input Rate Constraint:} \quad & \Delta u_{min} \le \Delta u(k) \le \Delta u_{max} \\ \text{Output constraint(If applicable):} \quad & y_{min} \le y(k) \le y_{max} \end{aligned} \tag{3.20}$$

In this research work, the MPC formulation described in equations (3.15, 3.17, 3.19, 3.20) is implemented into simulation via the Model Predictive Control Toolbox, in Matlab/Simulink. Figure 3.3 shows a sample screen of the MPC tool box in Matlab.

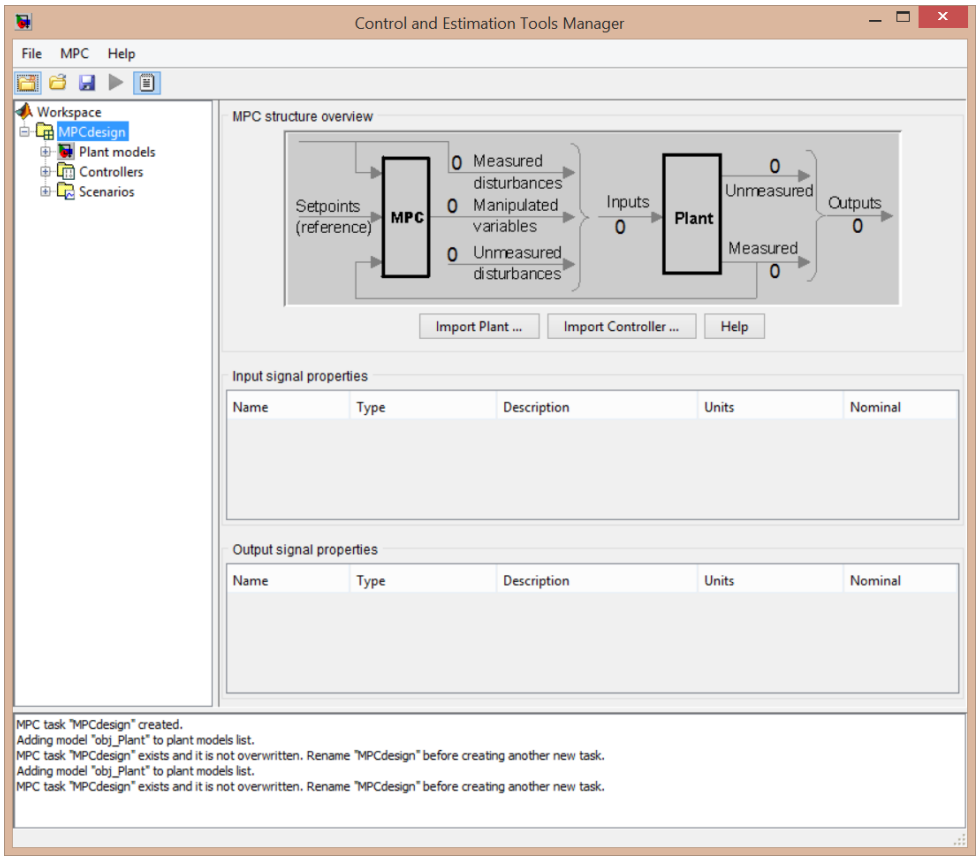

Figure 3.3: Model Predictive Control Toolbox GUI in Matlab. [69]

3.1.1 MPCA Plant model

This section describes the formulation of the MPCA plant model. As discussed earlier in this chapter, control allocation involves allocating the control task between multiple actuators, hence the actuator dynamics models are the MPC plant models. In this research work, the actuators are modelled to have a second order dynamics. Similar approaches are used in many aerospace research works on control allocation [6, 7, 8, 11, 13]. As this application of MPCA applies to a braking maneuver, the control task is to be allocated among hydraulic and regenerative brake. The schematic and signal flow describing the MPCA plant model is shown in Figure 3.4.

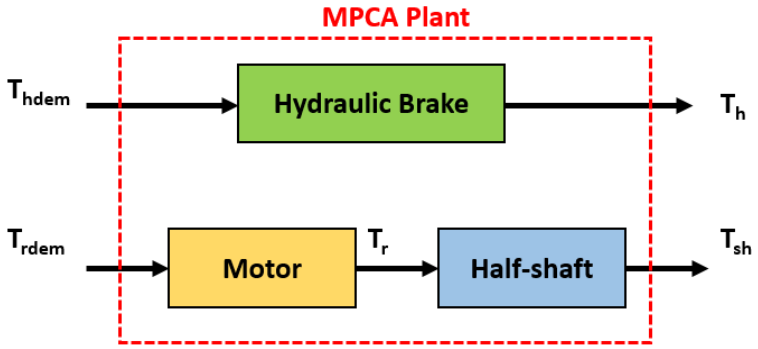

Figure 3.4: MPCA plant representation and signal flow

The actuator models in the time domain are as follows:

$$\ddot{T}_h + 2\xi_h\omega_{nh}\dot{T}_h + \omega_{nh}^2 T_h = \omega_{nh}^2 T_{hdem} \tag{3.21}$$

$$\ddot{T}_r + 2\xi_r\omega_{nr}\dot{T}_r + \omega_{nr}^2 T_r = \omega_{nr}^2 T_{rdem} \tag{3.22}$$

And in the frequency domain, they can be written as

$$\frac{T_h(s)}{T_{hdem}(s)} = \frac{\omega_{nh}^2}{s^2 + 2\xi_h\omega_{nh}s + \omega_{nh}^2} = G_h(s) \tag{3.23}$$

$$\frac{T_r(s)}{T_{rdem}(s)} = \frac{\omega_{nr}^2}{s^2 + 2\xi_r\omega_{nr}s + \omega_{nr}^2} = G_r(s) \tag{3.24}$$

As mentioned in chapter 2, since the powertrain configuration considered in this research work has half shaft dynamics, it is essential to include this effect in the MPC plant model. This will aid the controller to accurately predict the system states. In this work, a 2 DOF shaft model is used to describe the shaft dynamics, which is widely used in literature for anti-jerk control applications [30, 32, 33, 34, 35, 45, 46, 47]

$$\frac{T_{sh}(s)}{T_r(s)} = \frac{\omega_{nsh}^2}{s^2 + 2\xi_{sh}\omega_{nsh}s + \omega_{nsh}^2} = G_{sh}(s) \tag{3.25}$$

Substituting (3.25) in (3.24), we get

$$\frac{T_{sh}(s)}{T_{rdem}(s)} = G_r(s)G_{sh}(s) \tag{3.26}$$

Also, the total brake torque at the wheel is the addition of the hydraulic brake torque and the regenerative brake torque (shaft torque at the wheel):

$$T_h + T_{sh} = T_b \tag{3.27}$$

Hence equations (3.21)-(3.27) can be written in stat space format as:

$$\dot{X} = AX + BU \tag{3.28}$$

Where

$$X = \left[\dddot{T}_{sh}\ \ddot{T}_{sh}\ \dot{T}_{sh}\ T_{sh}\ \dot{T}_h\ T_h\right]^T$$

$$U = [\,T_{rdem}\ T_{hdem}]^T$$

$$A = \begin{bmatrix} 0 & 1 & 0 & 0 & 0 & 0 \\ -\omega_{nh}^2 & -2.\xi_h.\omega_{nh} & 0 & 0 & 0 & 0 \\ 0 & 0 & 0 & 1 & 0 & 0 \\ 0 & 0 & 0 & 0 & 1 & 0 \\ 0 & 0 & 0 & 0 & 0 & 1 \\ 0 & 0 & -\omega_{nr}^2.\omega_{nsh}^2 & a_{64} & a_{65} & a_{66} \end{bmatrix} \tag{3.29}$$

$$a_{64} = -2.(\xi_{sh}\omega_{nsh}\omega_{nr}^2 + \xi_r\omega_{nr}\omega_{nsh}^2)$$

$$a_{65} - (\omega_{nr}^2 + 4.\xi_{sh}\xi_r\omega_{nsh}\omega_{nr} + \omega_{nsh}^2)$$

$$a_{66} = -2.(\xi_{sh}\omega_{nsh} + \xi_r\omega_{nr})$$

$$B = \begin{bmatrix} 0 & 0 \\ \omega_{nh}^2 & 0 \\ 0 & 0 \\ 0 & 0 \\ 0 & 0 \\ 0 & -\omega_{nr}^2.\omega_{nsh}^2 \end{bmatrix}$$

3.1.2 MPC cost function

The MPC cost function used in this work is defined as follows:

$$\min_U \sum_{i=0}^{N_p} Y^T Q_y Y + \sum_{i=0}^{N_c-1} U^T Q_u U \tag{3.30}$$

The output error *Y*, of the MPC cost function is defined as:

$$Y = \begin{bmatrix} T_b - T_b^* \\ T_{sh} - T_{sh}^* \end{bmatrix} \tag{3.31}$$

This optimization problem is subjected to the following actuator constraints:

$$\begin{aligned} T_{rmin} \leq T_r \leq T_{rmax} \\ T_{hmin} \leq T_h \leq T_{hmax} \\ \dot{T}_{rmin} \leq \dot{T}_r \leq \dot{T}_{rmax} \\ \dot{T}_{hmin} \leq \dot{T}_h \leq \dot{T}_{hmax} \end{aligned} \tag{3.32}$$

The plant modeled in (3-8) is then discretized with respect to the MPC sampling time:

$$x_{k+1} = A_k\, x_k + B_k\, u_k \tag{3.33}$$

The MPCA scheme defined here has four tuning parameters: Prediction horizon N_p, Control Horizon N_c, input weighting matrix Q_u, and output weighting matrix Q_y.

$$Q_y = diag(\gamma_b, \gamma_{sh}) \tag{3.34}$$

$$Q_u = diag(\alpha_r, \alpha_h) \tag{3.35}$$

3.1.3 MPC tuning parameters

The input weighting matrix Q_u penalizes the effort of each actuator, whereas the output weighting matrix Q_y penalizes the output error. The parameters γ_b and γ_{sh} represent the multi-objective aspect of the proposed MPCA scheme. For the reference trajectories T_b* and T_{sh}*, the T_b* is directly taken from the total torque demanded from the ABS module, and the T_{sh}* is selected such that shaft torque should track the actual motor torque T_r, in order to reduce the driveline vibrations and the torque imbalance [45].

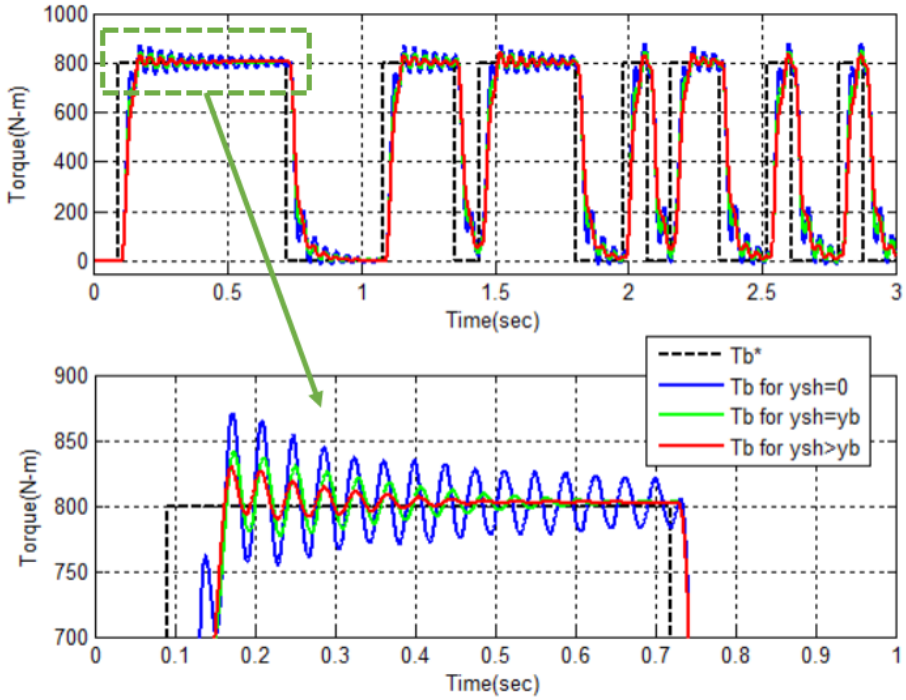

Figure 3.5: Comparison of torque response for different output weights

In order to explore the multi-objective aspect of the proposed MPCA scheme, the output weights γ_b and γ_{sh}, are selected accordingly. In this research work, two control objectives are considered: frequency-based torque allocation only, and torque allocation with vibration control. If the control objective is frequency-based torque allocation only, without considering the vibration damping aspect of the scheme, then the weight γ_{sh} is set to zero, and only γ_b is adjusted. If the control objective is vibration control along with control allocation, then the weight γ_{sh} is non-zero, and is tuned relative to γ_b. In order to test the effectiveness of the proposed MPCA schemes, and to substantiate the strategy proposed in this chapter, the MPCA controller is tested with a Pseudo Random Binary Signal (PRBS), and the results are analyzed.

Table 3.1: MPCA Tuning Parameters

Case:	$\gamma_{sh}=0$	$\gamma_{sh}=\gamma_b$	$\gamma_{sh}>\gamma_b$
γ_{sh}	0	10e4	15e4
γ_b	10e4	10e4	10e4
Sampling time	0.01 sec		
H_p	10		
H_c	2		

The tuning parameters used in this work are summarized in Table 3.1. Figure 3.5 compares the output torques for different weighting ($\gamma_{sh} = 0$, $\gamma_{sh} = \gamma_b$, and $\gamma_{sh} > \gamma_b$) with a pseudo random binary sequence (PRBS) signal, similar to the one used in [2].

A PRBS signal is kept the same for the three cases in order to have a fair comparison, and the magnitude of the PRBS torque was selected such that it is higher than the motor actuation limits, so that both the actuators can work together.

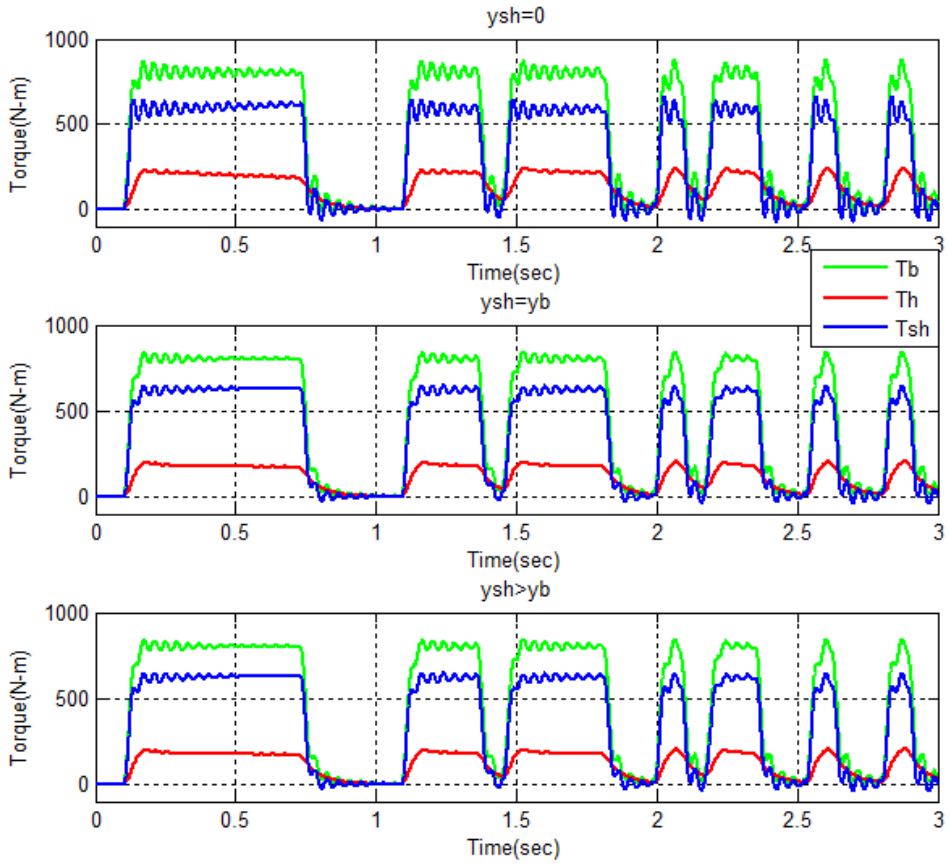

Figure 3.6: Torque split for different γ_{sh}

The effect of variation of γ_{sh} is presented in Figures 3.5, and 3.6. It can be observed that when γ_{sh} is set to zero, vibrations are evident in the total actual torque. These vibrations are mainly due to the flexibility of the driveshaft and are observed throughout the simulation when sudden torque demands are made. Then the parameter γ_{sh} is set equal to γ_b, which implies equal penalty to both the output errors, and it is observed that the peak-to-peak amplitude of the vibrations in the total torque is reduced. In the third case, when the magnitude of γ_{sh} is set relatively higher than γ_b, it

results in a slightly better performance than the previous case and the peak-to-peak amplitude of the vibrations in the total torque is further reduced.

3.2 FIVE PHASE ABS

The five phase ABS, is adapted from an existing ABS strategy from literature [54, 55, 56]. In general, ABS algorithms can be classified as direct-slip control and threshold based control. Direct slip control strategies are mathematically well defined and require lesser tuning as compared to threshold based strategies. However, direct slip control algorithms use the value of longitudinal wheel slip, which further depends on the vehicle longitudinal velocity, which is not available as a direct measurement from the available sensors in a vehicle. It further requires the design of estimators to determine its value of vehicle velocity. Threshold based strategies, on the other hand, require wheel speed/ wheel acceleration signal, which is easily available from wheel speed sensors. Threshold based algorithms also require more extensive tuning as compared to direct slip control algorithms. The five phase strategy is a threshold based algorithm, which only uses the signal of wheel acceleration during ABS operation.

$$x_1 = \lambda - \lambda^* \tag{3.36}$$

$$x_2 = r\,\dot{\omega} - a_x^* \tag{3.37}$$

This algorithm consists of five distinct phases and switching between these phases. The wheel acceleration signal is the criteria for switching between each of the states, and the criteria is specified by thresholds (ε_1, ε_2, ε_3, ε_4, ε_5), which are to be tuned accordingly. Each phase specifies the rate of change of brake torque. The strategy is explained in Figure 3.7, and is adapted from [54, 55, 56].

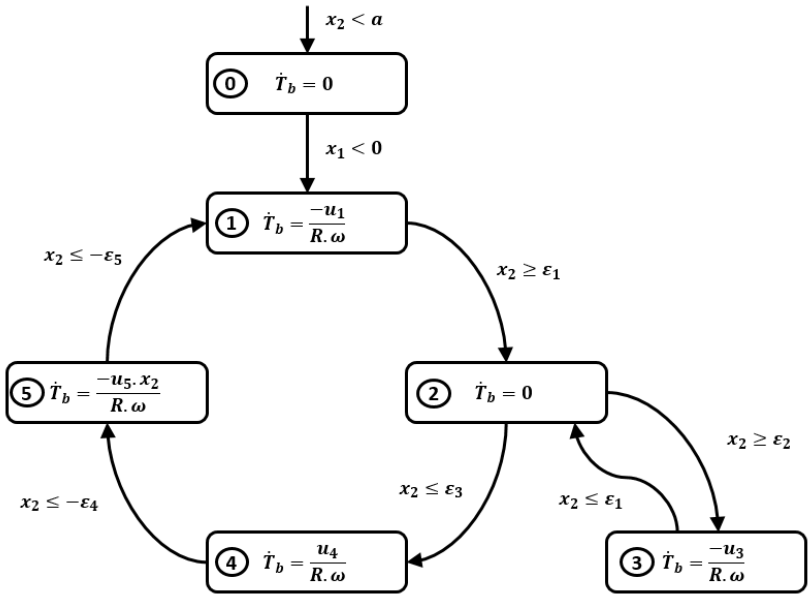

Figure 3.7: The five phase ABS control strategy, adopted from [55]

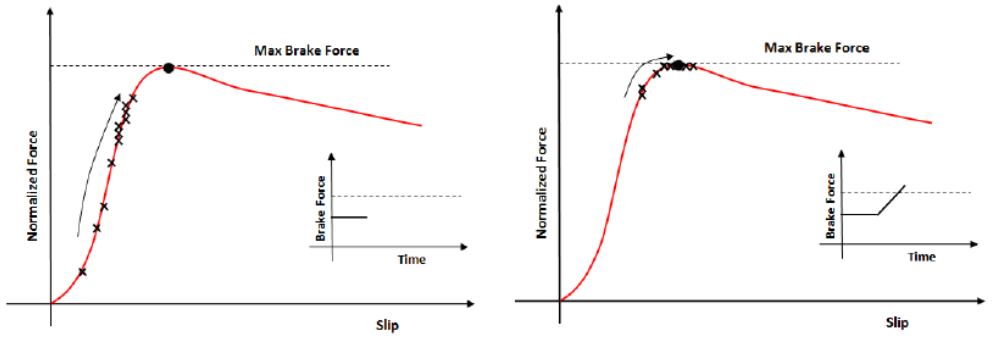

(a) The braking force is immediately applied of which stability is guaranteed deterministically

(b) The braking force keeps increasing

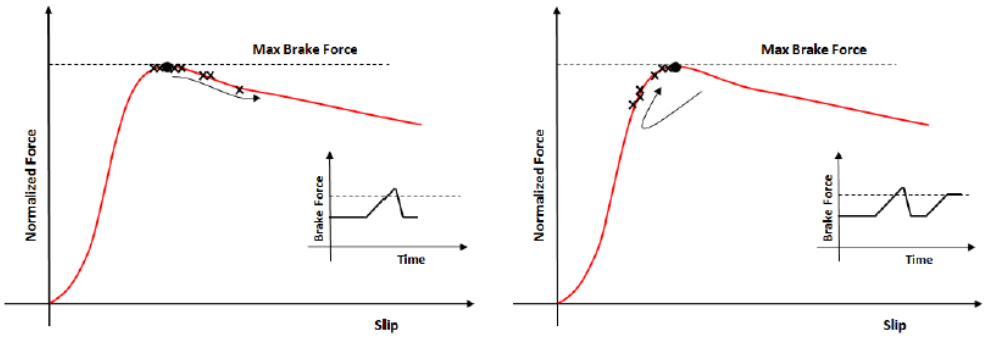

(c) When instability region is reached, braking force is set to decrease quickly

(d) Once wheel slip is in the stable region, holding the brake pressure

Figure 3.8: Plots showing the effect of different brake torque profile on available tractive force.[56]

Figure 3.8 further explains the working of the five phase ABS. As observed in Figure 3.8(a), at the beginning of the braking maneuver, application of sudden brake torque results in the wheel slip to increase (black arrow indicates the direction of wheel slip progression). If there was no ABS, then it would go past the peak of the tire force curve and stay at 100% slip (locked wheel). The objective of the ABS is to maintain the tire force in a region of maximum tire force (peak of the curve). Hence in Figure 3.8 (b), the brake torque is further increased, causing the wheel slip to further increase and hence the tire force. Once the tire force has increased past the peak, and has started to decrease, the brake torque is decreased, causing the wheel to accelerate, and hence the tire force starts to increase back towards the peak. The brake torque is decreased until the peak is crossed again, and once the tire force starts to decrease (indicated by the black arrow in Figure 3.8 (d)), the brake torque is increased, and this cycle is then repeated. The thresholds ε's decide when to stop increasing and decreasing the brake torque.

In order to confirm correct implementation of the five phase ABS algorithm in this work, the five phase controller was first tested with sample simulations. The results in this work were compared to the results published in [56]. The initial vehicle velocity was assumed to be 130kph, and the road surface was of mu 0.9, similar to the simulations conditions in [56]. The quarter car mass, wheel inertia, and the wheel radius used in this simulation are however different from the one used in [56], as the author did not reveal these parameters in his work. The tire model data, however is the same as the one used reference work [56] . Hence the results of the sample simulation are not exactly same but similar.

The longitudinal slip response and the ABS state variation is indicated in Figure 3.10, while the vehicle and wheel velocity response is observed in Figure 3.11. It can be observed that the initial portions of figures 3.10 and 3.11, from 1~1.7 sec is different for the sample simulation in this work, from the reference simulation plots. This is mainly due to the fact as to how fast the wheel velocity will decrease on application of brake torque at the wheels.

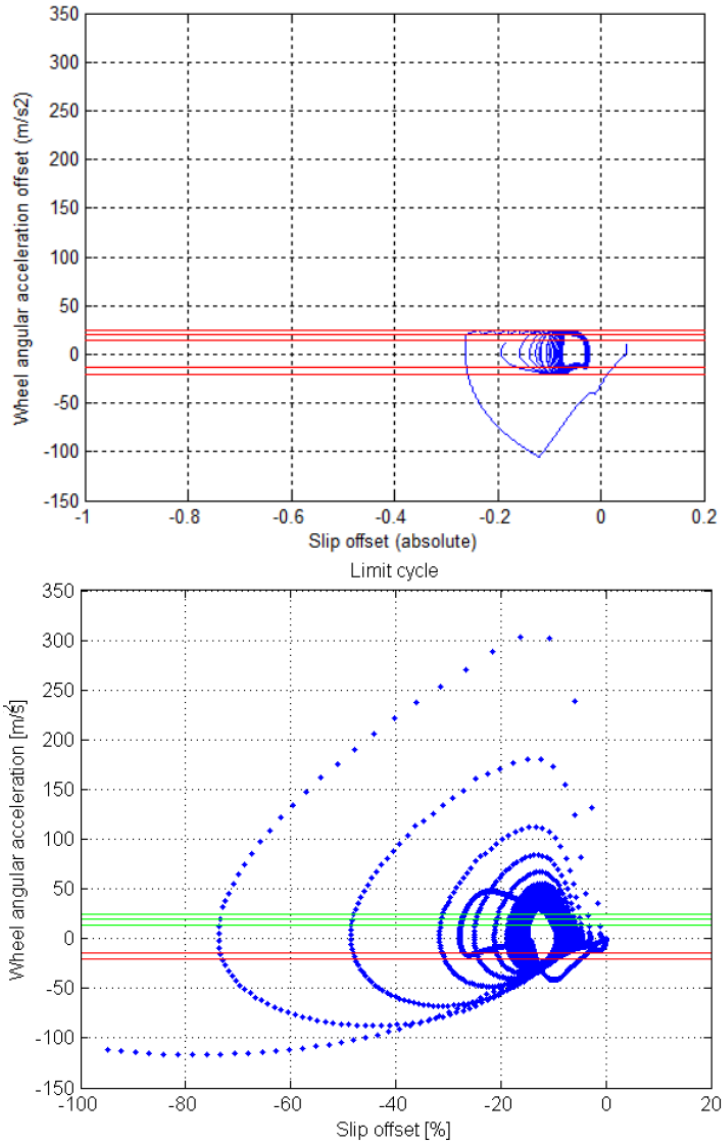

Figure 3.9: Limit cycle comparison: This work (top), reference plot from [56] (bottom)

As seen in Figure 3.11, for the results in this work, the wheel velocity decreases faster than the one from reference plot. This is because the wheel velocity calculation in the simulation is determined by the wheel inertia, wheel radius, and also the vehicle mass, all of which are not same as the ones used in the reference work as stated before. Hence this phenomenon is expected to be observed in the sample simulations. It can be observed that the slip cycling and ABS state in Figure 3.10, and the wheel velocity variation in Figure 3.11, in this work, are comparable to the reference simulation to a great extent. The limit cycle comparison for the sample simulation

is shown in Figure 3.9. It can be observed that the limit cycle is “less spread” for the sample simulation in this work. This is mainly due to the initial portion of the slip response (1~1.7sec) and the final portion (3.5~4sec) in Figure 3.10, being different in the sample simulation as compared to the reference plot, as explained previously. The significance of the ABS state, is that it indicates the time spent by the ABS logic in a particular phase, which assists in tuning the ABS control parameters, as explained in detail in the reference paper [56].

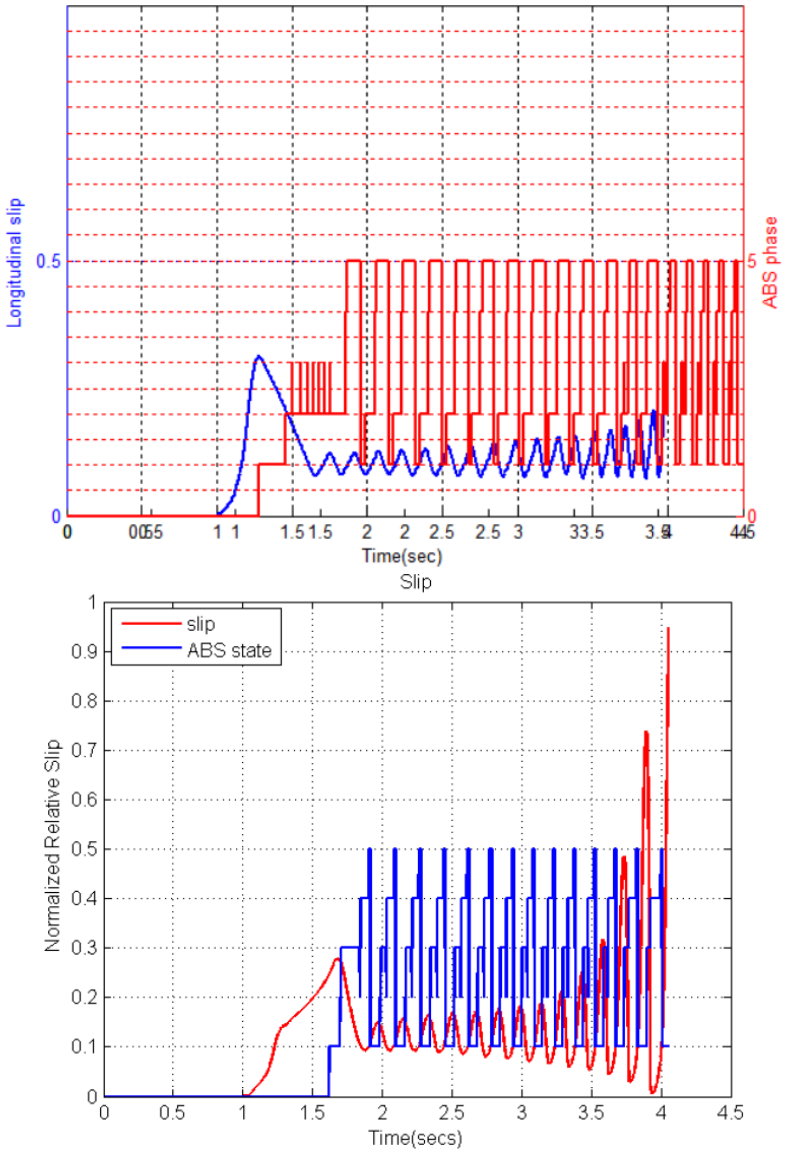

Figure 3.10: Longitudinal slip comparison: This work (top), reference plot from [56] (bottom)

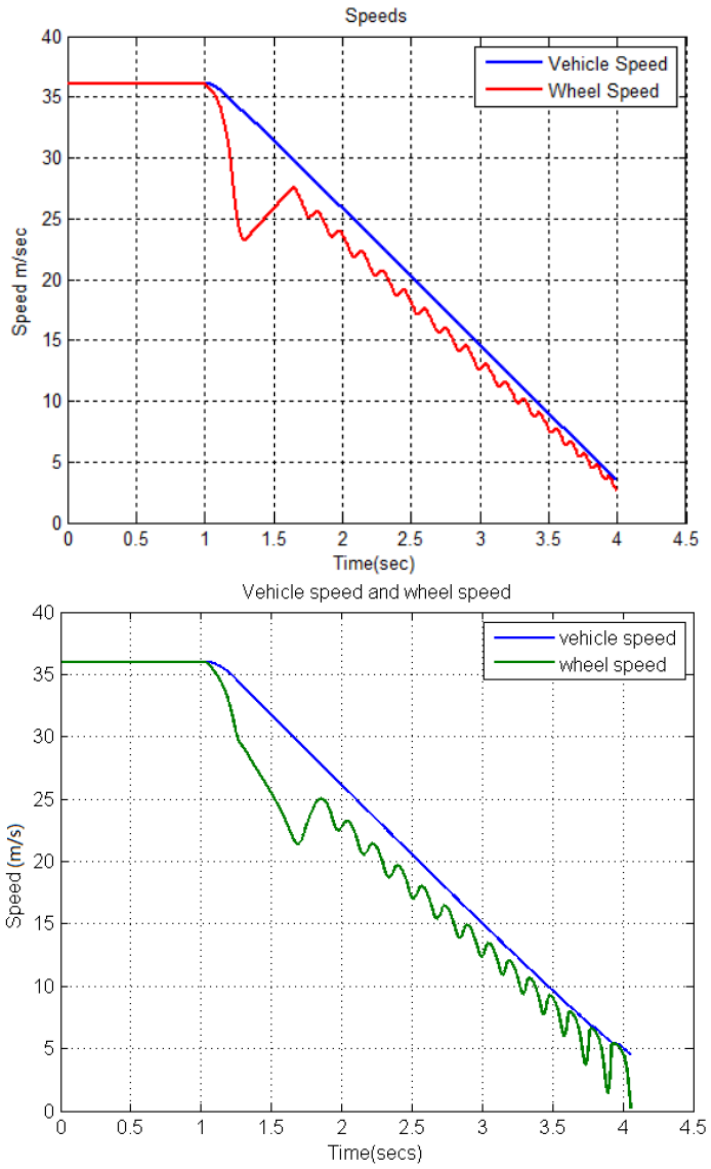

Figure 3.11: Velocities comparison: This work (top), reference plot from [56] (bottom)

3.3 PMSM CONTROL

In this research, a Permanent Magnet Synchronous Motor (PMSM) is used for the purpose of regenerative braking and the modelling and control is adopted from [58]. The PMSM model incorporated in this work is the popular d-q model [58, 59]. The equations defining the electric part of the model are:

$$\frac{d}{dt}(i_q) = (\, v_q - Ri_q - p\omega_r(L_d i_d + \lambda))/L_q \tag{3.38}$$

$$\frac{d}{dt}(i_d) = (v_d - Ri_d + p\omega_r L_q i_q)/L_d \tag{3.39}$$

The equations defining the mechanical part are:

$$T_e = 1.5\, p\{\lambda i_q + (L_d - L_q) i_q i_d\} \tag{3.40}$$

$$\frac{d}{dt} w_r = \frac{1}{J}(T_e - F w_r - T_m) \tag{3.41}$$

From the PMSM equations (3.38) and (3.39), it is observed that there is a dynamic coupling between the two equations due to the presence of the terms: $\omega_r i_q$ and $\omega_r i_d$, respectively. The PMSM equations are then decoupled, to eliminate the coupling between these terms. Decoupling results in simplification of the plant model equations and hence further simplifies the control task. This approach has also been used in literature [58, 59]. Hence two intermediate variables are thus defined U_d, and U_q.

$$U_d = v_d + \omega_r L_q i_q \tag{3.42}$$

$$U_q = v_q - \omega_m L_d I_d - \omega_m \lambda_f \tag{3.43}$$

Hence the de-coupled equations are:

$$\frac{d}{dt}(i_d) = (U_d - Ri_d)/L_d \tag{3.44}$$

$$\frac{d}{dt}(i_q) = (U_q - Ri_q)/L_q \tag{3.45}$$

From the resulting decoupled equations in (3.44) and (3.45), it can be observed that by introducing the intermediate variables, the q-axis and d-axis equations are de-coupled, i.e. the dynamically coupled terms are eliminated. Now, the intermediate variables U_d and U_q are then determined using the two Proportional-Integral (PI) Controllers. The error between the desired and actual d- and q-axis currents is minimized by these two PI controllers.

$$e_d = (I_d^* - I_d) \tag{3.46}$$

$$e_q = (I_q^* - I_q) \tag{3.47}$$

$$\widehat{U}_d = k_{pd} e_d + k_{id} \int_0^t e_d(\tau) d\tau \tag{3.48}$$

$$\widehat{U}_q = k_{pq} e_q + k_{iq} \int_0^t e_q(\tau) d\tau \tag{3.49}$$

Equations (3.42) and (3.43) are then combined with equations (3.48) and (3.49), and the control input signals v_q and v_d are then applied to the PMSM model. From the above approach, it can be observed that the parameters i_q and i_d are the required inputs to the PI controllers. In reality, since the currents are available in 3 phase, the available measured 3 phase signals from the PMSM model are then converted to the d-q axis signals by using Park-Clark transform, as shown in Figure 3.12.

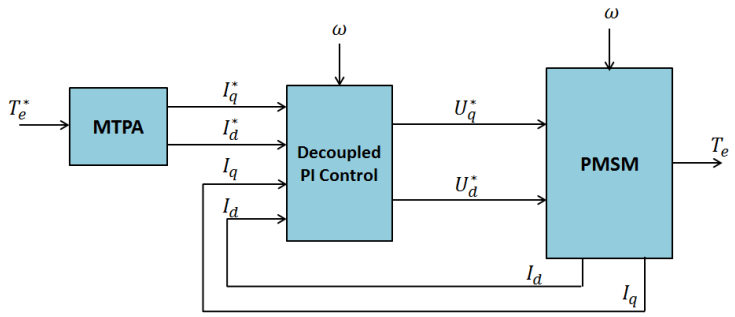

Figure 3.12: PMSM model with decoupled control

The PMSM control strategy used in this work is Maximum Torque Per Ampere (MTPA), when the motor speed is less than the base speed, and Flux weakening, otherwise, similar to [58,59]. The error between the currents I_q* and I_q; and I_d* and I_d, are minimized with the use of two different PI controllers. The output of the PI controllers is the d and q axis voltages.

In order to generate the MTPA trajectory, an approach similar to [58] is used. The MTPA trajectory is generated by means of a second order curve fitting from [59].

The performance of the PMSM model is then validated through simulation with published results in [59]. Figure 3.13 shows motor responses with MTPA control for full load simulation. The motor speed follows the reference speed (1500 rpm) and motor electromagnetic torque is controlled to the full load torque (40 Nm) at about 0.1s. And motor d, q axis and three phase currents are also controlled to steady-state values which are related to motor torque and parameters based on MTPA control. These responses are similar to the published results in [59].

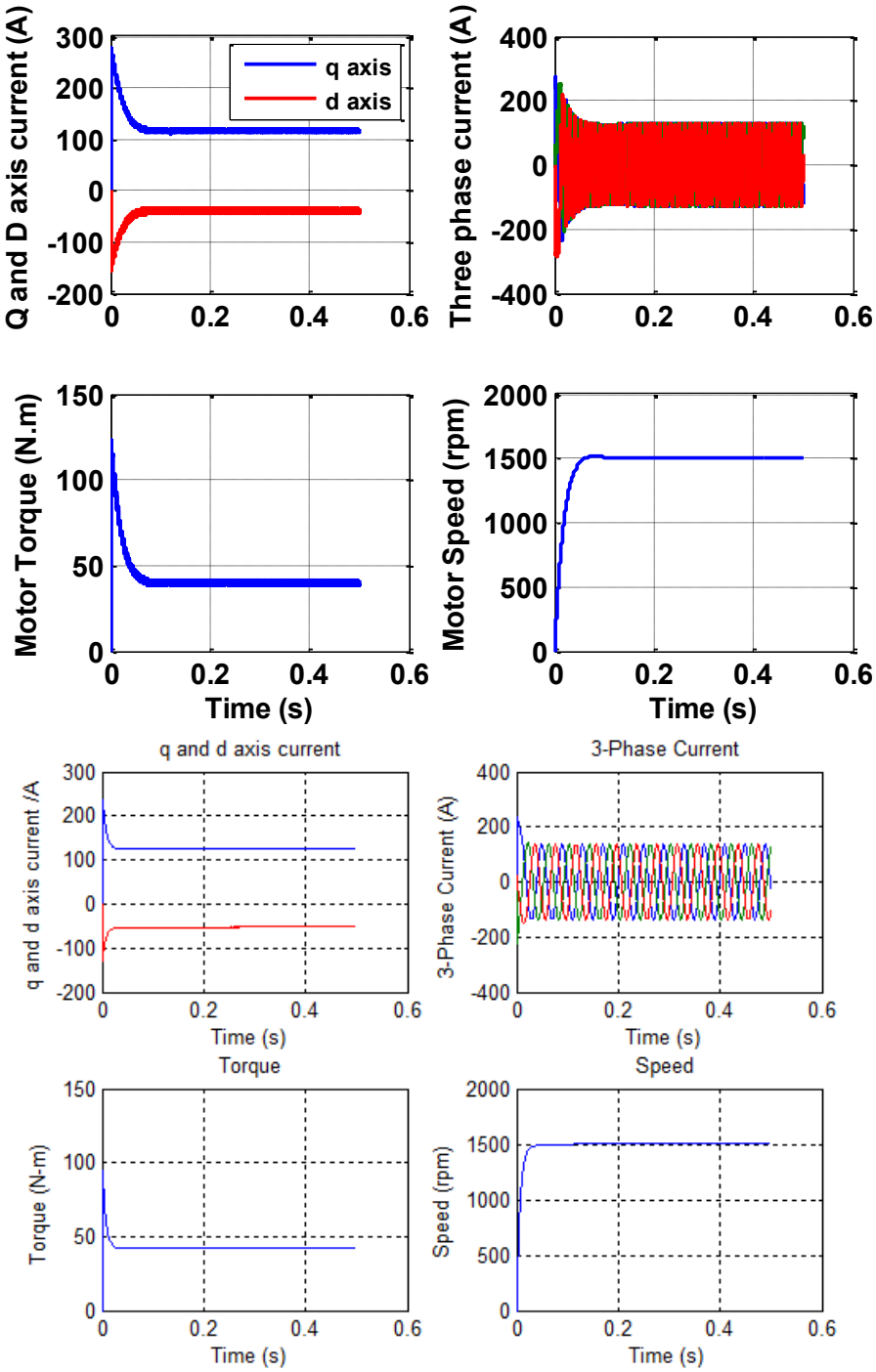

Figure 3.13: PMSM control validation for full load MTPA condition: (Top) results published in [59] and (bottom) results of the simplified PMSM model used in this work.

3.4 COMBINED SYSTEM TUNING

This section describes the methodology of selecting the MPC weights for the combined system. As an example, the system with a single wheel model is considered, but the same approach can be applied to the system with full car model as well. Consider the system configuration defined in Figure 3.14.

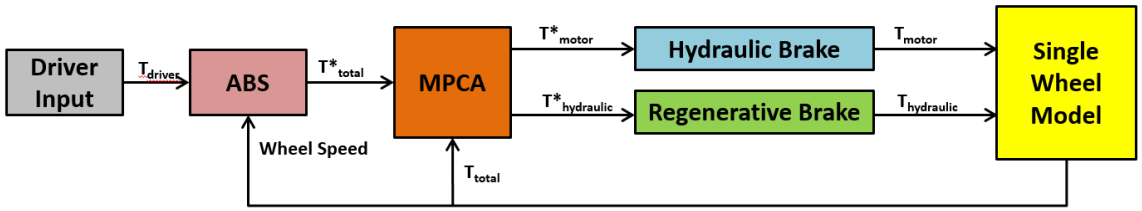

Figure 3.14: System configuration with single wheel model.

As discussed earlier in this chapter, this work has a total of 3 control systems: MPCA, ABS and the PMSM decoupled control. In order to demonstrate the tuning of the MPCA for the entire system, the tuning parameters of the other two control systems, i.e. the ABS and PMSM control, are kept constant throughout this exercise. In this work, as discussed in section 3.1, the performance of the MPCA depends on the selection of 2 parameters: the total torque tracking weight γ_b and the vibration damping weight γ_{sh}. Section 3.1.3 discussed about the effect of selecting these weights for a sample PRBS signal, while this section will discuss the effect of selecting these weights for the overall combined system. In order to demonstrate the tuning of the MPCA, two different cases are considered: firstly without considering any vibration control, and secondly, considering vibration control. These scenarios are discussed later in Chapter 4, and are defined as MPCA I for no vibration control, and MPCA II for with vibration control. The parameters of the single wheel model are given in Table 3.2, and are same as the ones used in Chapter 4

Table 3.2: Single wheel model Parameters

Parameter	Symbol	Value
Quarter Car Mass	M	498 kg
Wheel inertia	J_w	1kg-m^2
Tire rolling radius	R	0.32 m
Motor inertia	J_m	0.42 kg-m^2
Min./Max. Motor Torque	T_{rmin}/T_{rmax}	-630/+630 N-m
Min./Max. Hydraulic torque	T_{hmin}/T_{hmax}	0/3500 N-m

The initial vehicle speed is 100 kph, and the brake is applied at simulation time t=1sec. It is assumed that the engine is decoupled via a clutch during the braking scenario, and hence the effect of positive engine torque is neglected. The battery SoC is assumed to be less than its fully charged threshold, and hence the regenerative brake torque is available throughout the simulation. The five phase ABS reference slip deceleration and the deceleration thresholds are kept the same for all simulations, to have a fair comparison and are indicated in Table 3.3:

Table 3.3: ABS Tuning Parameters for single wheel model

Parameter	Value
λ^*	0.12
$\varepsilon 1$	10
$\varepsilon 2$	11
$\varepsilon 3$	9
$\varepsilon 4$	9
$\varepsilon 5$	10

The single wheel model is simulated for a tire-road friction coefficient (μ) of 0.9. In practice this may refer to a dry asphalt or dry concrete road surface. In the five phase ABS Logic, the reference wheel deceleration (a_x^*) for the high mu case (μ=0.9), is chosen as 8.82 m/s^2.

3.4.1 MPCA I (for tuning the value of γ_b)

This section describes the methodology of selecting the MPCA output weights for the system with no vibration control objective (MPCA I). Hence the main objective of the system is to closely track the total torque, thus closely tracking the reference slip, and hence decreasing the stopping distance. For this case the vibration damping objective described by gain γ_{sh} is given zero priority and hence this gain is set to zero. To demonstrate the effect of γ_b variation, three different cases with different values of γ_b are considered. In this exercise only the value of γ_b is varied, while the remaining parameters remain the same, as described in Table 3.4. Hence to summarize, the system, with initial conditions described in section 3.4 and the MPC parameters described in table 3.4 is simulated, and the results are obtained.

Table 3.4: MPCA parameters:

Parameter	Case 1	Case 2	Case 3
Sampling Time	0.01 sec		
Prediction Horizon	10		
Control Horizon	2		
Max/Min Hydraulic Brake	3500/0 N-m		
Max/Min Regen. Brake	±630 N-m		

γ_b	80000	100000	120000
γ_{sh}	0		

It can be observed in Figure 3.15 that as the value of γ_b is increased from cases 1 to3, the total torque response vary accordingly.

Table 3.5: Stopping distance summary for $\mu = 0.9$ case, single wheel

Stopping Distance(m)	Case 1	Case 2	Case 3
During ABS	38.86	37.95	39.57
Overall	50.61	49.77	51.32

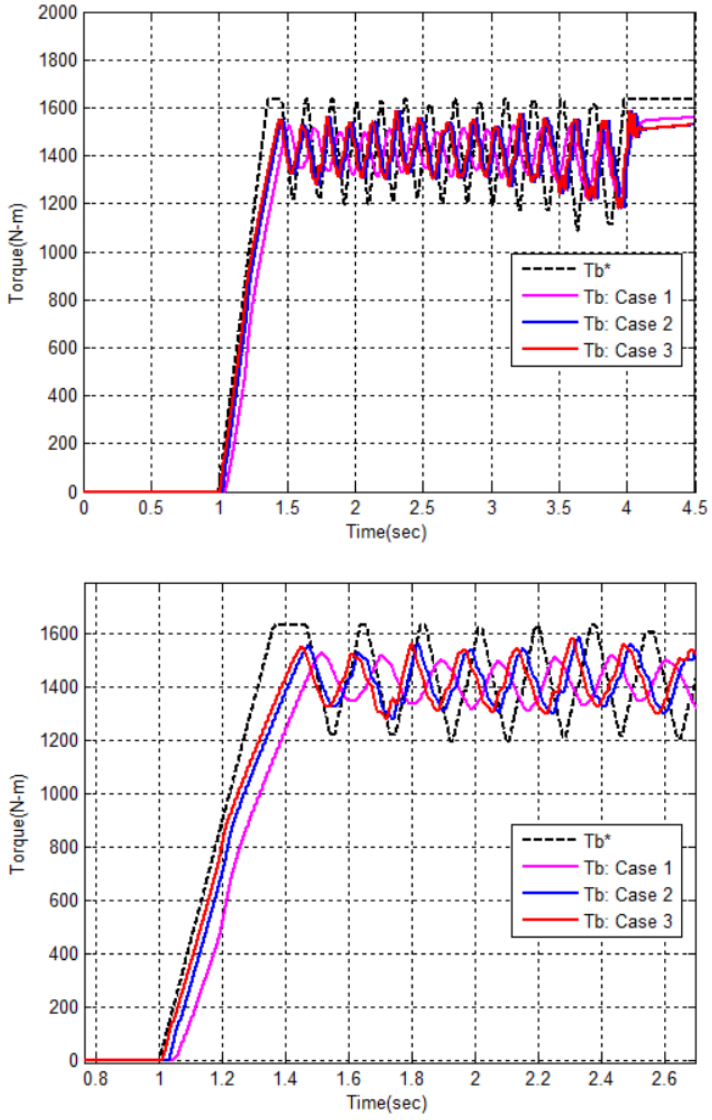

Figure 3.15: Total torque response for the 3 cases: (top) Entire Simulation and (bottom) Zoomed in view.

For case 2, as the weight is increased from case 1, the total torque tracking is better and faster, as compared to case 1. This can be expected, because as we increase the gain, more weight is given to the tracking the total torque. A similar trend is observed in Figures 3.16, 3.17 and 3.18, where the respective responses are delayed for case 1 as compared to case 2.

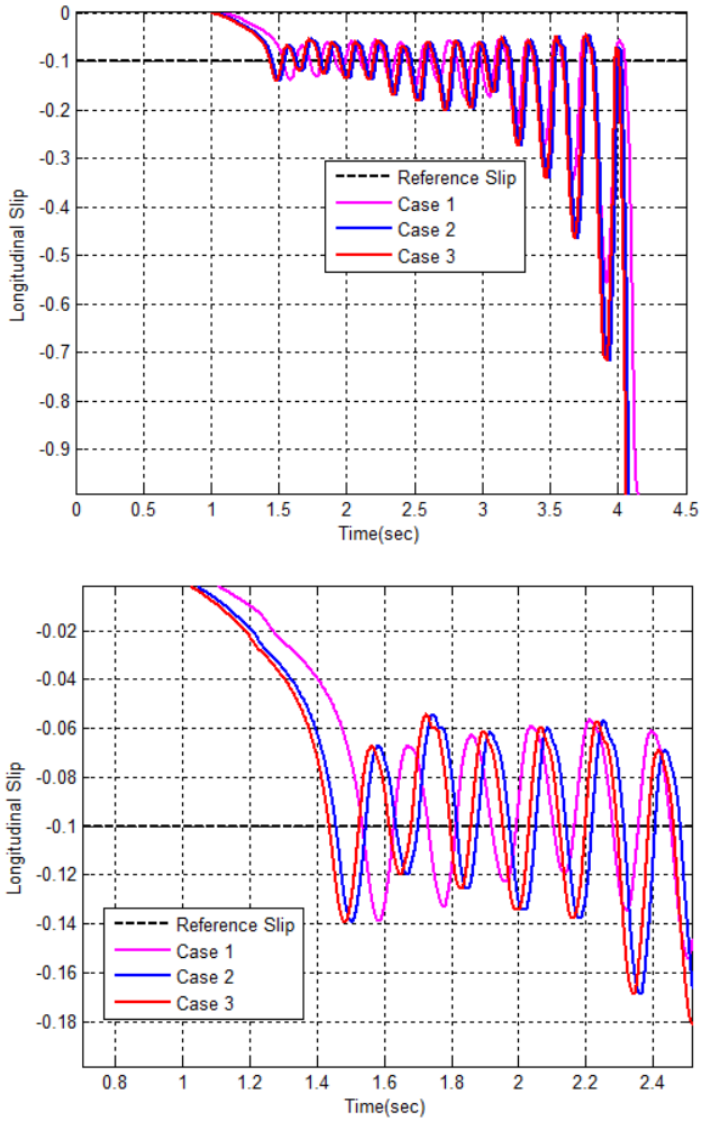

Figure 3.16: Longitudinal Slip response for the 3 cases: (top) Entire Simulation and (bottom) Zoomed in view.

Hence as we discuss the cases 1 and 2 of increasing the gain γ_b, it is important to establish a limit up to which one can increase the value of the gain. In order to demonstrate this, a case 3 was added with the gain set to 120000. For case 3, in Figure 3.16, it can be observed that the slip is more tightly controlled, as compared to cases 1 and 2, however, in the zoomed in plot between

interval 1.4 and 2.4 sec, the slip is controlled below the reference slip, implying non-optimal utilization of the tire traction which will further lead to a sub-optimal stopping distance performance, as indicated in Table 3.5.

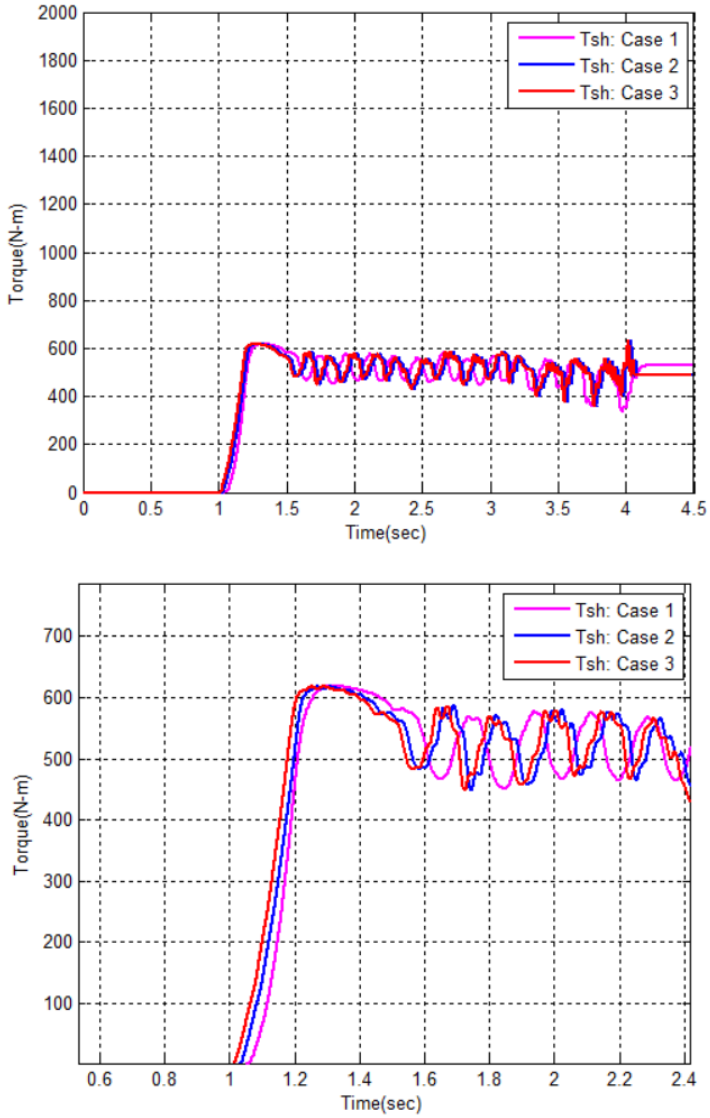

Figure 3.17: Shaft torque response for the 3 cases: (top) Entire Simulation and (bottom) Zoomed in view.

Figure 3.17 and 3.18 indicate the actuator torque for the 3 cases. As shown in Figure 3.17 and 3.18, the torque response for case 2 is quicker than cases 1 and 3, for both hydraulic as well as the shaft torques. The objective of this activity is to demonstrate the methodology for choosing the optimal γ_b. In order to achieve good stopping distance and torque tracking performance, one cannot choose the highest possible γ_b, as this value will affect the total torque tracking, which

will in turn affect ABS stopping distance. Hence when choosing the value of γ_b, one should also ensure that the ABS is operating around the value of optimal slip, as indicated by the comparison between cases 1, 2 and case 3.

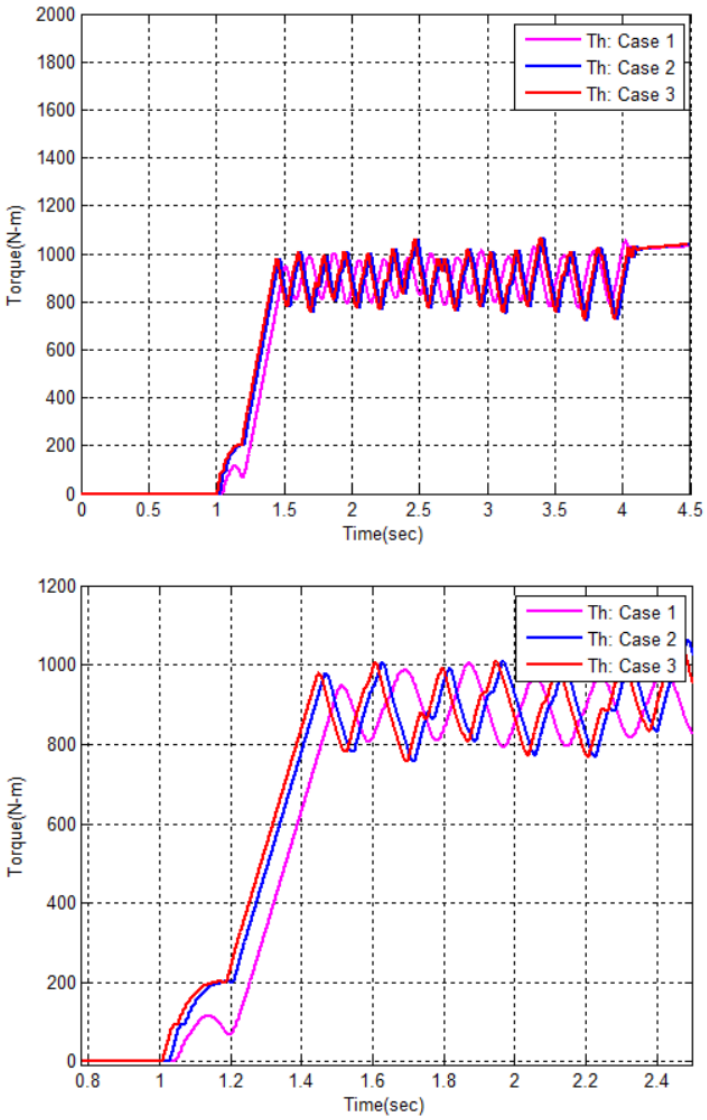

Figure 3.18: Hydraulic torque response for the 3 cases: (top) Entire Simulation and (bottom) Zoomed in view.

In this way the optimal value of γ_b, was selected. In this procedure, as mentioned before, only the torque tracking and stopping distance was considered, while maintaining all the ABS as well the MPC tuning parameters the same throughout.

3.4.2 MPCA II (for tuning the value of γ_{sh})

This section describes the methodology of selecting the MPCA output weights for the system with vibration control objective (MPCA II). Hence the main objective of the system is to minimize the peak to peak magnitude of the shaft angular deflection, as indicated by its Fast Fourier Transform (FFT), and while having a considerable decrease in the stopping distance. For this case the vibration damping objective described by gain γ_{sh} is given non-zero priority and hence this gain is set to non-zero. To demonstrate the effect of γ_{sh} variation, three different cases with different values of γ_{sh} are considered. In this exercise only the value of γ_{sh} is varied, while the remaining parameters remain the same, as described in Table 3.6. Hence to summarize, the system, with initial conditions described in section 3.4 and the MPC parameters described in table 3.4 is simulated, and the results are obtained. In all the simulations of this section, the value of γ_b is selected as the optimal value from the previous section.

Table 3.6: MPCA parameters:

Parameter	Case 1	Case 2	Case 3
Sampling Time	0.01 sec		
Prediction Horizon	10		
Control Horizon	2		
Max/Min Hydraulic Brake	3500/0 N-m		
Max/Min Regen. Brake	±630 N-m		
γ_b	100000		
γ_{sh}	100000	110000	130000

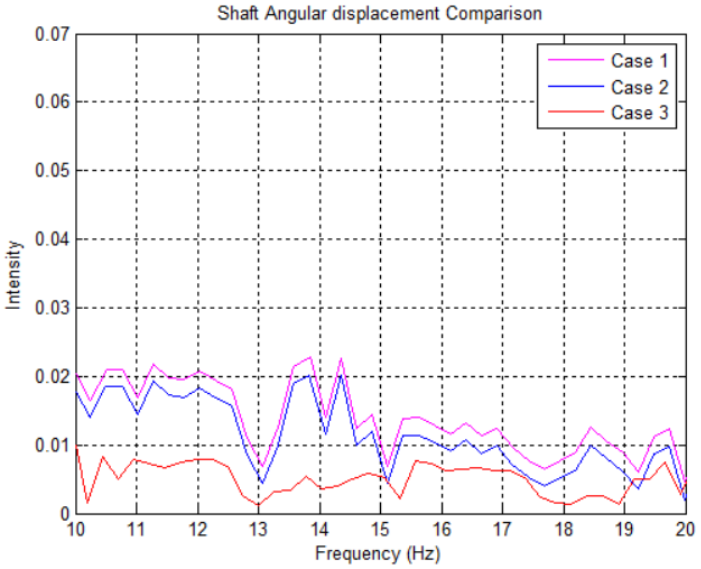

Figure 3.19: FFT of the Shaft angular displacement for the 3 cases

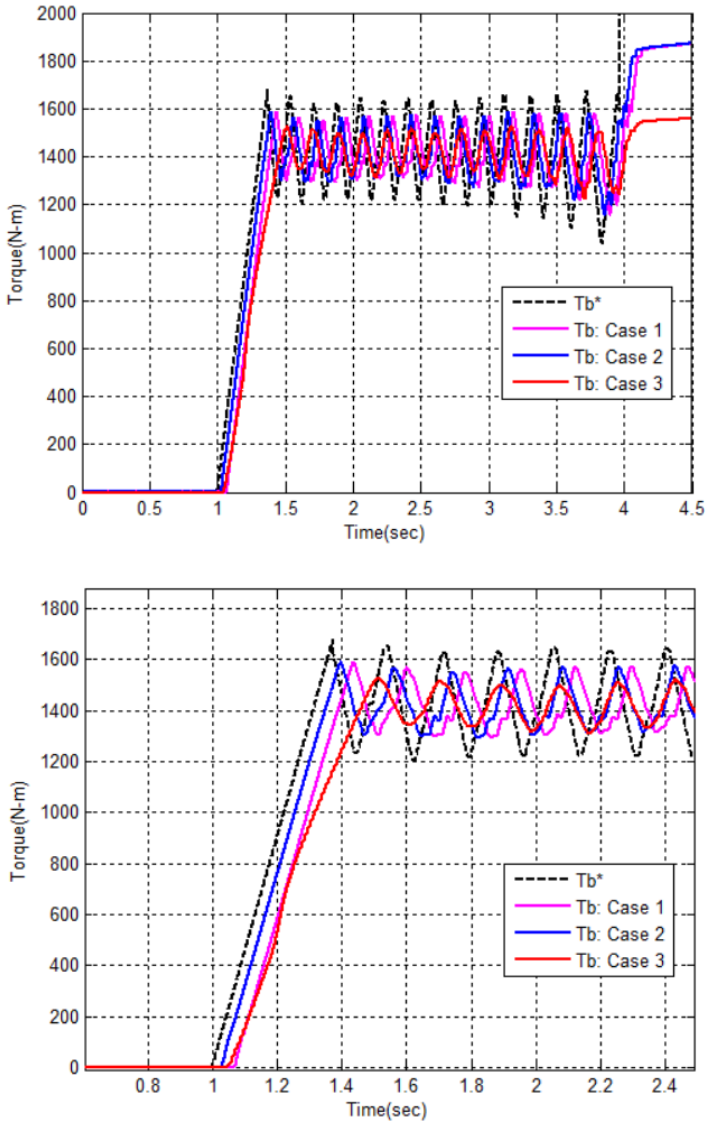

Figure 3.20: Total torque response for the 3 cases: (top) Entire Simulation and (bottom) Zoomed in view

Figure 3.19 indicates the FFT of the shaft angular displacement for the 3 cases. A general observation from the FFT is that as one proceeds from case one to case 3, the FFT decreases for each case. This makes perfect sense as the value of γ_{sh} is the least for case 1 and the most for case 3, implying that the vibration control gain is the most for case 3. Ideally one would select case 3 as the final optimal case as it gives the least intensity of vibration, but it is important to look at the other responses as well. As observed from the total torque response from Figure 3.20, it is observed that when the when the vibration control is the highest in case 3, the total torque response is heavily delayed.

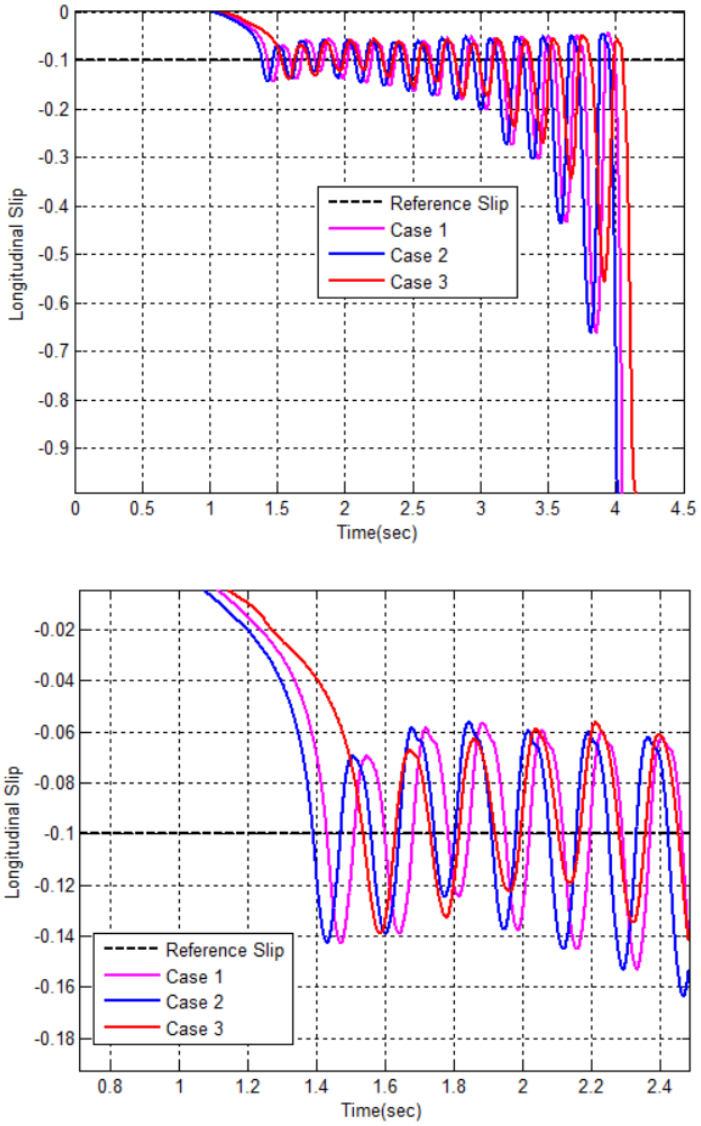

Figure 3.21: Longitudinal Slip response for the 3 cases: (top) Entire Simulation and (bottom) Zoomed in view.

Also in Figure 3.21, it further consolidates the observation in the previous Figure, that for case 3, the overall system performance is delayed, which results in delayed rise of the vehicle slip at 1.6 sec in Figure 3.21. This further affects the stopping distance performance of the system as expected, as shown in Table 3.7:

Table 3.7: Stopping distance summary for $\mu = 0.9$ case, single wheel

Stopping Distance(m)	Case 1	Case 2	Case 3
During ABS	38.91	38.42	40.06
Overall	50.43	49.94	51.58

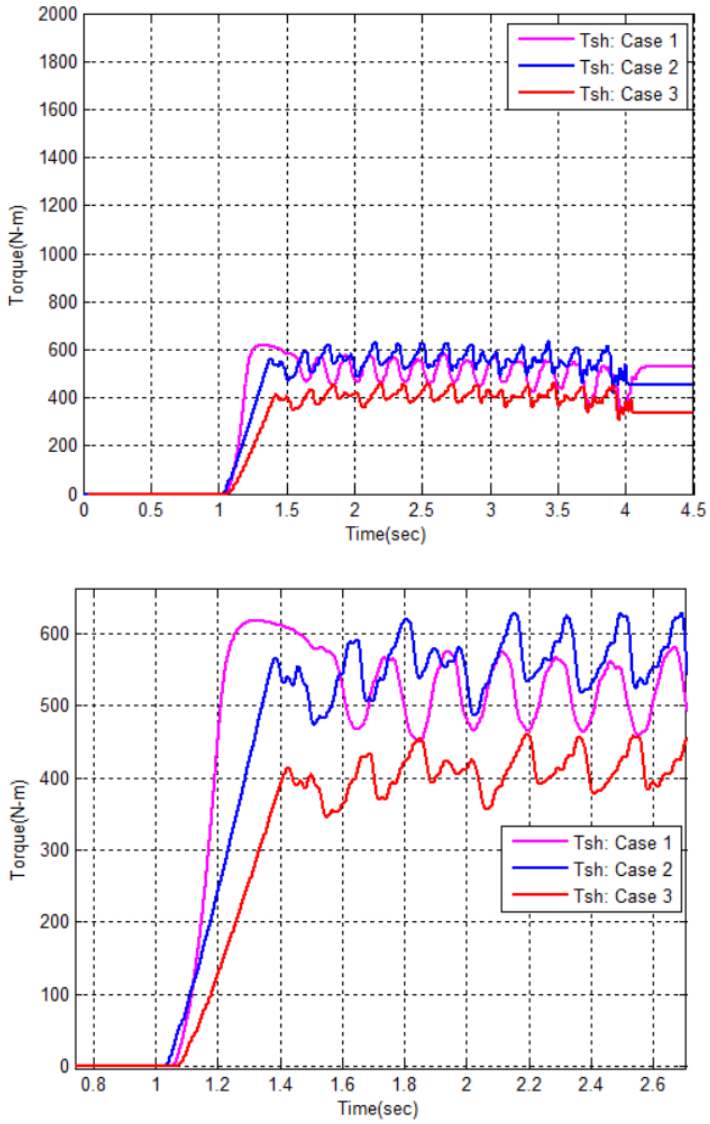

Figure 3.22: Shaft torque response for the 3 cases: (top) Entire Simulation and (bottom) Zoomed in view

Also, as expected from Figure 3.22, for case 3, due to 'excessive' vibration control gain, the torque allocation does not utilize the maximum motor torque, but is reduced in magnitude and delayed to dampen the vibrations. This results in a higher actuator torque to be supplied by the hydraulic brakes, which is observed in Figure 3.23. Hydraulic brakes then result in a slightly slower modulation, which further results in a slower overall performance.

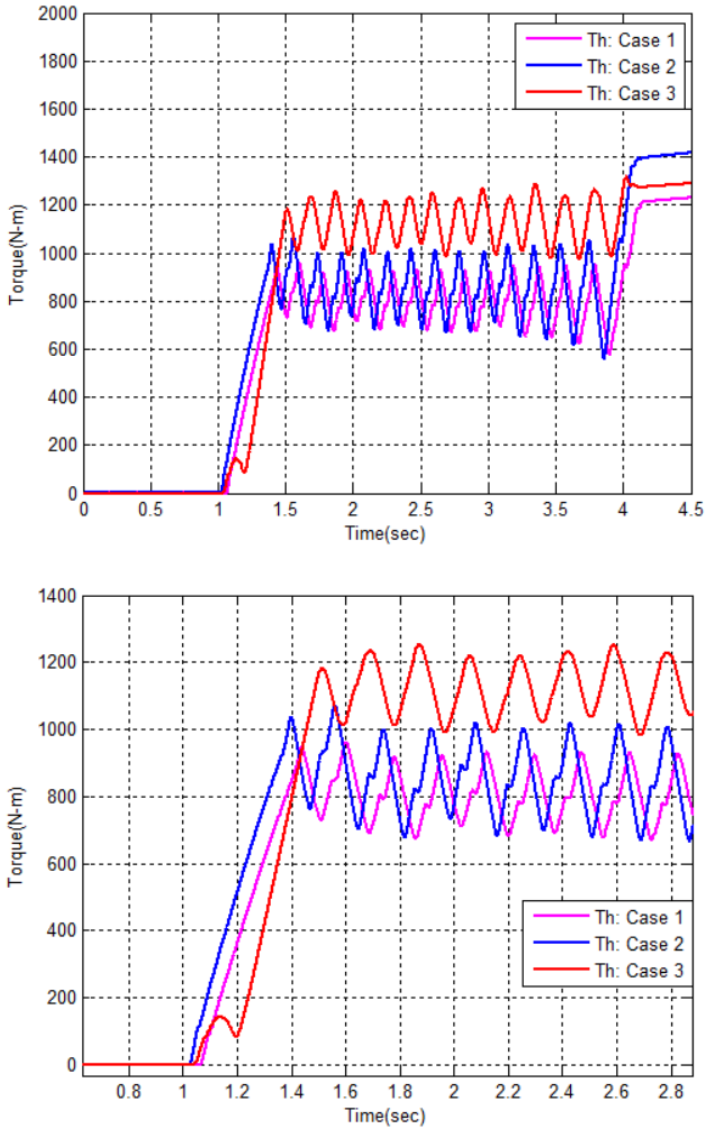

Figure 3.23: Total torque response for the 3 cases: (top) Entire Simulation and (bottom) Zoomed in view

Hence from Figures 3.19 to 3.23, it can be concluded that the optimum value of γsh will correspond to 110000, i.e. case 2, as it gives the least stopping distance and a good FFT result.

Hence to conclude the overall system tuning, the following steps were followed in order to tune the systems further discussed in Chapter 4 (applies to single wheel as well as Carsim configuration:

1. For a particular Road condition, tune the ABS for the Hydraulic only case, and obtain the five phase tuning parameters. Once these parameters are obtained, keep them constant for all the simulations for that particular road condition, in order to have a fair comparison.

2. Using the parameters obtained in step 1, follow the procedure described in section 3.4.1 to obtain the value of γ_b. for MPCA I case
3. Now using the value of γ_b obtained in step 2, follow the procedure discussed in section 3.4.2 to obtain the value of γ_{sh} for the MPCA II case.

3.5 CONCLUSION

This chapter discusses about the control strategies used in this research. The main contribution of this research is the MPCA strategy defined in section 3.1. This chapter discusses the MPC plant, cost function and tuning parameter development. The developed MPCA strategy is then tested with a PRBS signal, in order to show the effect of the tuning parameters on the controller performance. Then, the five phase ABS, and the PMSM control strategies are discussed. The five phase ABS and PMSM control strategy is validated with the published results, for similar conditions. Finally, the tuning procedure for the combined system performance is also discussed.

Chapter 4: Simulation Results and Discussion

The control strategy developed in the previous chapter is tested in this chapter, through simulation. In the previous chapter, the effectiveness of the proposed dual objective MPCA scheme is verified, by simulating it with a sample PRBS signal. In this chapter, the proposed MPCA scheme is further investigated by combining it with an ABS logic, actuator models and vehicle dynamics model. The schematic of the overall simulation model used in this work (explained in detail in chapter 2) is shown in Figure 4.1

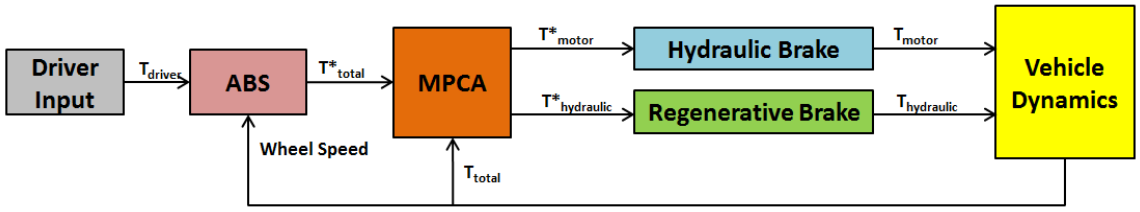

Figure 4.1: Simulation model schematic

In order evaluate the performance of proposed MPCA strategy, two performance metrics are used: vehicle stopping distance, and shaft vibration intensity. The vibration intensity is determined by calculating the Fast Fourier Transform (FFT) of the shaft angular displacement signal. Also, the stopping distance is represented in two different ways: firstly, "During ABS" i.e. the stopping distance from the point where ABS is activated, to when instant it is switched off, and the "Overall" stopping distance, measured from the instant the Brake is applied, to the instant when the vehicle comes to a halt (velocity = 0). This enables us to measure the stopping distance during ABS, thus neglecting the end-effects when the wheel speed reaches zero, and the wheel locks. Two MPCA strategies are considered in this work: ABS with regenerative brake

boost, without considering vibration damping objective (hereafter referred to as MPCA I) and ABS with regenerative brake

boost with added vibration damping objective (hereafter referred to as MPCA II). As discussed in chapter 3, for MPCA I, the vibration damping gain γ_{sh} is set to zero, with a non-zero γ_b, and for MPCA II the vibration control gain γ_{sh} is tuned with respect to γ_b. The parameters used in the MPCA block are indicated in Table 4.1.

Table 4.1: MPCA parameters:

Parameter	Symbol	Value
Sampling Time	T_s	0.01 sec
Prediction Horizon	N_p	10
Control Horizon	N_c	2
Max/Min Hydraulic Brake	T_{hmax}/T_{hmin}	3500/0 N-m
Max/Min Regenerative Brake	T_{rmax}/T_{rmin}	-630/+630 N-m

In this work, a front wheel driven hybrid electric vehicle is used for simulation study. Hence the MPCA is applied to the front wheel ABS only. In a Carsim vehicle model, the improvement in stopping distance will be a function of the ABS modulation at all the four wheels. Hence two different sets of simulations are considered: firstly with a single wheel model and then with a full vehicle model in Carsim software. The simulation with a single wheel model allows us to directly compare the stopping distances at one particular wheel. This study is then extended for a full Carsim vehicle model, to show its application in more realistic situations. In order to test the robustness of the proposed scheme over a range of operating conditions, three test scenarios are considered:

1. High Mu test: Tire-Road friction coefficient of 0.9.
2. Mid Mu test: Tire-Road friction coefficient of 0.5.
3. Low Mu Test: Tire-Road Friction coefficient of 0.2.

The corresponding tire-force vs. slip plot for different road conditions is shown in Figure 4.2

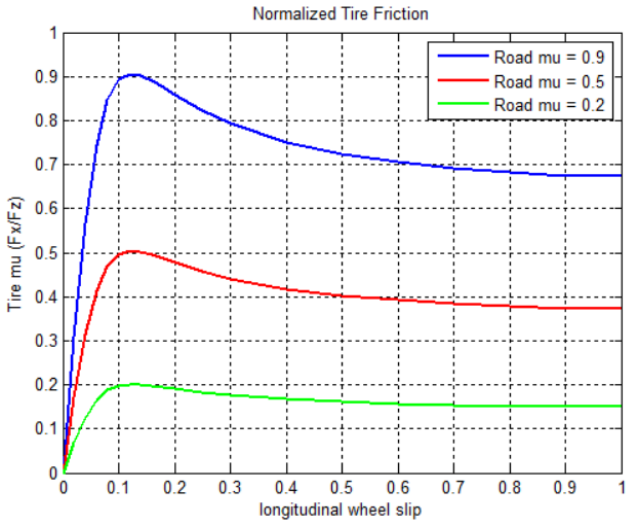

Figure 4.2: Tire friction (Normalized Tire Force) coefficient vs. slip plot

4.1 SINGLE WHEEL MODEL

A single wheel model with shaft dynamics defined in chapter 2, is used in this simulation. The simulation configuration for this case is indicated in Figure 4.3.

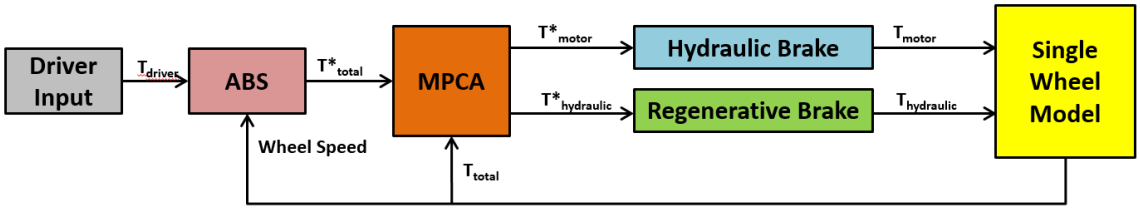

Figure 4.3: Simulation model Schematic for Single wheel model simulations

The parameters of the single wheel model are given in Table 4.2:

Table 4.2: Single wheel model Parameters

Parameter	Symbol	Value
Quarter Car Mass	M	498 kg
Wheel inertia	J_w	1kg-m^2
Tire rolling radius	R	0.32 m
Motor inertia	J_m	0.42 kg-m^2
Min./Max. Motor Torque	T_{rmin}/T_{rmax}	-630/+630 N-m
Min./Max. Hydraulic torque	T_{hmin}/T_{hmax}	0/3500 N-m

The initial vehicle speed is 100 kph, and the brake is applied at simulation time t=1sec. It is assumed that the engine is decoupled via a clutch during the braking scenario, and hence the effect of positive engine torque is neglected. The battery SoC is assumed to be less than its fully charged threshold, and hence the regenerative brake torque is available throughout the simulation. The five phase ABS reference slip deceleration and the deceleration thresholds are kept the same for all simulations, to have a fair comparison and are indicated in Table 4.3:

Table 4.3: ABS Tuning Parameters for single wheel model

Parameter	Value
λ^*	0.12
$\varepsilon 1$	10
$\varepsilon 2$	11
$\varepsilon 3$	9
$\varepsilon 4$	9
$\varepsilon 5$	10

4.1.1 High μ Test (μ=0.9)

The single wheel model is simulated as per the simulation conditions described in section 4.1, for a tire-road friction coefficient (μ) of 0.9. In practice this may refer to a dry asphalt or dry concrete road surface. In the five phase ABS Logic, the reference wheel deceleration (a_x^*) for the high mu case (μ=0.9), is chosen as 8.82 m/s^2.

The comparison of longitudinal slip in this case is indicated in Figure 4.4. It can be observed that the ABS cycling, i.e. slip tracking is only slightly faster for the MPCA I and II cases, as compared to the hydraulic only case. This is mainly because of using electric motor as an actuator during ABS cycling. The inclusion of the electric motor as an additional actuator, effectively extends the bandwidth of the system, and results in relatively faster slip tracking. In Figure 4.5, it can be observed that the range in which the limit cycle operates for the 3 cases is the same.

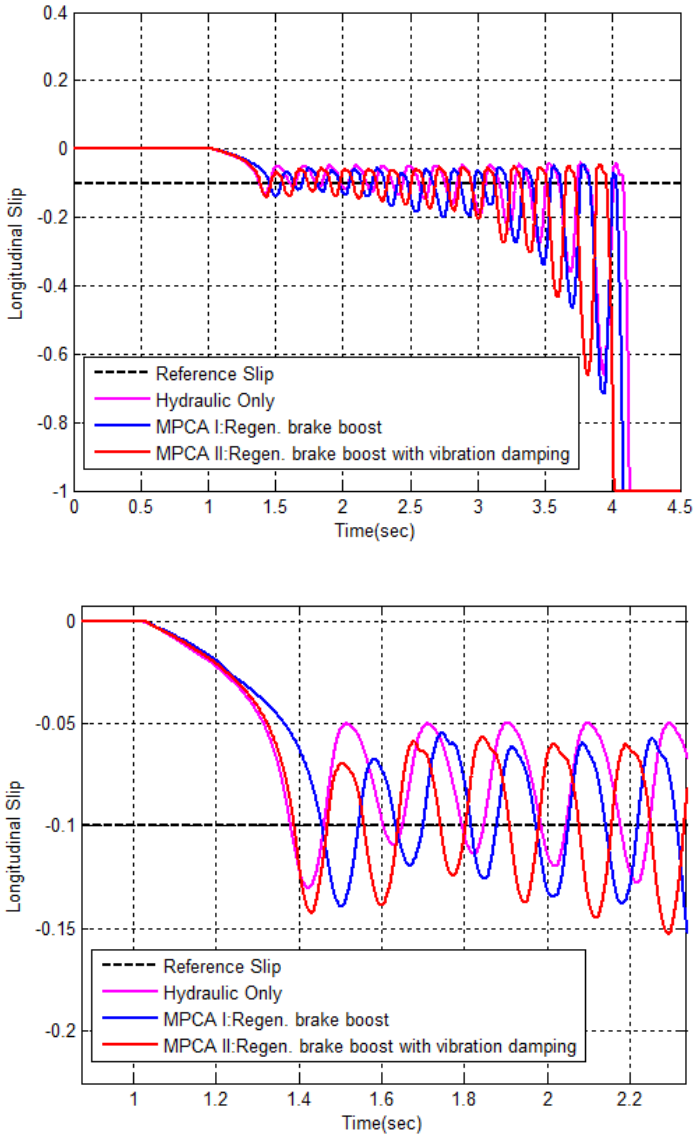

Figure 4.4: Comparison of the vehicle longitudinal slip for the 3 strategies for μ = 0.9 road surface: (top) entire simulation, and (bottom) Zoomed in view.

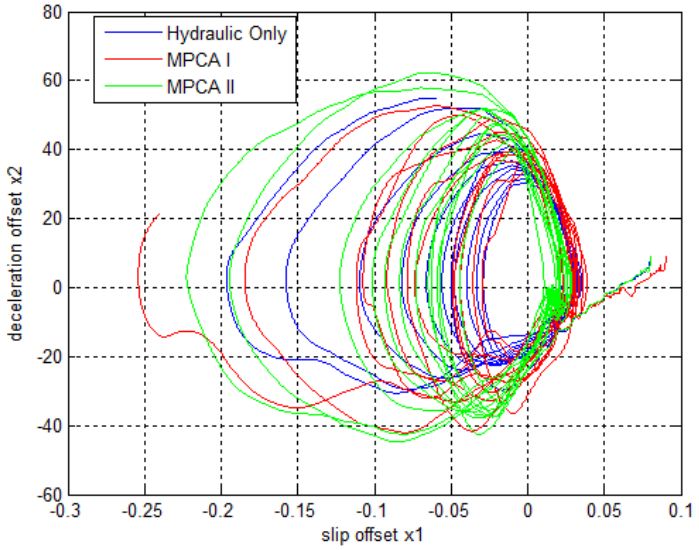

Figure 4.5: Comparison of the ABS limit cycles for the 3 strategies μ = 0.9 road surface.

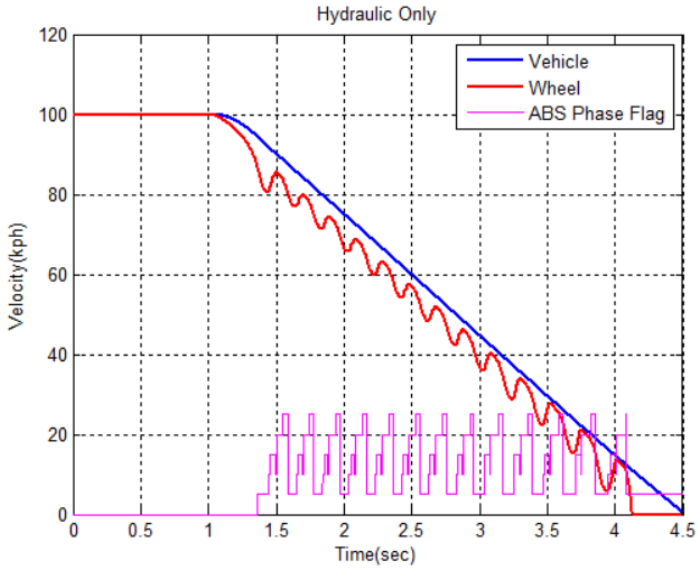

Figure 4.6: Vehicle and wheel velocities, and ABS Phase Flag for the hydraulic ABS only case for μ = 0.9 road surface

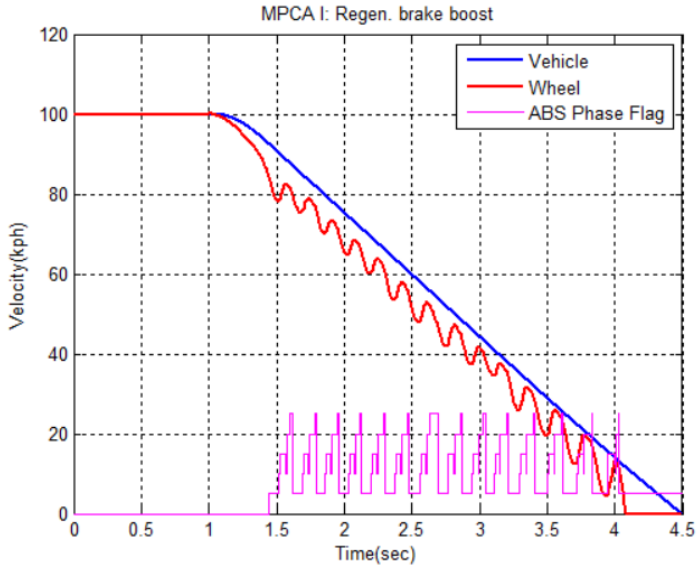

Figure 4.7: Vehicle and wheel velocities, and ABS Phase Flag for the MPCA I case for μ = 0.9 road surface

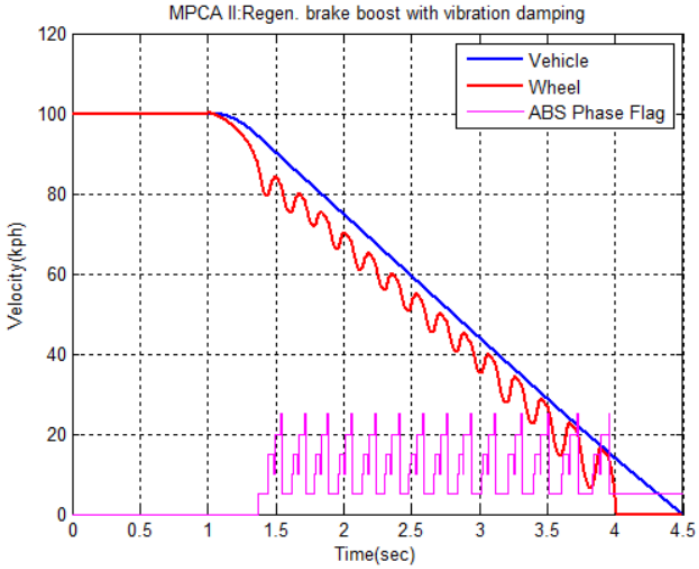

Figure 4.8: Vehicle and wheel velocities, and ABS Phase Flag for the MPCA II case for μ = 0.9 road surface.

Figures 4.6, 4.7, and 4.8 show the vehicle and wheel velocity responses for the 3 cases. It can be observed from the figures that at t=1sec, when the brakes are applied, the vehicle velocity response starts to decrease, as expected. The wheel velocity response starts to "cycle" as per the brake torque applied at the wheel. These are the typical responses one would expect, when the ABS is in action. It can further be observed from the plots that the wheel velocity starts to

"cycle" around 1.4sec for all the 3 cases. This is the time at which the wheel slip first crosses the reference wheel slip, as can be confirmed from Figure 4.4. The ABS phase flag indicates the cycling of the ABS control, and also confirms the ABS cycling starting at 1.4sec. Also, the ABS is set to de-activate as the vehicle velocity falls below 10 kph in simulation, and can also be observed from the figures 4.4, 4.6, 4.7 and 4.8.

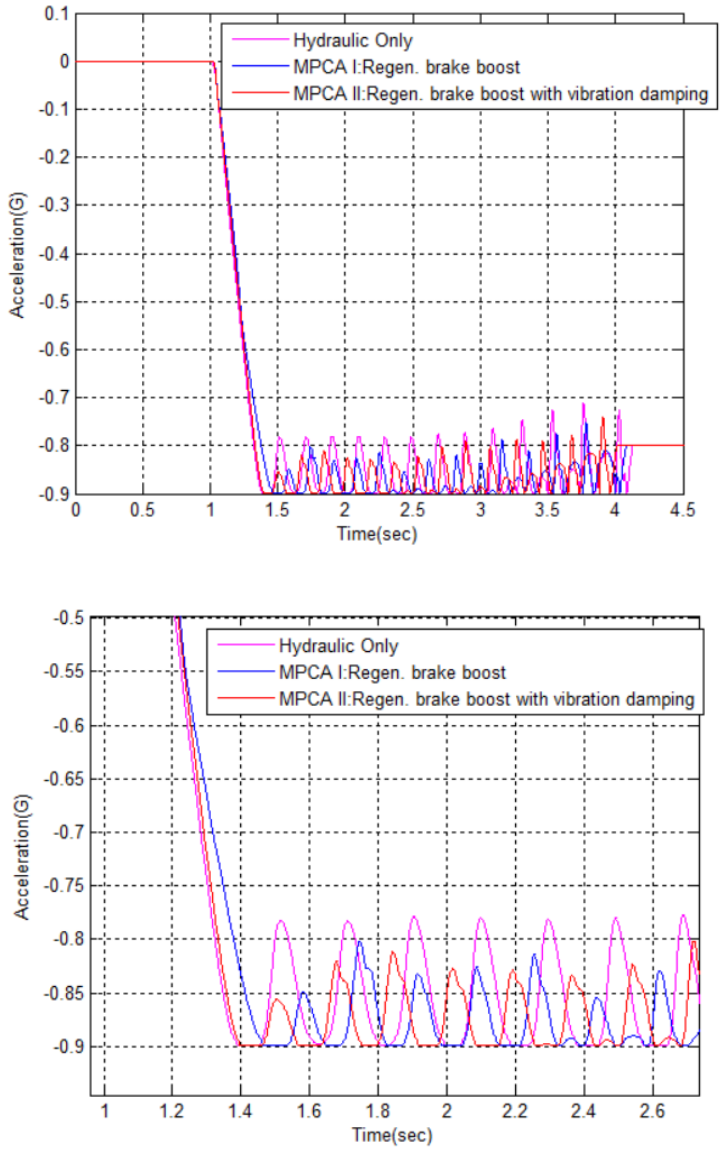

Figure 4.9: Comparison of the vehicle deceleration for the 3 strategies for μ = 0.9 road surface, for a single wheel model (top) Full simulation and (bottom) Zoomed in view.

Figure 4.9 indicates the vehicle deceleration response for the 3 strategies. This plot further consolidates the conclusion for Figure 4.4. It can be observed that the vehicle deceleration for

MPCA I and II cases is more “concentrated” towards larger deceleration. This is mainly due to the faster overall ABS cycling and tighter slip control offered by the MPCA I and II cases.

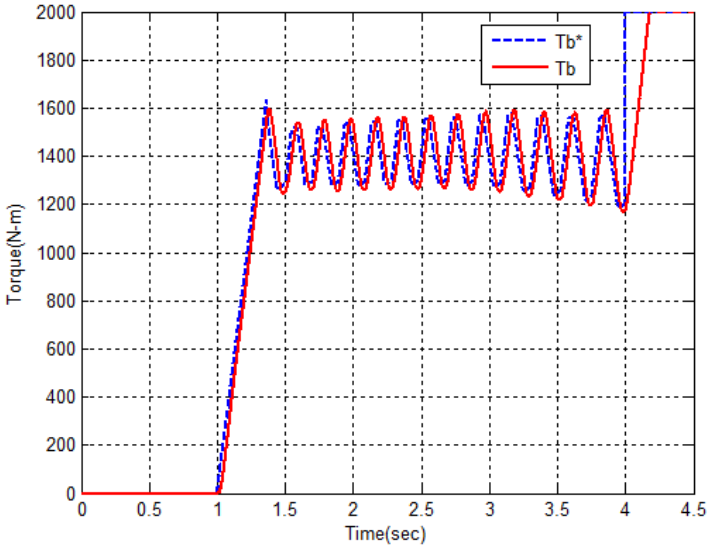

Figure 4.10: Comparison of Brake Torques for the hydraulic ABS only case for μ = 0.9 road surface

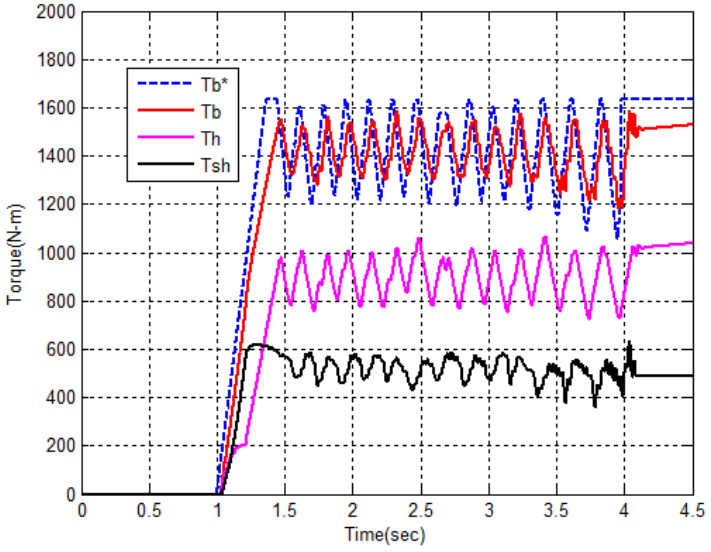

(a)

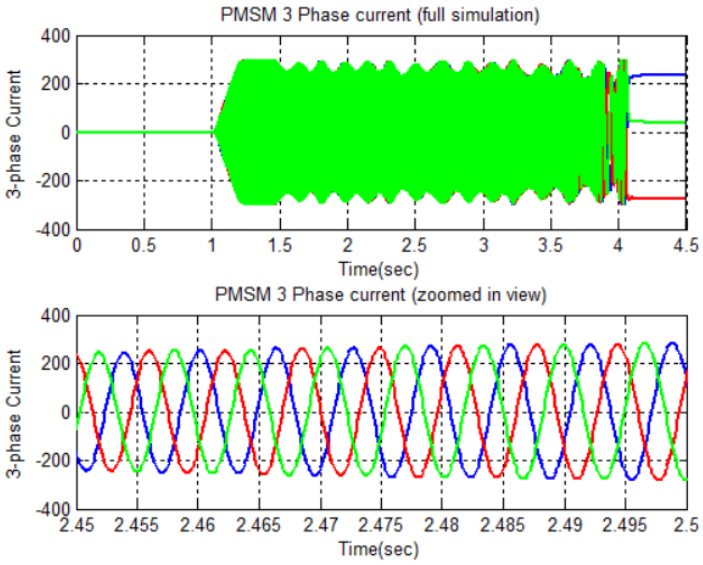

(b)

Figure 4.11: (a) Comparison of Brake Torques and (b) PMSM 3 Phase Current; for the MPCA I case for μ = 0.9 road surface

Figures 4.10, 4.11(a), and 4.12(a) indicate the various actuator torques observed in the simulation for μ = 0.9 road condition. Firstly, it can be observed that the total actual torque in all the 3 cases, operate in the same torque range (1400~1500 N-m), which imply that the 3 cases are indeed comparable. It can be observed that the total ABS torque modulates slightly faster for the MPCA I and II cases than the hydraulic only case. This is again because of the electric motor extending the bandwidth of the system. The modulation is however, only slightly faster as the addition of shaft dynamics also adds a delay to the regenerative brake torque applied to the wheel. The shaft dynamics delay, however, does not affect the hydraulic only case, as the hydraulic torque is applied directly at the wheel, and not via the half shaft. Figures 4.11(b) and 4.12(b) indicate the respective 3-phase motor current, which correspond to the Motor (shaft) torque indicated in Figures 4.11(a) and 4.12(a). A general and expected observation from these is that the envelope of the motor current matches that of the Motor torque, in the time scale. In Figure 4.11(a), the motor torque rises to the maximum (600Nm) from 0, at around 1.25 sec, the motor current in Figure 4.11(b) also rises from the 0 to the maximum in the same time. Also in Figure 4.11(a), the motor stops modulating at around 4.1 sec, so does the motor current in Figure 4.11(b). This trend can also be observed for the MPCA II case in Figures 4.12 (a) and (b)

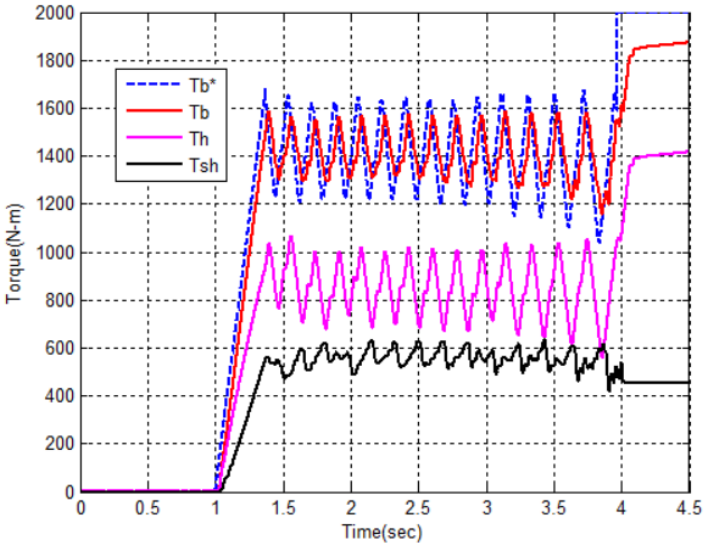

(a)

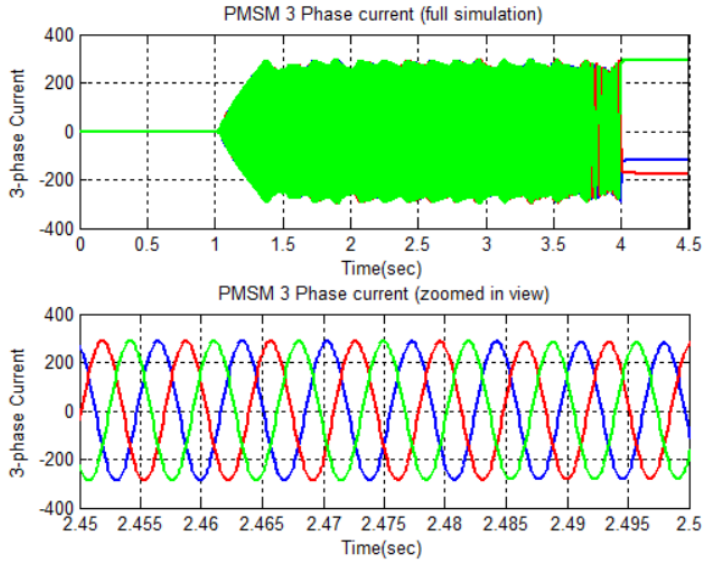

(b)

Figure 4.12: (a) Comparison of Brake Torques and (b) PMSM 3 Phase Current; for the MPCA II case for $\mu = 0.9$ road surface

Figure 4.11(a) shows the brake torques during the ABS operation with MPCA I, where T_b* indicates the demanded brake torque and T_b represents total applied brake torque (sum of the hydraulic brake torque, T_h, and the electric motor torque, T_{sh}. As shown in Figure 4.11(a), MPCA I effectively allocates the demanded torque based on the bandwidth, in which the electric motor is allocated the high-frequency part of the torque signal and the hydraulic brakes are

allocated the low-frequency part of the torque signal. In this case, the control effort is focused on tracking the demanded brake torque (T_b*) with the torque split without considering shaft vibration reduction. The MPC tuning parameters used in this case are: γ_b is set to 100000 and γ_{sh} is set to zero.

Figure 4.12(a) compares the brake torques during ABS operation with MPCA II. The torque split is not as effective compared to the earlier case since it also considers vibration control. A non-zero-value of γ_{sh} (110000) has been used in the cost function of the MPCA. With that, the hydraulic brakes modulate almost in phase with the regenerative brakes to reduce the shaft vibration, as shown in Figure 4.13. Although it vastly improves the shaft vibration damping, the frequency-based torque split performance has been degraded, and the motor torque is slightly delayed at the start of the simulation.

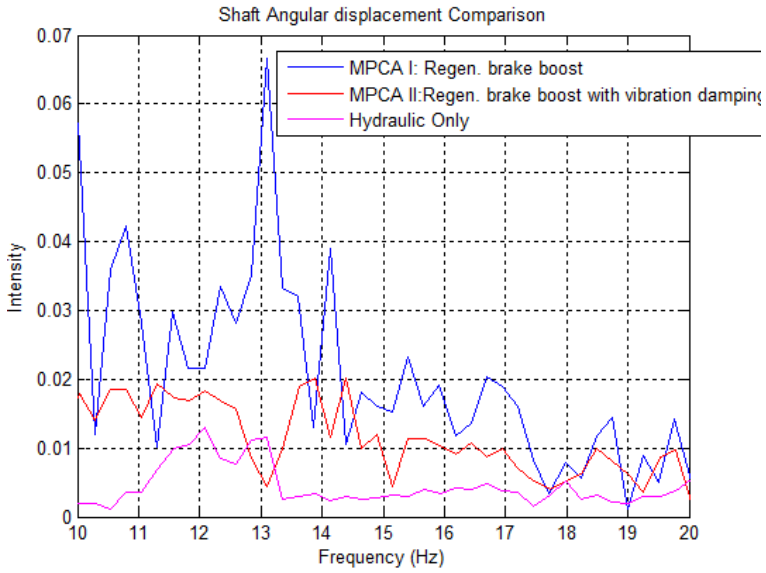

Figure 4.13: Comparison of the FFT of the shaft angular displacement for $\mu = 0.9$ road surface.

It can be observed that the peak to peak vibrations at the natural frequency of the shaft (around 13 Hz) is reduced in the case of MPCA II. Hence to summarize, the tuning parameters used in the MPCA II case are: γb is set to 100000, and γsh is set to 110000.

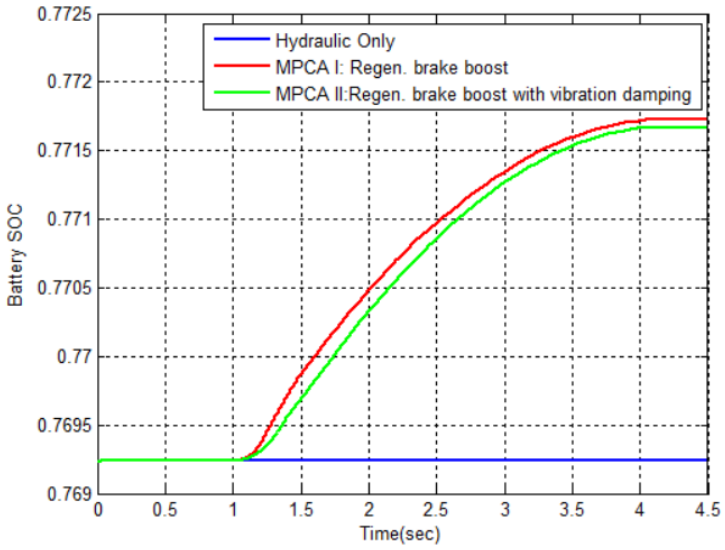

Figure 4.14: Comparison of the Battery SOC Response for μ = 0.9 road surface simulation, for single wheel model.

Table 4.4: Stopping distance summary for μ = 0.9 case, single wheel

Stopping Distance(m)	Hydraulic Only	MPCA I	MPCA II
During ABS	39.02	37.95	38.42
Overall	50.97	49.77	49.94

The effectiveness of the combined braking strategies over hydraulic strategies can be observed from the stopping distance comparison in Table 4.4. It is observed that due to faster torque modulation in the combined braking torques observed in figures 4.11 and 4.12, as compared to hydraulic only case in Figure 4.10. This leads to slightly faster slip control in Figure 4.4, which further leads to an improvement in stopping distance. Figure 4.14 indicates the comparison of the Battery SoC for the 3 strategies. It is observed that as expected, there is no energy recovered in the Hydraulic only case, while some amount of energy is recovered in the MPCA-I and II cases. This is hence a secondary advantage of implementing MPCA. However, one can argue that energy recovery cannot be a primary objective in the case of emergency braking for two reasons: first, this being a safety-critical control, one must prioritize safety instead of recovered energy, and second: one does not encounter emergency braking situations more often, in order to rely on ABS for energy recovery.

4.1.2 Mid μ Test (μ=0.5)

The Single wheel model is simulated as per the simulation conditions described in section 4.1, for a tire-road friction coefficient (μ) of 0.5. In practice this may refer to a dry packed gravel

road. In the five phase ABS Logic, the reference wheel deceleration (a_x*) for the mid mu case (μ=0.5), is chosen as 4.905 m/s^2.

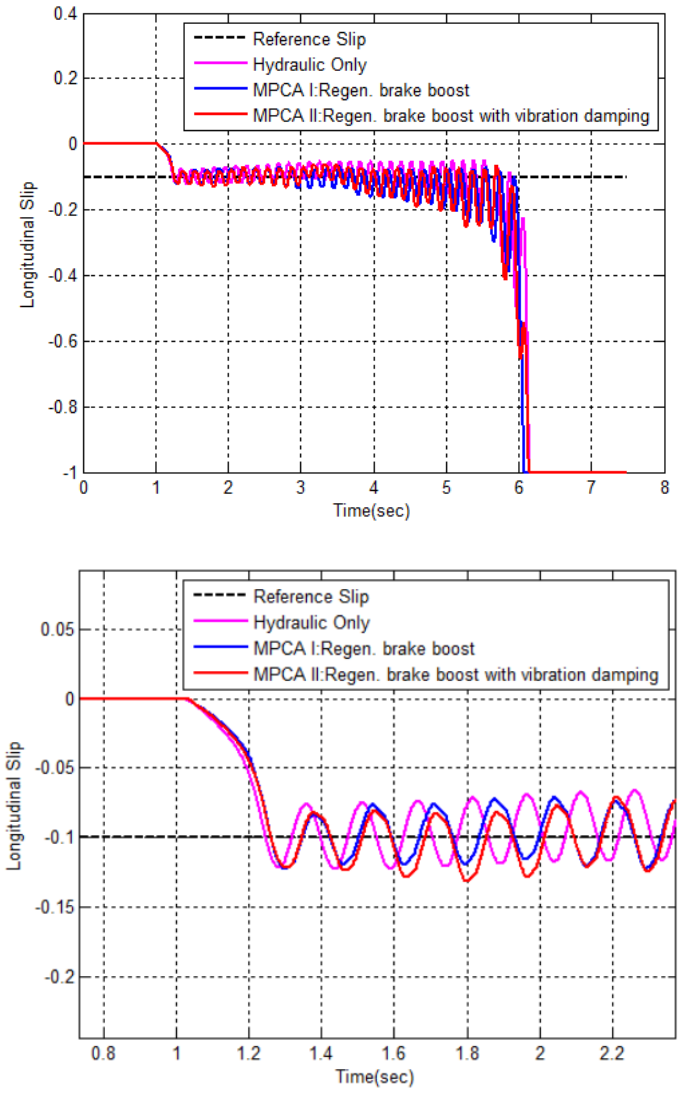

Figure 4.15: Comparison of the vehicle longitudinal slip for the 3 strategies for μ = 0.5 road surface: (top) entire simulation, and (bottom) Zoomed in view.

The comparison of longitudinal slip in this case is indicated in Figure 4.15. It can be observed that the ABS cycling, i.e. slip tracking is slightly faster for the MPCA I and II cases, as compared to the hydraulic only case. This is mainly because of using electric motor as an actuator during ABS cycling.

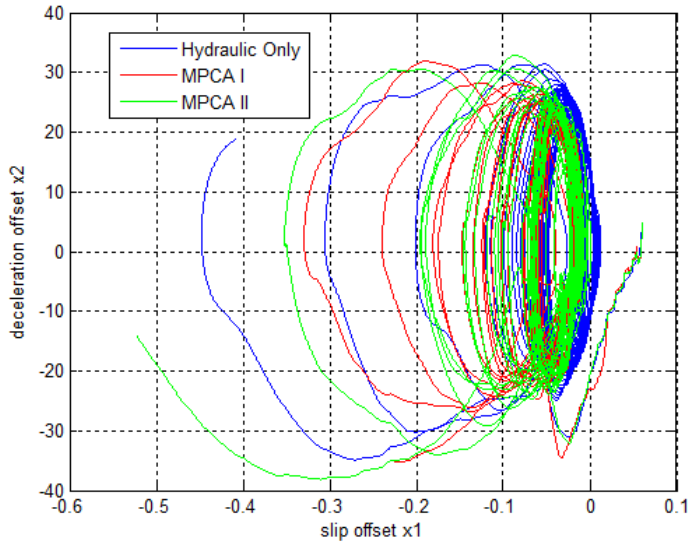

Figure 4.16: Comparison of the ABS limit cycles for the 3 strategies for μ = 0.5 road surface.

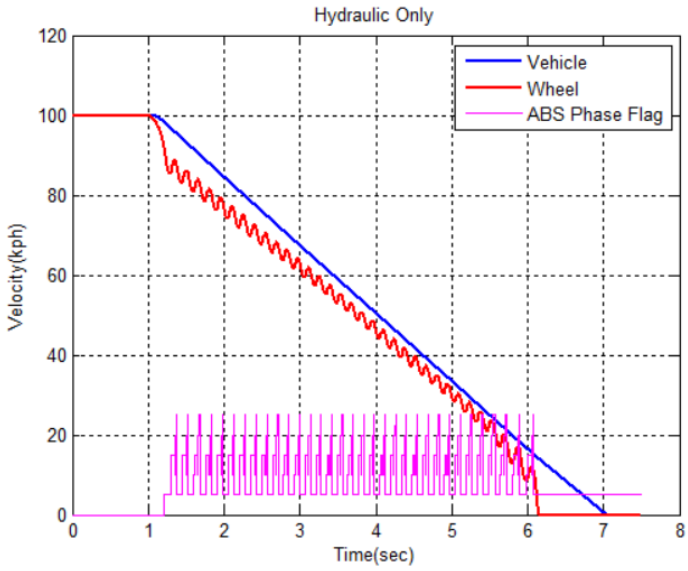

Figure 4.17: Vehicle and wheel velocities, and ABS phase flag for the hydraulic ABS only case for μ = 0.5 road surface

The inclusion of the electric motor as an additional actuator, effectively extends the bandwidth of the system, and results in relatively faster slip tracking. In Figure 4.16, it can be observed that the range in which the limit cycle operates for the 3 cases is the same.

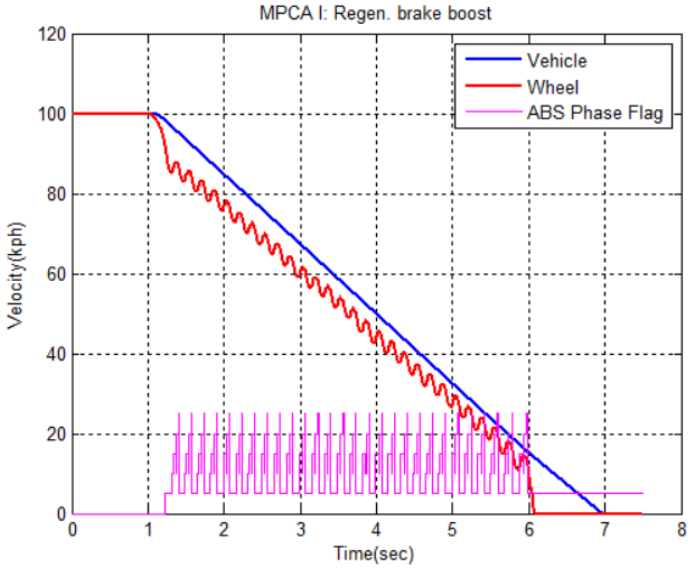

Figure 4.18: Vehicle and wheel velocities, and ABS phase flag for the MPCA I case for μ = 0.5 road surface

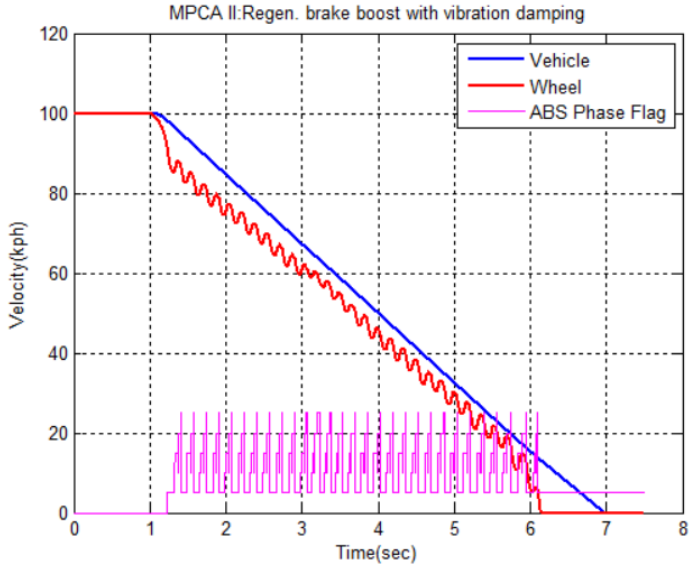

Figure 4.19: Vehicle and wheel velocities, and ABS phase flag for the MPCA II case for μ = 0.5 road surface

Figures 4.17, 4.18, and 4.19 show the vehicle and wheel velocity responses for the 3 cases. It can be observed from the figures that at t=1sec, when the brakes are applied, the vehicle velocity response starts to decrease, as expected. The wheel velocity response starts to "cycle" as per the brake torque applied at the wheel. These are the typical responses one would expect, when the ABS is in action. It can further be observed from the plots that the wheel velocity starts to "cycle" around 1.3sec for all the 3 cases. This is the time at which the wheel slip first crosses the

reference wheel slip, as can be confirmed from Figure 4.15 The ABS phase flag indicates the cycling of the ABS control, and also confirms the ABS cycling starting at 1.3sec Also, the ABS is set to de-activate as the vehicle velocity falls below 10 kph in simulation, and can also be observed from the figures 4.15, 4.17, 4.18 and 4.19.

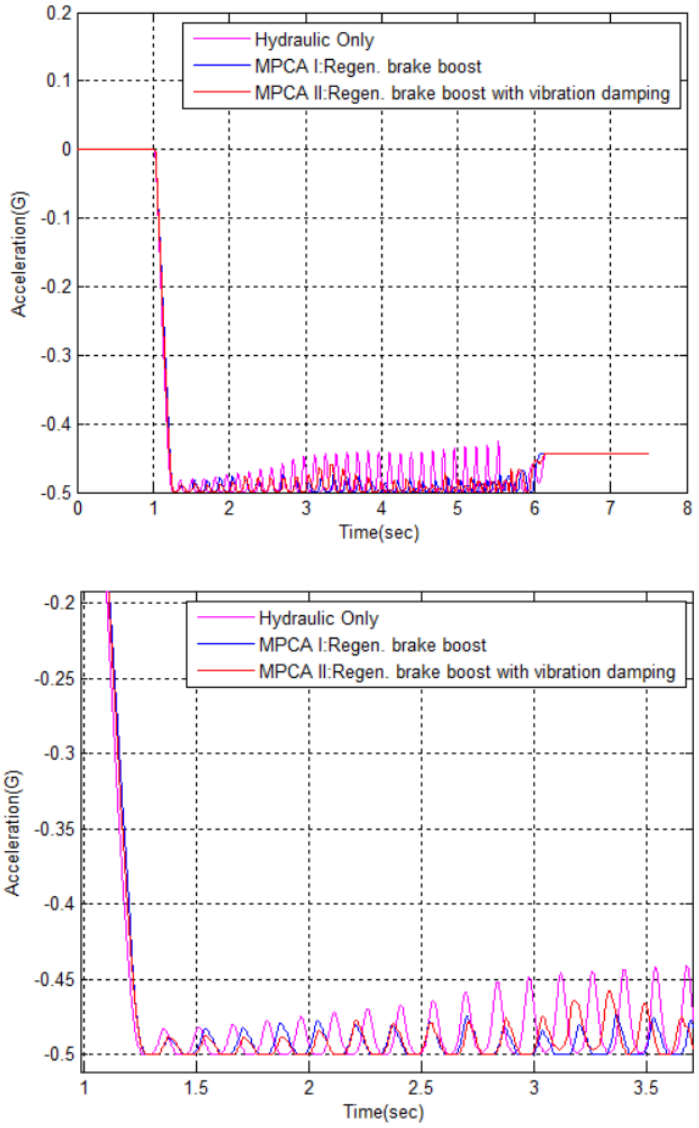

Figure 4.20: Comparison of the vehicle deceleration for the 3 strategies for μ = 0.5 road surface, for a single wheel model: (Top) entire simulation, and (Bottom) Zoomed in view

Figure 4.20 indicates the vehicle deceleration response for the 3 strategies. This plot further consolidates the conclusion for Figure 4.15. It can be observed that the vehicle deceleration for MPCA I and II cases is more "concentrated" towards larger deceleration. This is mainly due to the faster overall ABS cycling and tighter slip control offered by the MPCA I and II cases.

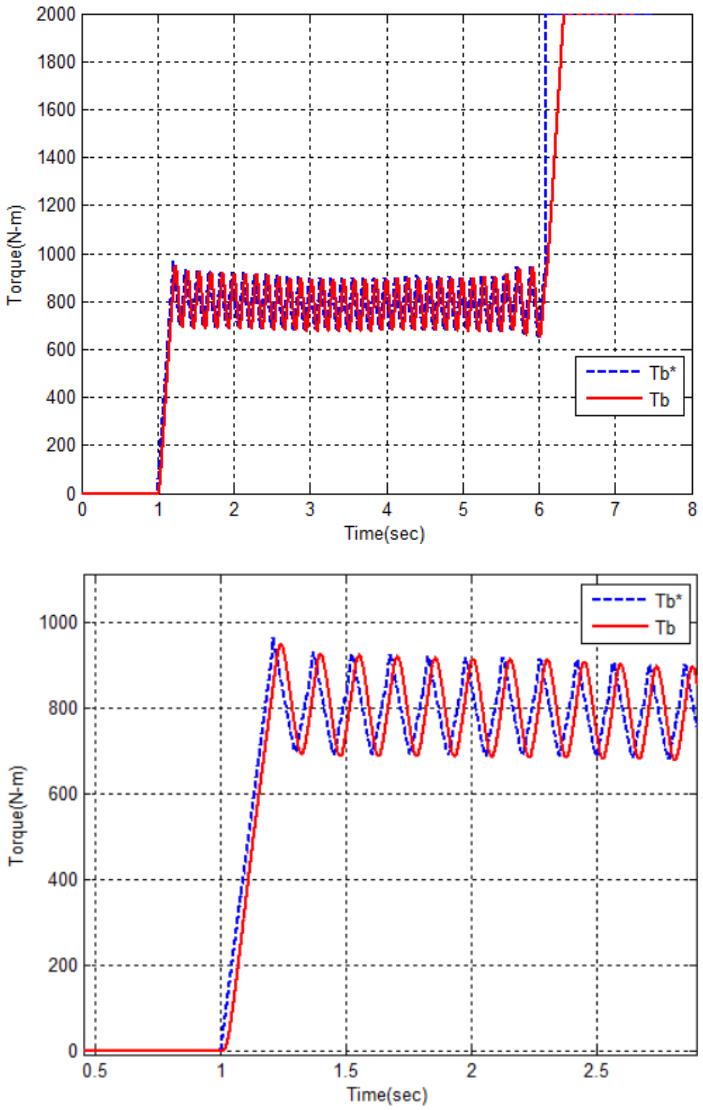

Figure 4.21: Comparison of Brake Torques for the hydraulic ABS only case for μ = 0.5 road surface: (Top) entire simulation, and (Bottom) Zoomed in view

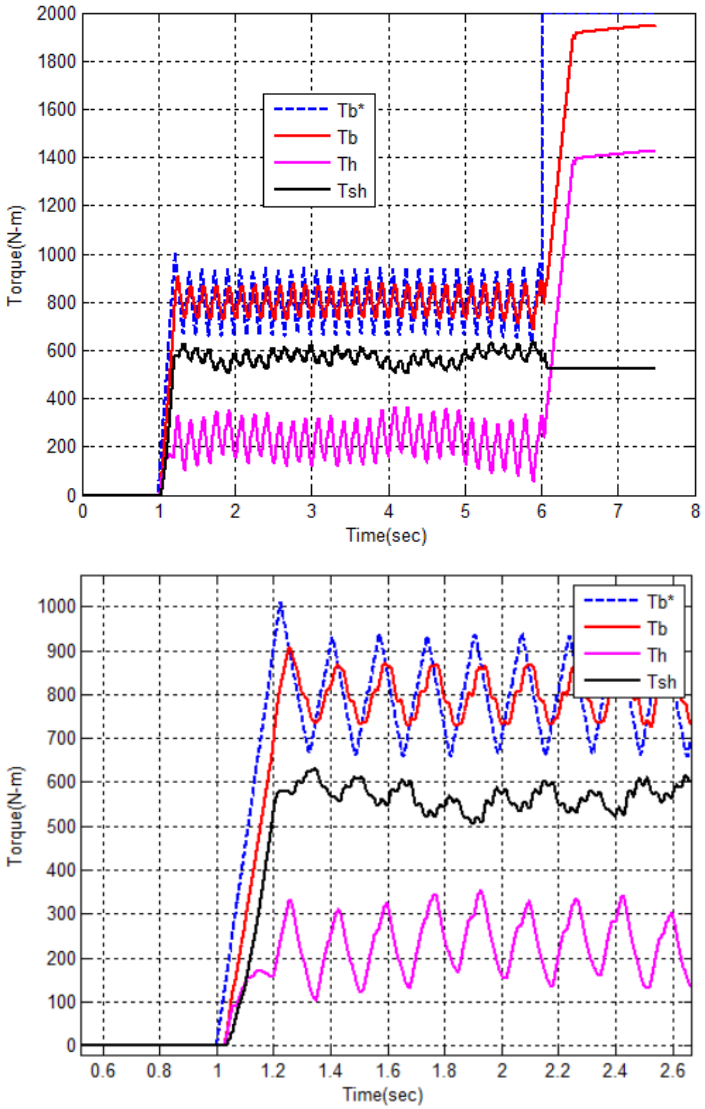

Figure 4.22: Comparison of Brake Torques for the MPCA I case for μ = 0.5 road surface: (Top) entire simulation, and (Bottom) Zoomed in view

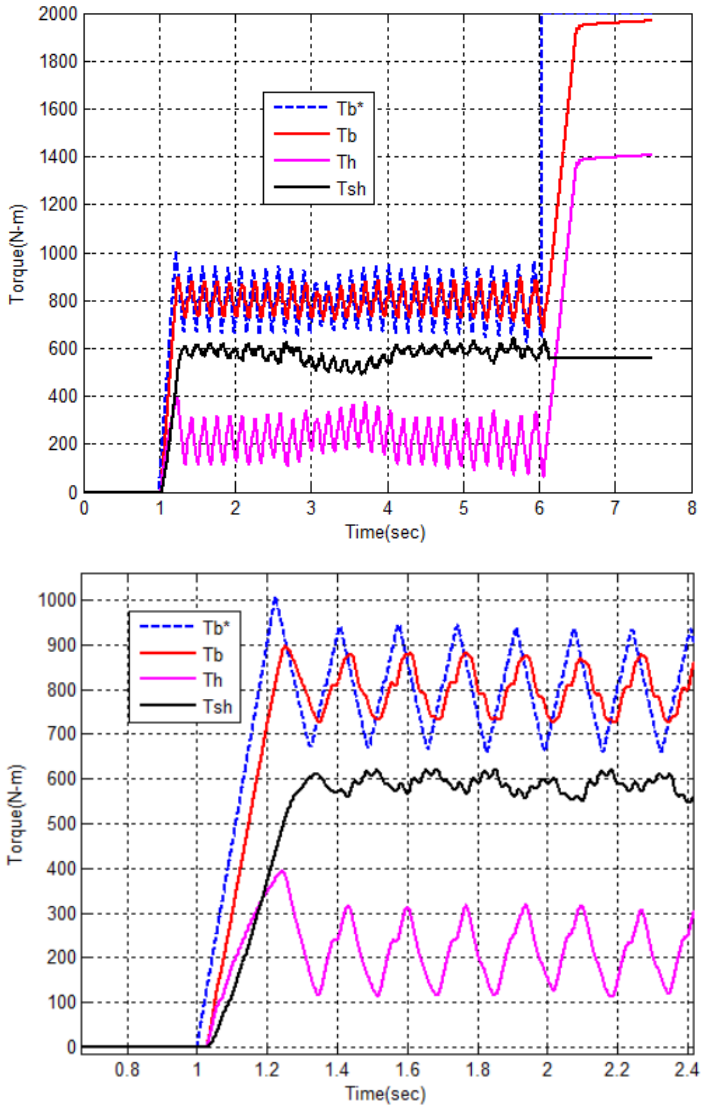

Figure 4.23: Comparison of Brake Torques for the MPCA II case for μ = 0.5 road surface: (Top) entire simulation, and (Bottom) Zoomed in view

Figures 4.21, 4.22, and 4.23 indicate the various actuator torques observed in the simulation for μ = 0.5 road condition. Firstly, it can be observed that the total actual torque in all the 3 cases, operate in the same torque range (650~950 N-m), which imply that the 3 cases are indeed comparable. It can be observed that the total ABS torque modulates slightly faster for the MPCA I and II cases than the hydraulic only case. This is again because of the electric motor extending the bandwidth of the system. The modulation is however, only slightly faster as the addition of shaft dynamics also adds a delay to the regenerative brake torque applied to the wheel. The shaft

dynamics delay, however, does not affect the hydraulic only case, as the hydraulic torque is applied directly at the wheel, and not via the half shaft.

Figure 4.22 shows the brake torques during the ABS operation with MPCA I, where T_b* indicates the demanded brake torque and T_b represents total applied brake torque (sum of the hydraulic brake torque, T_h, and the electric motor torque, T_{sh}. As shown in Figure 4.22, MPCA I effectively allocates the demanded torque based on the bandwidth, in which the electric motor is allocated the high-frequency part of the torque signal and the hydraulic brakes are allocated the low-frequency part of the torque signal. In this case, the control effort is focused on tracking the demanded brake torque (T_b *) with the torque split without considering shaft vibration reduction. The MPC tuning parameters used in this case are: γ_b is set to 120000 and γ_{sh} is set to zero.
Figure 4.23 compares the brake torques during ABS operation with MPCA II. The torque split is not as effective compared to the earlier case since it also considers vibration control. A non-zero-value of γ_{sh} (130000) has been used in the cost function of the MPCA. With that, the hydraulic brakes modulate almost in phase with the regenerative brakes to reduce the shaft vibration, as shown in Figure 4.24. Although it vastly improves the shaft vibration damping, the frequency-based torque split performance has been degraded, and the motor torque is slightly delayed at the start of the simulation. It can be observed that the peak to peak vibrations at the natural frequency of the shaft (around 13 Hz) is reduced in the case of MPCA II.

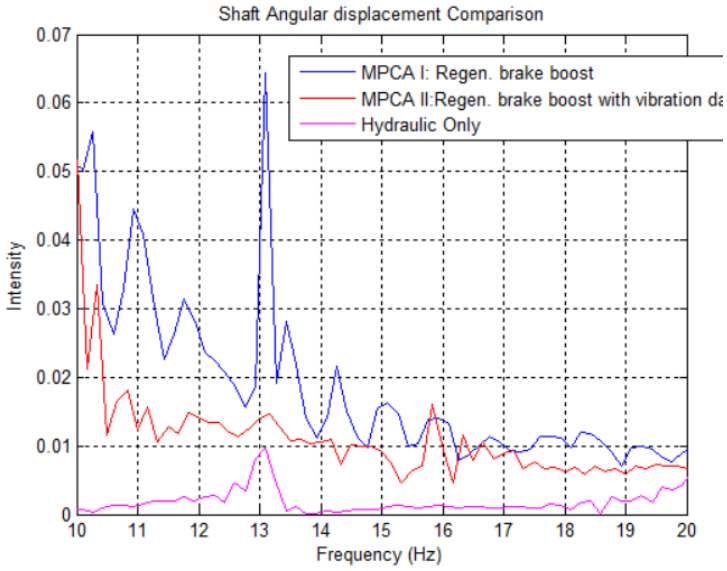

Figure 4.24: Comparison of the FFT of the shaft angular displacement for $\mu = 0.5$ road surface.

Hence to summarize, the tuning parameters used in the MPCA II case are: γ_b is set to 120000, and γ_{sh} is set to 130000.

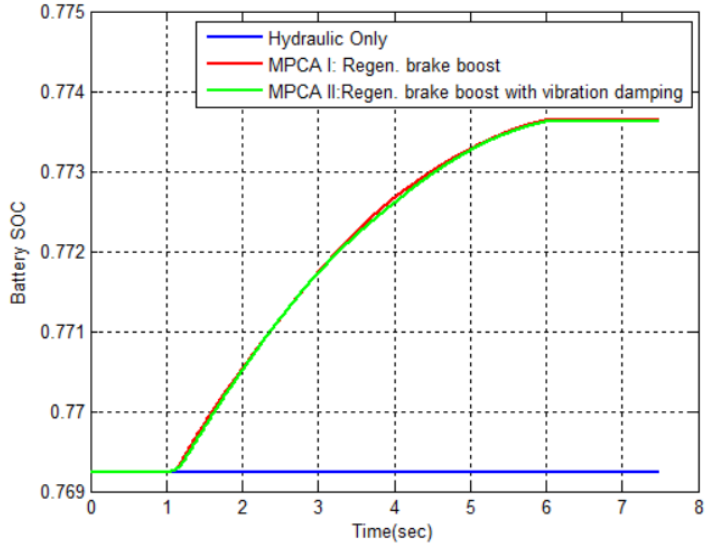

Figure 4.25: Comparison of the Battery SOC Response for μ = 0.5 road surface simulation, for single wheel model.

Table 4.5: Stopping distance summary for μ = 0.5 case, single wheel

Stopping Distance(m)	Hydraulic Only	MPCA I	MPCA II
During ABS	73.86	72.96	73.29
Overall	84.54	83.53	83.73

The effectiveness of the combined braking strategies over hydraulic strategies can be observed from the stopping distance comparison in Table 4.5. It is observed that due to faster torque modulation in the combined braking torques observed in figures 4.22 and 4.23, as compared to hydraulic only case in Figure 4.20. This leads to slightly faster slip control in Figure 4.15, which further leads to an improvement in stopping distance. Figure 4.25 indicates the comparison of the Battery SoC for the 3 strategies. It is observed that as expected, there is no energy recovered in the Hydraulic only case, while some amount of energy is recovered in the MPCA-I and II cases. This is hence a secondary advantage of implementing MPCA. However, one can argue that energy recovery cannot be a primary objective in the case of emergency braking for two reasons: first, this being a safety-critical control, one must prioritize safety instead of recovered energy, and second: one does not encounter emergency braking situations more often, in order to rely on ABS for energy recovery.

4.1.3 Low μ Test (μ=0.2)

The single wheel model is simulated as per the simulation conditions described in section 4.1, for a tire-road friction coefficient (μ) of 0.2. In practice this may refer to a snow covered road surface. In the five phase ABS Logic, the reference wheel deceleration (a_x*) for the low mu case (μ=0.2), is chosen as 1.96 m/s^2.

The comparison of longitudinal slip in this case is indicated in Figure 4.26. It can be observed that the ABS cycling, i.e. slip tracking is slightly faster for the MPCA I and II cases, as compared to the hydraulic only case.

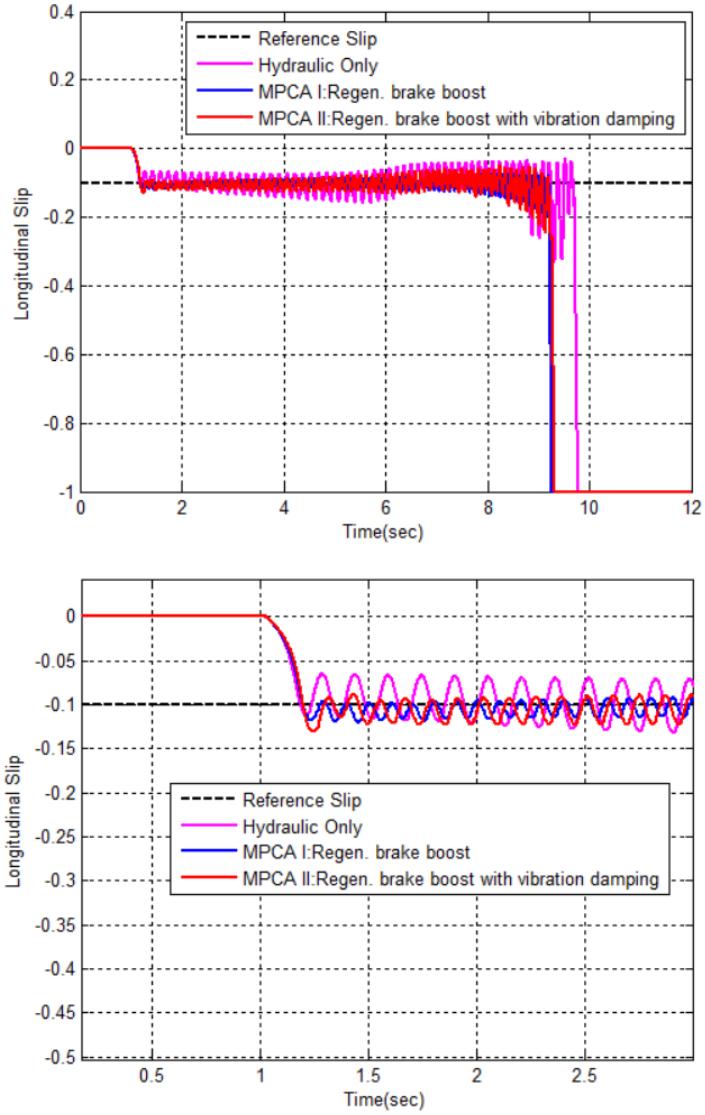

Figure 4.26: Comparison of the vehicle longitudinal slip for the 3 strategies for μ = 0.2 road surface: (top) entire simulation, and (bottom) Zoomed in view.

This is mainly because of using electric motor as an actuator during ABS cycling. The inclusion of the electric motor as an additional actuator, effectively extends the bandwidth of the system, and results in relatively faster slip tracking. In Figure 4.27, it can be observed that the range in which the limit cycle operates for the 3 cases is the same.

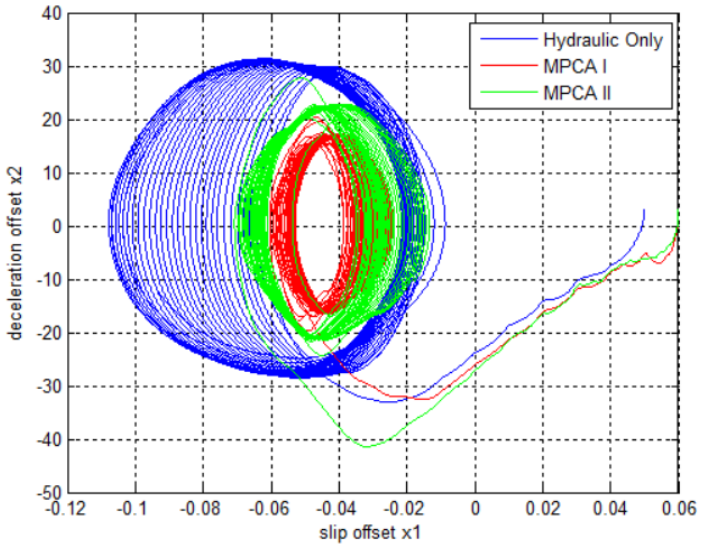

Figure 4.27: Comparison of the ABS limit cycles for the 3 strategies for μ = 0.2 road surface.

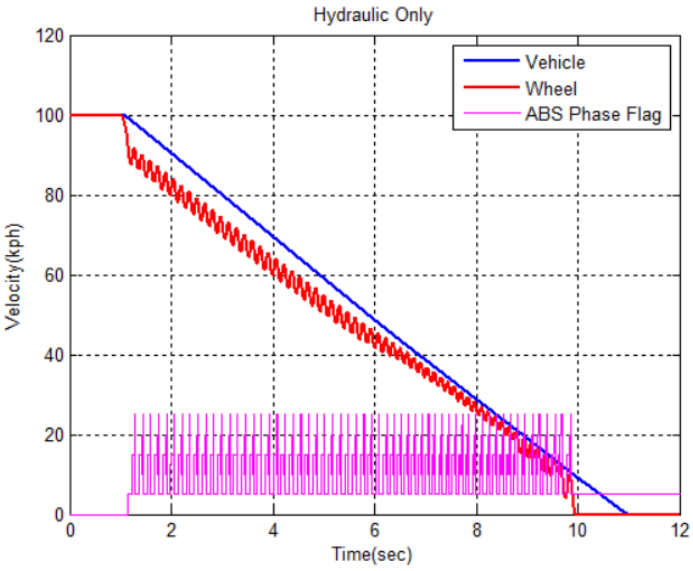

Figure 4.28: Vehicle and wheel velocities, and ABS phase flag for the hydraulic ABS only case for μ = 0.2 road surface

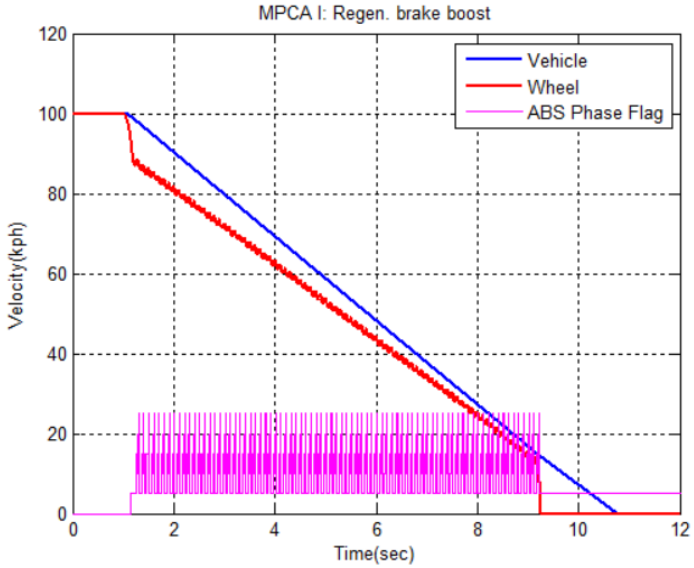

Figure 4.29: Vehicle and wheel velocities, and ABS phase flag for the MPCA I case for μ = 0.2 road surface

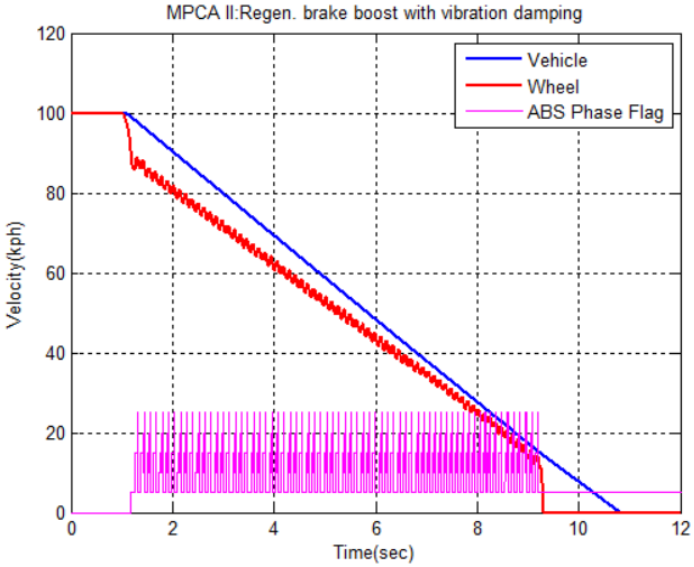

Figure 4.30: Vehicle and wheel velocities, and ABS phase flag for the MPCA II case for μ = 0.2 road surface

Figures 4.28, 4.29, and 4.30 show the vehicle and wheel velocity responses for the 3 cases. It can be observed from the figures that at t=1sec, when the brakes are applied, the vehicle velocity response starts to decrease, as expected. The wheel velocity response starts to "cycle" as per the brake torque applied at the wheel. These are the typical responses one would expect, when the ABS is in action. It can further be observed from the plots that the wheel velocity starts to "cycle" around 1.2sec for all the 3 cases. This is the time at which the wheel slip first crosses the

reference wheel slip, as can be confirmed from Figure 4.26 The ABS phase flag indicates the cycling of the ABS control, and also confirms the ABS cycling starting at 1.2sec Also, the ABS is set to de-activate as the vehicle velocity falls below 10 kph in simulation, and can also be observed from the figures 4.26, 4.28, 4.29 and 4.30.

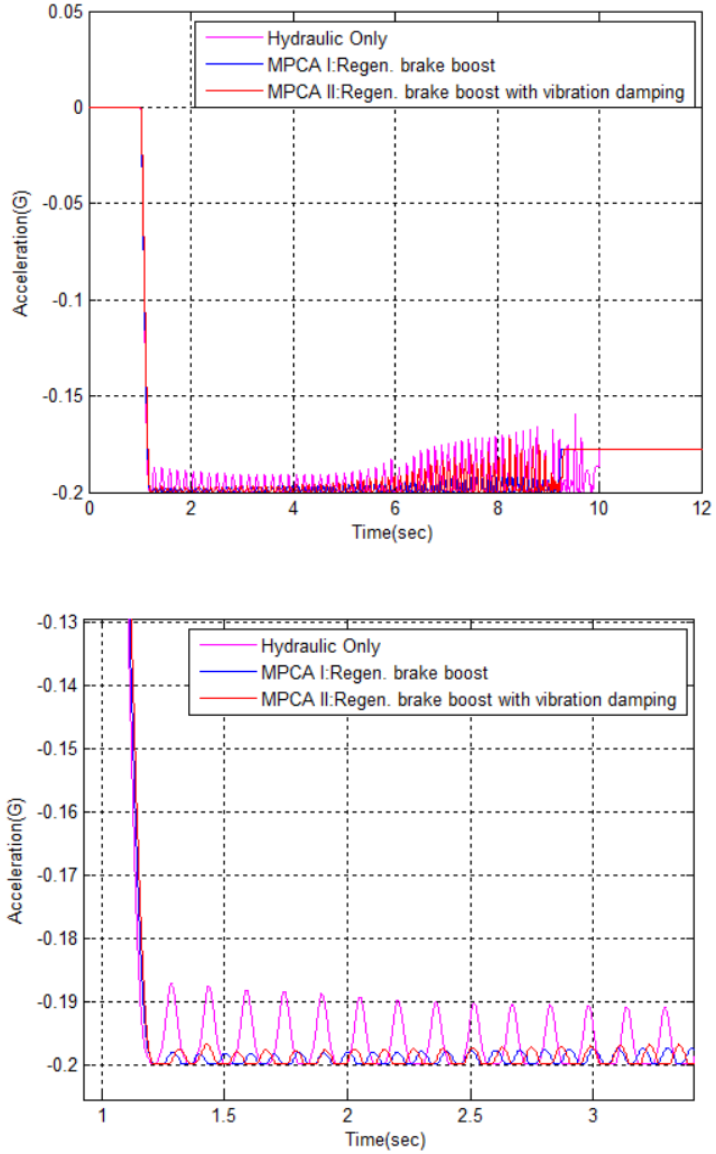

Figure 4.31: Comparison of the vehicle deceleration for the 3 strategies for μ = 0.2 road surface, for a single wheel model: (Top) entire simulation, and (Bottom) Zoomed in view

Figure 4.31 indicates the vehicle deceleration response for the 3 strategies. This plot further consolidates the conclusion for Figure 4.26. It can be observed that the vehicle deceleration for

MPCA I and II cases is more “concentrated” towards larger deceleration. This is mainly due to the faster overall ABS cycling and tighter slip control offered by the MPCA I and II cases.

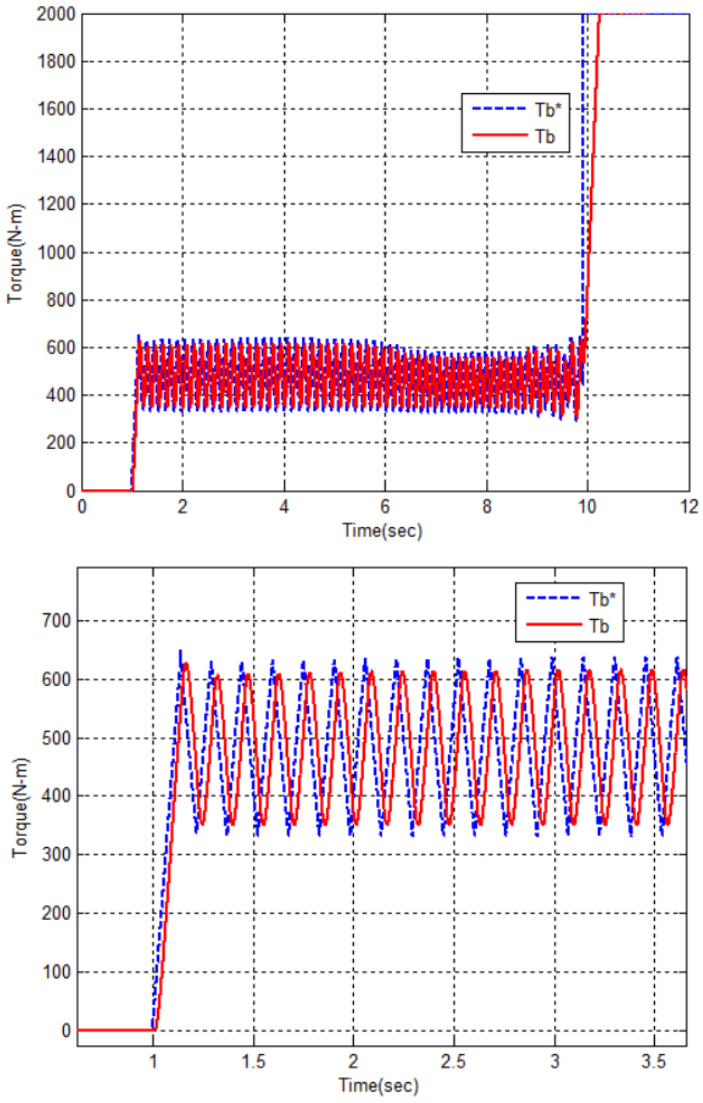

Figure 4.32: Comparison of Brake Torques for the hydraulic ABS only case for μ = 0.2 road surface: (Top) entire simulation, and (Bottom) Zoomed in view

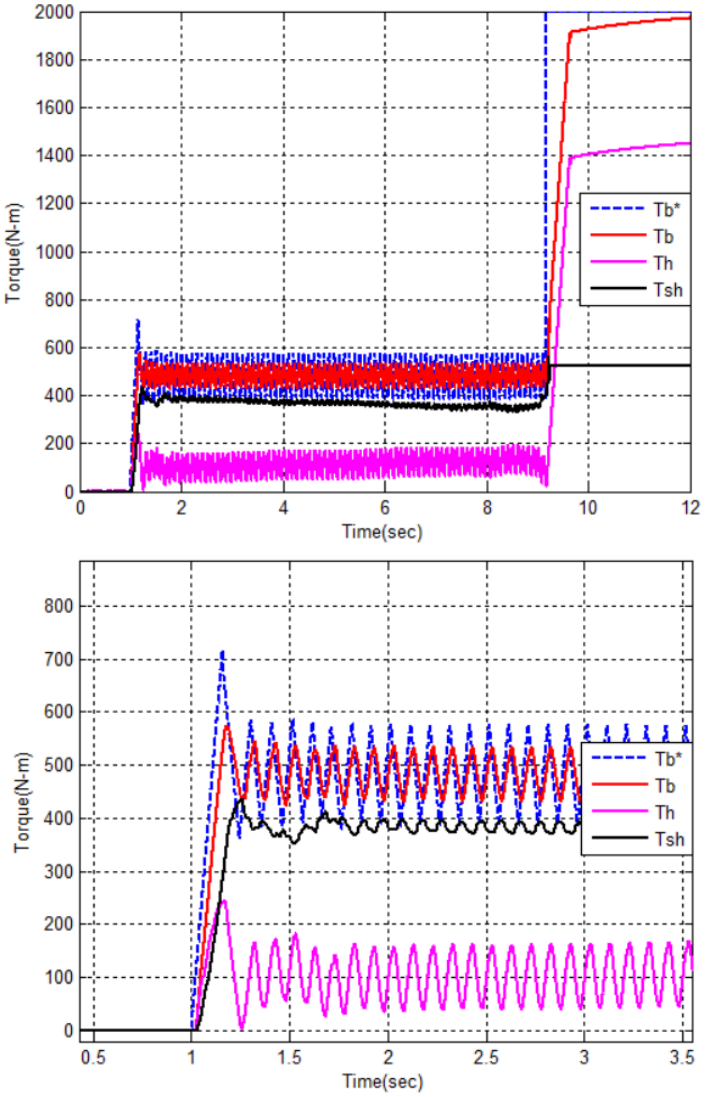

Figure 4.33: Comparison of Brake Torques for the MPCA I case for μ = 0.2 road surface: (Top) entire simulation, and (Bottom) Zoomed in view

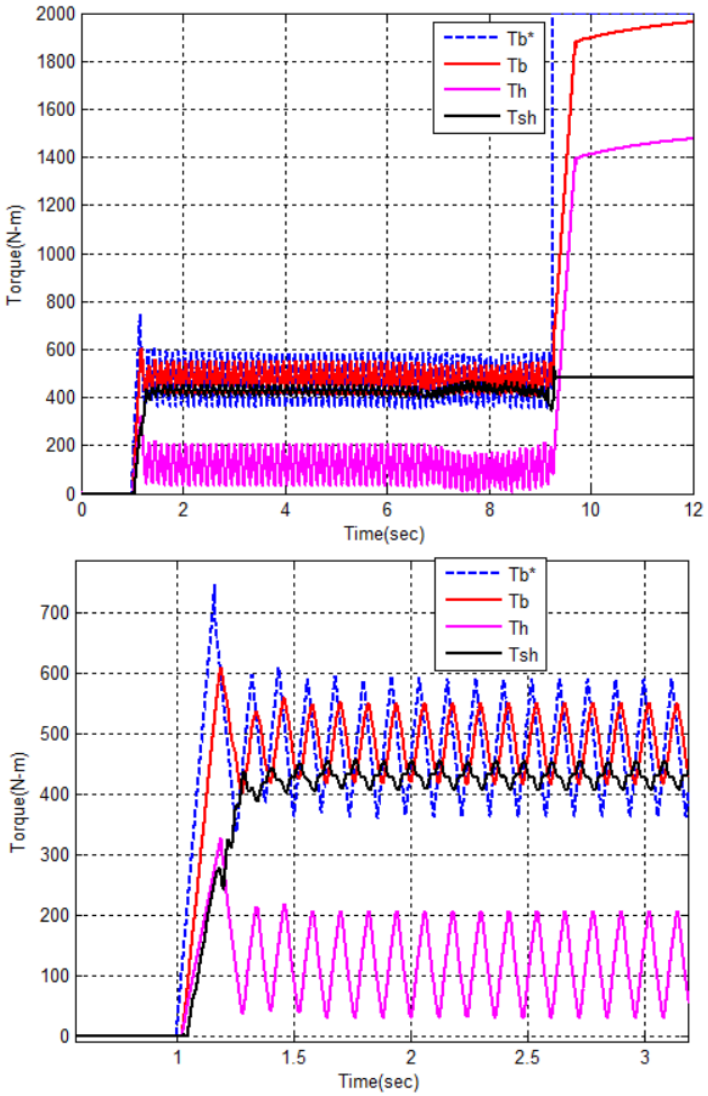

Figure 4.34: Comparison of Brake Torques for the MPCA II case for μ = 0.2 road surface: (Top) entire simulation, and (Bottom) Zoomed in view

Figures 4.32, 4.33 and 4.34 indicate the various actuator torques observed in the simulation for μ = 0.2 road condition. Firstly, it can be observed that the total actual torque in all the 3 cases, operate in the same torque range (400~600 N-m), which imply that the 3 cases are indeed comparable. It can be observed that the total ABS torque modulates slightly faster for the MPCA I and II cases than the hydraulic only case. This is again because of the electric motor extending the bandwidth of the system. The modulation is however, only slightly faster as the addition of shaft dynamics also adds a delay to the regenerative brake torque applied to the wheel. The shaft dynamics delay, however, does not affect the hydraulic only case, as the hydraulic torque is applied directly at the wheel, and not via the half shaft.

Figure 4.33 shows the brake torques during the ABS operation with MPCA I, where T_b* indicates the demanded brake torque and T_b represents total applied brake torque (sum of the hydraulic brake torque, T_h, and the electric motor torque, T_{sh}. As shown in Figure 4.33, MPCA I effectively allocates the demanded torque based on the bandwidth, in which the electric motor is allocated the high-frequency part of the torque signal and the hydraulic brakes are allocated the low-frequency part of the torque signal. In this case, the control effort is focused on tracking the demanded brake torque (T_b*) with the torque split without considering shaft vibration reduction. The MPC tuning parameters used in this case are: γ_b is set to 140000 and γ_{sh} is set to zero.

Figure 4.34 compares the brake torques during ABS operation with MPCA II. The torque split is not as effective compared to the earlier case since it also considers vibration control. A non-zero-value of γ_{sh} (150000) has been used in the cost function of the MPCA. With that, the hydraulic brakes modulate almost in phase with the regenerative brakes to reduce the shaft vibration, as shown in Figure 4.35. Although it vastly improves the shaft vibration damping, the frequency-based torque split performance has been degraded, and the motor torque is slightly delayed at the start of the simulation. It can be observed that the peak to peak vibrations at the natural frequency of the shaft (around 13 Hz) is reduced in the case of MPCA II.

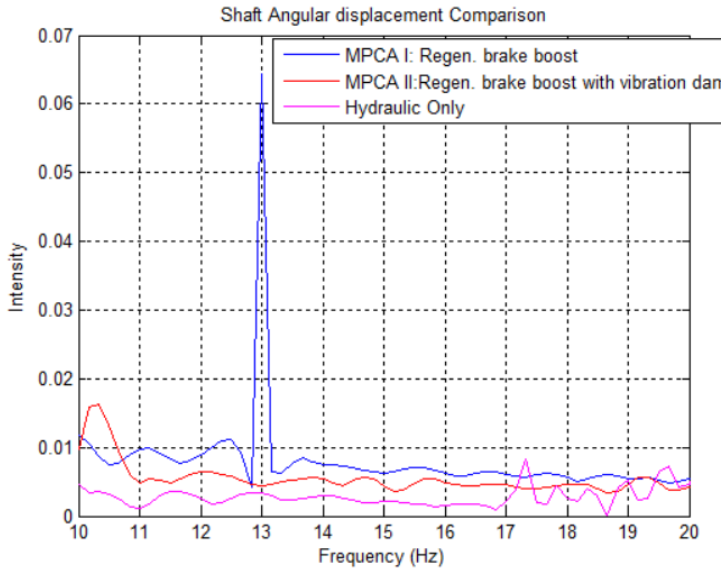

Figure 4.35: Comparison of the FFT of the shaft angular displacement for $\mu = 0.2$ road surface.

Hence to summarize, the tuning parameters used in the MPCA II case are: γ_b is set to 140000, and γ_{sh} is set to 150000.

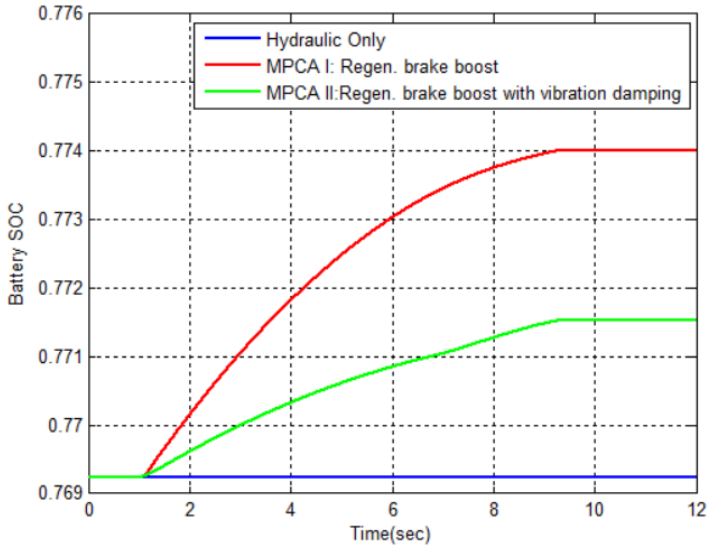

Figure 4.36: Comparison of the Battery SOC Response for μ = 0.2 road surface simulation, for single wheel model.

Table 4.6: Stopping distance summary for μ = 0.2 case, single wheel

Stopping Distance(m)	Hydraulic Only	MPCA I	MPCA II
During ABS	151.3	147.4	148.4
Overall	165.2	162.3	163.5

The effectiveness of the combined braking strategies over hydraulic strategies can be observed from the stopping distance comparison in Table 4.6. It is observed that due to faster torque modulation in the combined braking torques observed in figures 4.33 and 4.34, as compared to hydraulic only case in Figure 4.32. This leads to slightly faster slip control in Figure 4.26, which further leads to an improvement in stopping distance. Figure 4.36 indicates the comparison of the Battery SoC for the 3 strategies. It is observed that as expected, there is no energy recovered in the Hydraulic only case, while some amount of energy is recovered in the MPCA-I and II cases. This is hence a secondary advantage of implementing MPCA. However, one can argue that energy recovery cannot be a primary objective in the case of emergency braking for two reasons: first, this being a safety-critical control, one must prioritize safety instead of recovered energy, and second: one does not encounter emergency braking situations more often, in order to rely on ABS for energy recovery.

4.2 CARSIM VEHICLE MODEL.

The simulation study is then extended for a full vehicle model in Carsim defined in chapter 2.

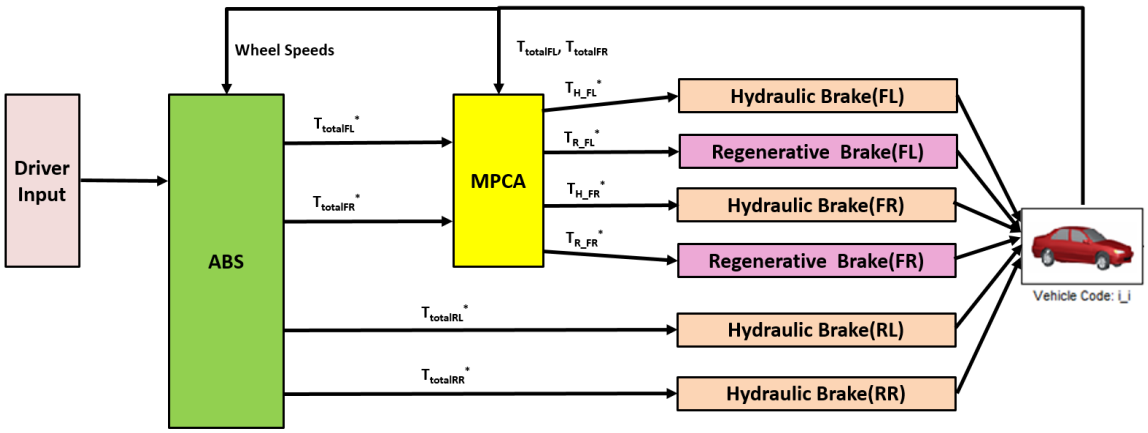

Figure 4.37: Simulation model Schematic for Carsim simulations

The parameters of the Carsim model are given in Table 4.7. The initial vehicle speed is 100 kph, and the brake is applied at simulation time t=1sec, in order to allow the forces in the suspension data set of Carsim to settle and reach steady state.

Table 4.7: Carsim model Parameters (B-Class Hatchback)

Parameter	Symbol	Value
Vehicle Mass (LLVW)	M	1955 kg
Wheel inertia	J_w	1kg-m^2
Height of C.G.	H	0.5 m
C.G. distance from front axle	A	1.021 m
Wheelbase	L	2.68 m
Tire rolling radius	R	0.32 m
Motor inertia	J_m	0.42 kg-m^2
Min./Max. Motor Torque	T_{rmin}/T_{rmax}	-630/+630 N-m
Min./Max. Hydraulic torque	T_{hmin}/T_{hmax}	0/3500 N-m

It is assumed that the engine is decoupled via a clutch during the braking scenario, and hence the effect of positive engine torque is neglected. The battery SoC is assumed to be less than its fully charged threshold, and hence the regenerative brake torque is available throughout the simulation. The five phase ABS reference slip deceleration and the deceleration thresholds are kept the same for all simulations, to have a fair comparison, and are indicated in Table 4.8.

Table 4.8: ABS Tuning Parameters, for Carsim

Parameter	Value
λ^*	0.12
$\varepsilon 1$	10
$\varepsilon 2$	11

ε3	9
ε4	9
ε5	10

In order to test the robustness of the proposed scheme over a range of operating conditions, three test scenarios are considered:

1. High Mu test: Tire-Road friction coefficient of 0.9.
2. Mid Mu test: Tire-Road friction coefficient of 0.5.
3. Low Mu Test: Tire-Road Friction coefficient of 0.2.

4.2.1 High μ Test (μ=0.9)

The Single wheel model is simulated as per the simulation conditions described in section 4.1, for a tire-road friction coefficient (μ) of 0.9. In practice this may refer to a dry asphalt or dry concrete road surface. In the five phase ABS Logic, the reference wheel deceleration (a_x*) for the high mu case (μ=0.9), is chosen as 8.82 m/s^2.

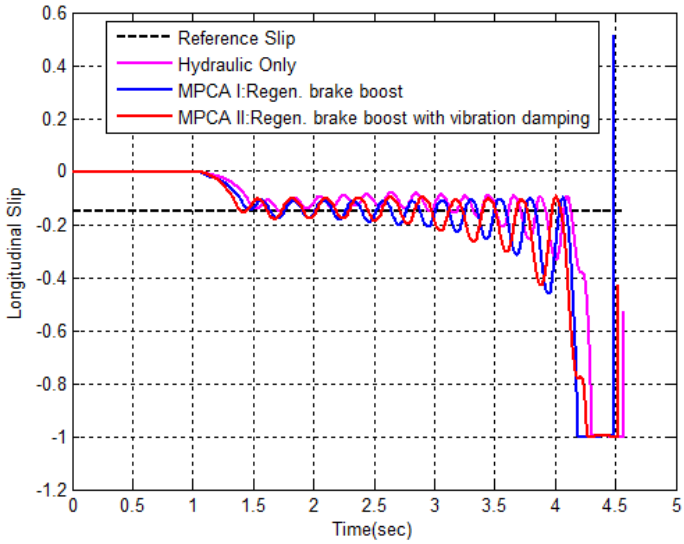

Figure 4.38: Comparison of the vehicle longitudinal slip for the Front left wheel for the 3 strategies for μ = 0.9 road surface.

The comparison of longitudinal slip in this case is indicated in Figure 4.38. It can be observed that the ABS cycling, i.e. slip tracking is slightly faster for the MPCA I and II cases, as compared

to the hydraulic only case. This is mainly because of using electric motor as an actuator during ABS cycling.

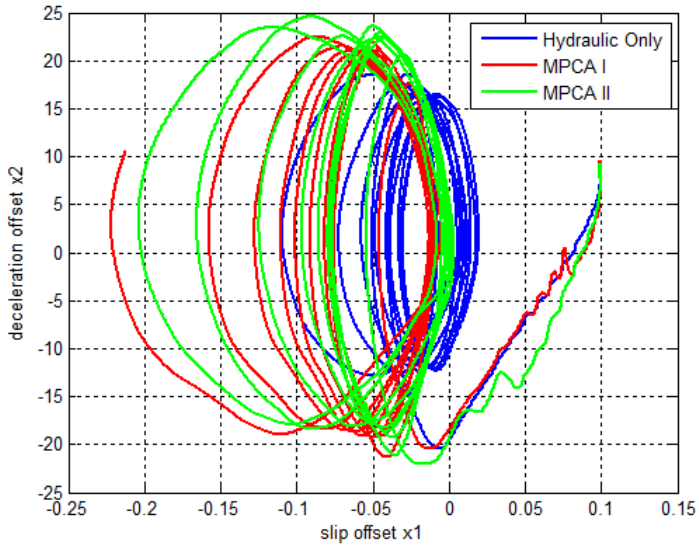

Figure 4.39: Comparison of the ABS limit cycles for the Front left wheel for the 3 strategies for $\mu = 0.9$ road surface.

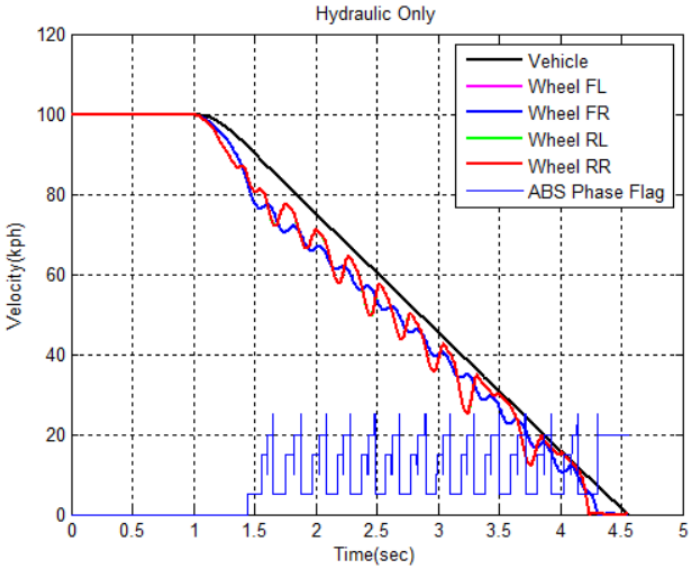

Figure 4.40: Vehicle and wheel velocities for the hydraulic ABS only case for $\mu = 0.9$ road surface and the ABS phase flag for the Front Left wheel.

The inclusion of the electric motor as an additional actuator, effectively extends the bandwidth of the system, and results in relatively faster slip tracking. In Figure 4.39, it can be observed that the range in which the limit cycle operates for the 3 cases is the same.

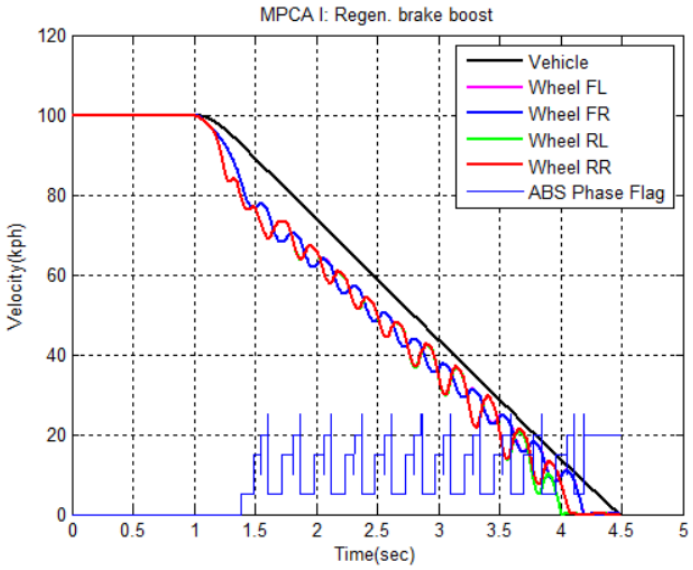

Figure 4.41: Vehicle and wheel velocities for the MPCA I case for μ = 0.9 road surface and the ABS phase flag for the Front Left wheel.

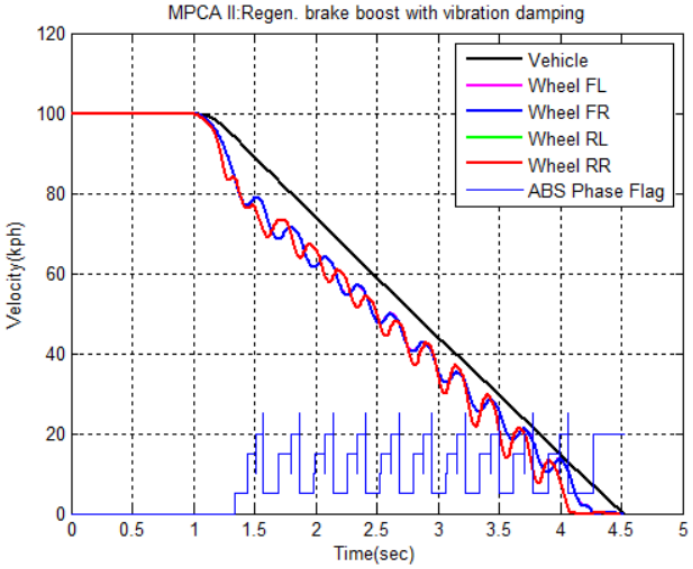

Figure 4.42: Vehicle and wheel velocities for the MPCA II case for μ = 0.9 road surface and the ABS phase flag for the Front Left wheel.

Figures 4.40, 4.41, and 4.42 show the vehicle and wheel velocity responses for the 3 cases. It can be observed from the figures that at t=1sec, when the brakes are applied, the vehicle velocity response starts to decrease, as expected. The wheel velocity response starts to "cycle" as per the brake torque applied at the wheel. These are the typical responses one would expect, when the ABS is in action. It can further be observed from the plots that the wheel velocity starts to "cycle" around 1.5sec for all the 3 cases. This is the time at which the wheel slip first crosses the

reference wheel slip, as can be confirmed from Figure 4.38. The ABS phase flag indicates the cycling of the ABS control, and also confirms the start of ABS control at about 1.5sec. Also, the ABS is set to de-activate as the vehicle velocity falls below 10 kph in simulation, and can also be observed from the figures 4.38, 4.40, 4.41 and 4.42.

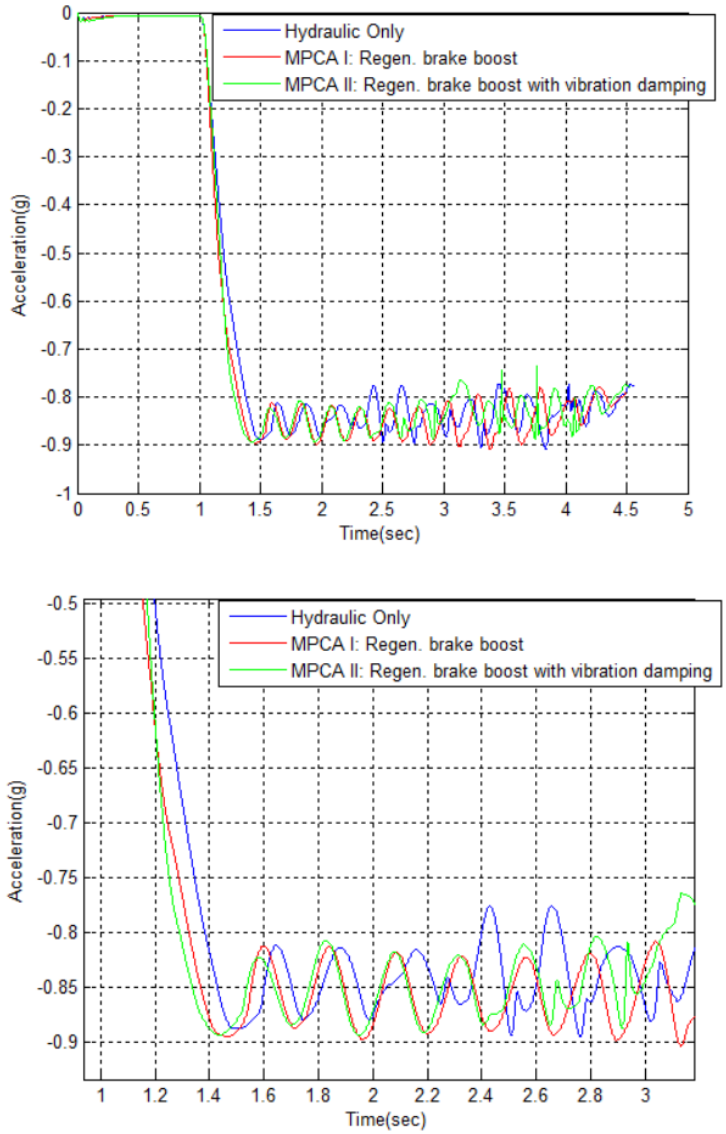

Figure 4.43: Comparison of the vehicle deceleration for the 3 strategies for μ = 0.9 road surface, for a Carsim model: (top) entire simulation, and (bottom) Zoomed in view.

Figure 4.43 indicates the vehicle deceleration response for the 3 strategies. It can be observed that the vehicle deceleration for the MPCA cases is more concentrated towards the higher deceleration side. However, as compared to the single wheel model, one cannot conclude from

this plot, the effectiveness of the MPCA strategies. This is because the Vehicle deceleration for a full vehicle model is influenced by the brake torques at all its wheels, but regenerative braking (and hence MPCA I and II) is available at only the front wheels as the vehicle in consideration is a front wheel drive.

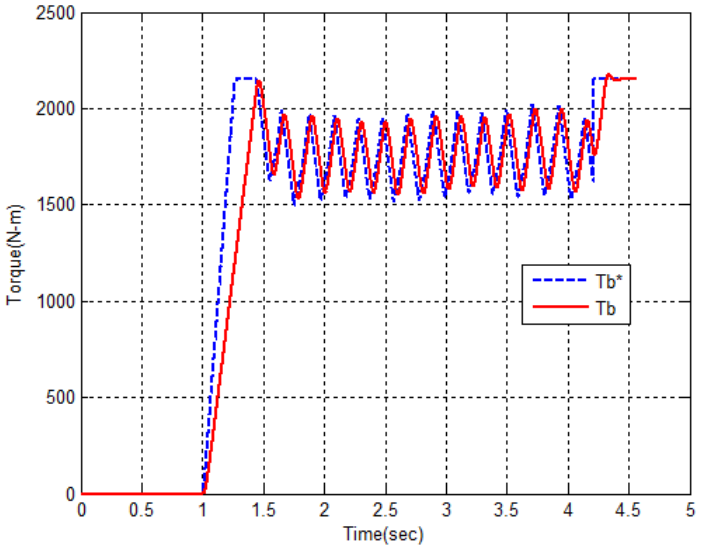

Figure 4.44: Comparison of Brake Torques for the Front left wheel for the hydraulic ABS only case for μ = 0.9 road surface

Figures 4.44, 4.45 and 4.45 indicate the various actuator torques observed in the simulation for μ = 0.9 road condition. Firstly, it can be observed that the total actual torque in all the 3 cases, operate in the same torque range (1500~2000 N-m), which imply that the 3 cases are indeed comparable. It can be observed that the total ABS torque modulates slightly faster for the MPCA I and II cases than the hydraulic only case. This is again because of the electric motor extending the bandwidth of the system. The modulation is however, only slightly faster as the addition of shaft dynamics also adds a delay to the regenerative brake torque applied to the wheel. The shaft dynamics delay, however, does not affect the hydraulic only case, as the hydraulic torque is applied directly at the wheel, and not via the half shaft. Figures 4.45(b) and 4.46(b) indicate the respective 3-phase motor current, which correspond to the Motor (shaft) torque indicated in Figures 4.45(a) and 4.46(a). A general and expected observation from these is that the envelope of the motor current matches that of the Motor torque, in the time scale. In Figure 4.45(a), the motor torque rises to the maximum (600Nm) from 0, at around 1.15 sec, the motor current in Figure 4.45(b) also rises from the 0 to the maximum in the same time. Also in Figure 4.45(a), the

motor stops modulating at around 4.2 sec, so does the motor current in Figure 4.45(b). This trend can also be observed for the MPCA II case in Figures 4.46 (a) and (b)

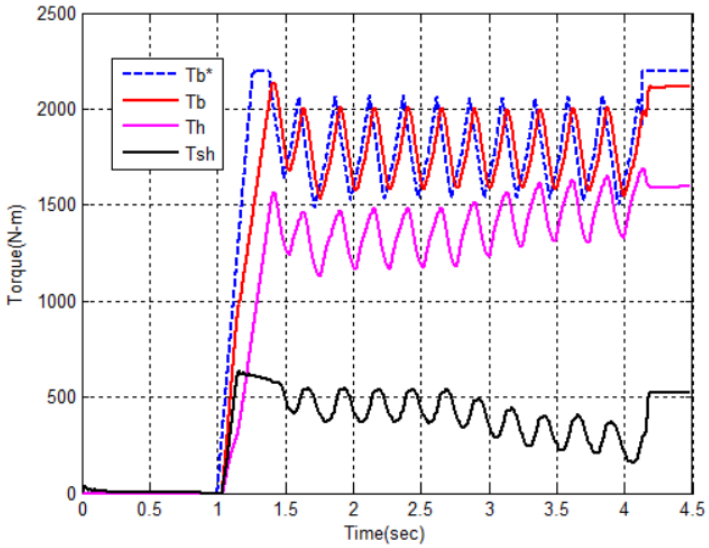

(a)

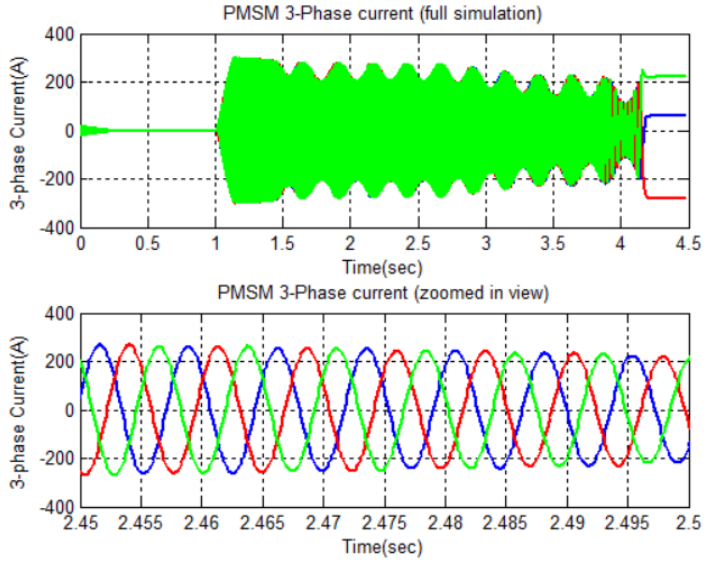

(b)

Figure 4.45: (a) Comparison of Brake Torques and (b) PMSM 3 Phase Current; for the Front left wheel for the MPCA I case for μ = 0.9 road surface

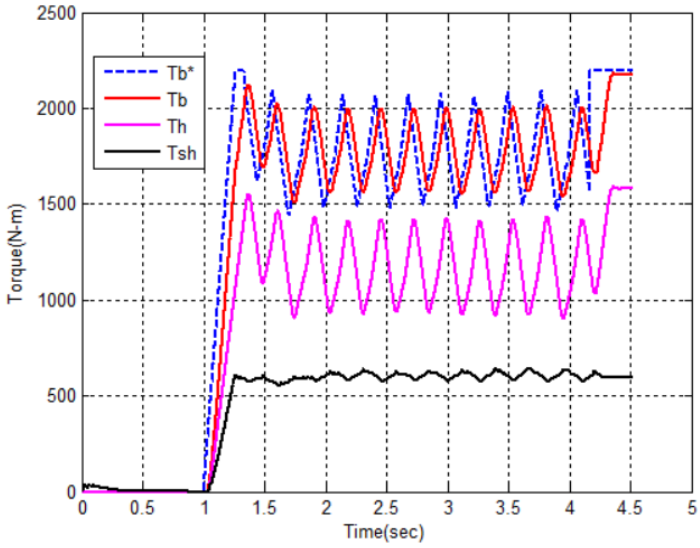

(a)

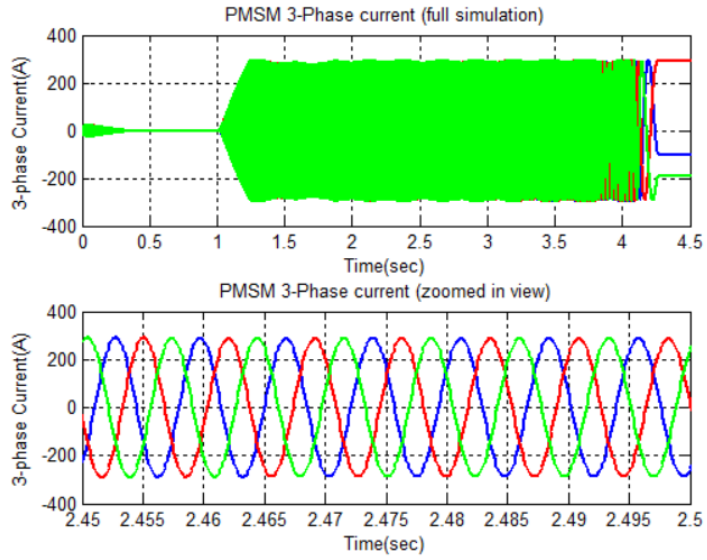

(b)

Figure 4.46: (a) Comparison of Brake Torques and (b) PMSM 3 Phase Current; for the Front left wheel for the MPCA II case for μ = 0.9 road surface

Figure 4.45 shows the brake torques during the ABS operation with MPCA I, where T_b* indicates the demanded brake torque and T_b represents total applied brake torque (sum of the hydraulic brake torque, T_h, and the electric motor torque, T_{sh}. As shown in Figure 4.45, MPCA I effectively allocates the demanded torque based on the bandwidth, in which the electric motor is allocated the high-frequency part of the torque signal and the hydraulic brakes are allocated the low-frequency part of the torque signal. In this case, the control effort is focused on tracking the

demanded brake torque (T_b*) with the torque split without considering shaft vibration reduction. The MPC tuning parameters used in this case are: γ_b is set to 100000 and γ_{sh} is set to zero.

Figure 4.46 compares the brake torques during ABS operation with MPCA II. The torque split is not as effective compared to the earlier case since it also considers vibration control. A non-zero-value of γ_{sh} (110000) has been used in the cost function of the MPCA. With that, the hydraulic brakes modulate almost in phase with the regenerative brakes to reduce the shaft vibration, as shown in Figure 4.47. Although it vastly improves the shaft vibration damping, the frequency-based torque split performance has been degraded, and the motor torque is slightly delayed at the start of the simulation.

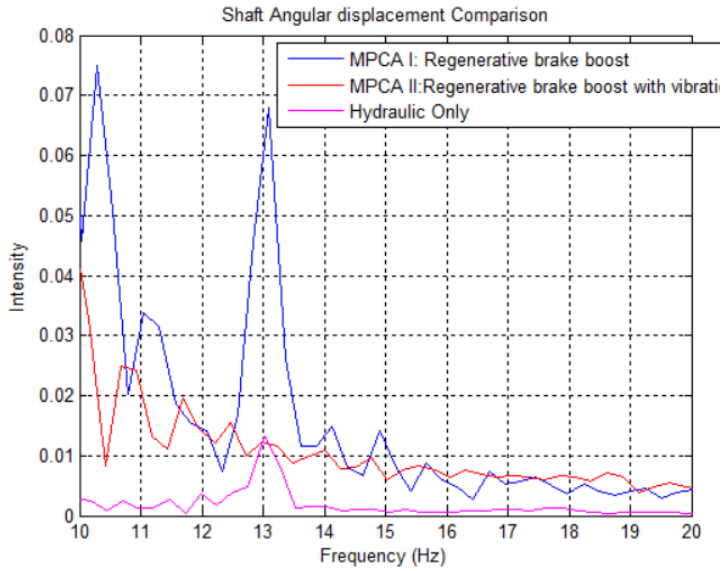

Figure 4.47: Comparison of the FFT of the shaft angular displacement for the Front left wheel for $\mu = 0.9$ road surface.

It can be observed that the peak to peak vibrations at the natural frequency of the shaft (around 13 Hz) is reduced in the case of MPCA II. Hence to summarize, the tuning parameters used in the MPCA II case are: γ_b is set to 100000, and γ_{sh} is set to 110000.

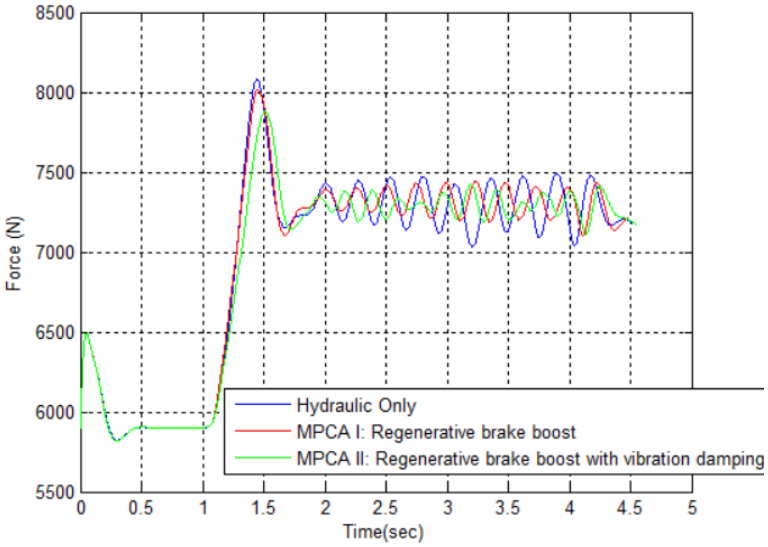

Figure 4.48: Comparison of Tire Normal Force response for the Front left wheel for the 3 strategies for μ = 0.9 road surface

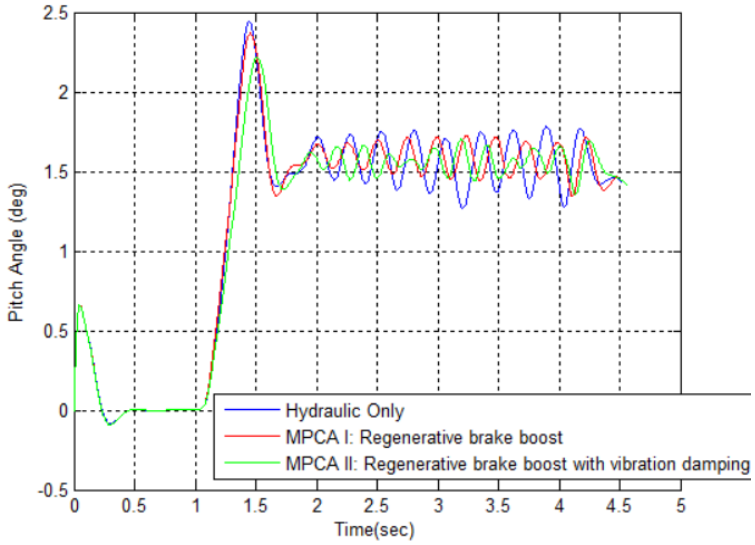

Figure 4.49: Comparison of vehicle pitch angle response for the 3 strategies for μ = 0.9 road surface

Figures 4.48 and 4.49 show the Normal force response (for the front left wheel) and the vehicle pitch angle response respectively. Initial overshoot of both the responses is due to the forces in the Suspension model of Carsim not reaching steady state. Hence the braking is applied at 1 sec, so that the forces reach steady state and "settle down". The weight transfer during braking is positive, as can be expected for the front wheel. It is observed that the Peak to Peak magnitude of the variation in Normal force, and pitch angle during ABS activation is least for MPCA II,

followed by MPCA I and most for Hydraulic only case, implying that the MPCA II strategy proposed in this work is successful. This can further be related to a more "comfortable" ride for the occupants in the vehicle, as the peak to peak magnitude of the Pitch angle is decreased in the MPCA II case.

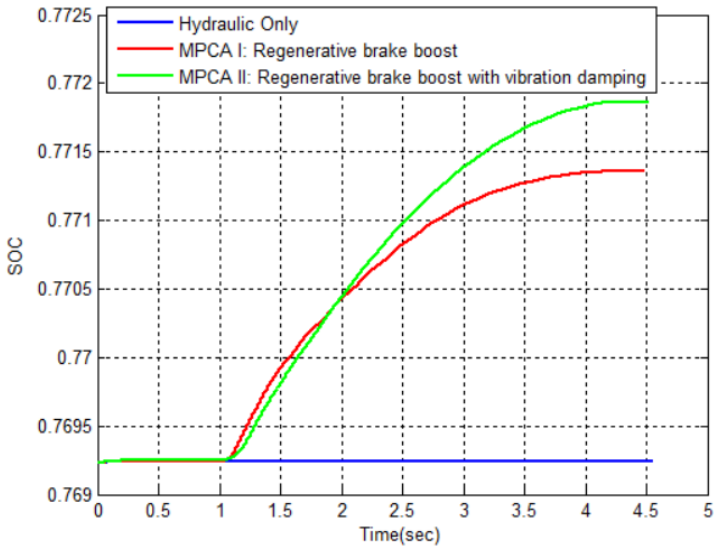

Figure 4.50: Comparison of the Battery SOC Response for μ = 0.9 road surface simulation, for Carsim vehicle model.

As can be observed in Figure 4.50, the intensity of vibration in the MPCA II case is improved at around the natural frequency of the shaft (~13Hz).

Table 4.9: Stopping distance summary for μ = 0.9 case, Carsim

Stopping Distance(m)	Hydraulic Only	MPCA I	MPCA II
During ABS	37.09	35.77	36.07
Overall	51.56	50.00	50.42

The effectiveness of the combined braking strategies over hydraulic strategies can be observed from the stopping distance comparison in Table 4.9. It is observed that due to faster torque modulation in the combined braking torques observed in figures 4.45 and 4.46, as compared to hydraulic only case in Figure 4.44. This leads to slightly faster slip control in Figure 4.38, which further leads to an improvement in stopping distance. Figure 4.50 indicates the comparison of the Battery SoC for the 3 strategies. It is observed that as expected, there is no energy recovered in the Hydraulic only case, while some amount of energy is recovered in the MPCA-I and II cases. This is hence a secondary advantage of implementing MPCA. However, one can argue that

energy recovery cannot be a primary objective in the case of emergency braking for two reasons: first, this being a safety-critical control, one must prioritize safety instead of recovered energy, and second: one does not encounter emergency braking situations more often, in order to rely on ABS for energy recovery.

4.2.2 Mid μ Test (μ=0.5)

The single wheel model is simulated as per the simulation conditions described in section 4.1, for a tire-road friction coefficient (μ) of 0.9. In practice this may refer to a dry packed gravel road. In the five phase ABS Logic, the reference wheel deceleration (a_x*) for the mid mu case (μ=0.5), is chosen as 4.905 m/s^2.

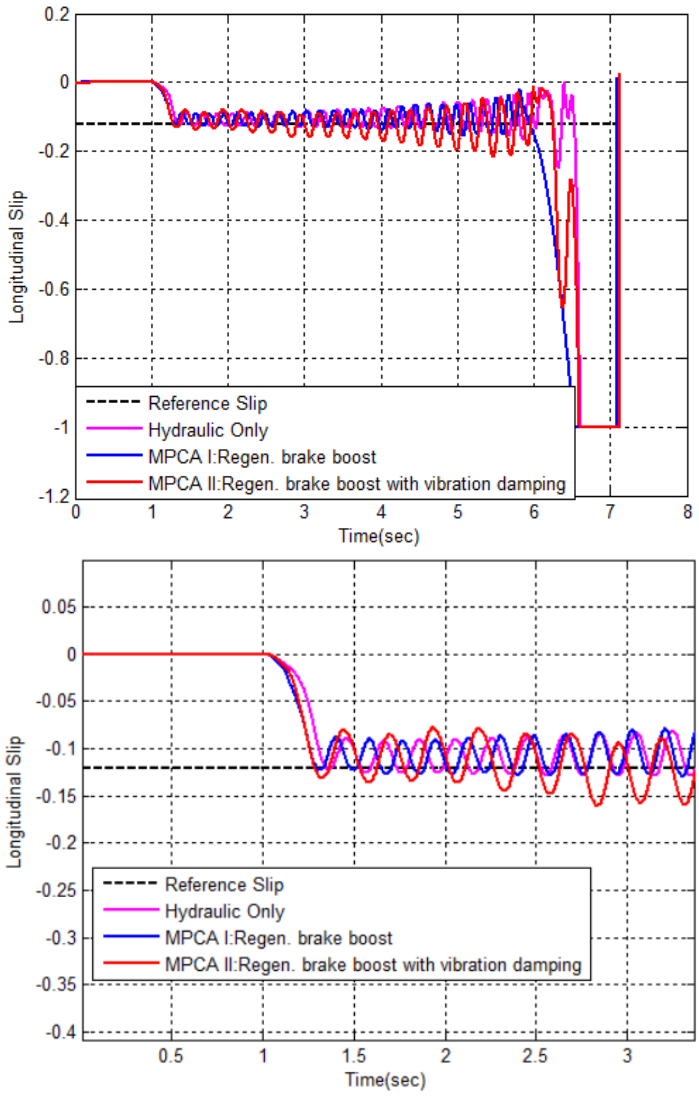

Figure 4.51: Comparison of the vehicle longitudinal slip for the Front left wheel for the 3 strategies for μ = 0.5 road surface: (Top) entire simulation, and (Bottom) Zoomed in view.

The comparison of longitudinal slip in this case is indicated in Figure 4.51. It can be observed that the ABS cycling, i.e. slip tracking is slightly faster for the MPCA I and II cases, as compared to the hydraulic only case. This is mainly because of using electric motor as an actuator during ABS cycling. The inclusion of the electric motor as an additional actuator, effectively extends the bandwidth of the system, and results in relatively faster slip tracking. In Figure 4.52, it can be observed that the range in which the limit cycle operates for the 3 cases is the same.

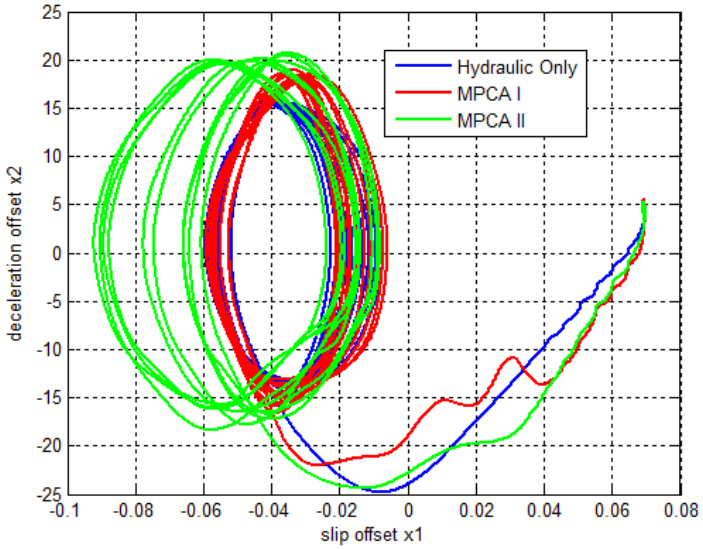

Figure 4.52: Comparison of the ABS limit cycles for the Front left wheel for the 3 strategies for μ = 0.5 road surface.

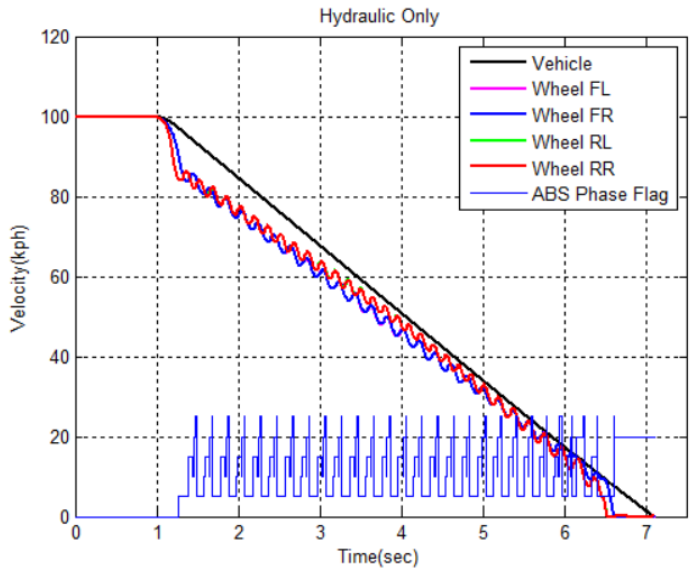

Figure 4.53: Vehicle and wheel velocities for the hydraulic ABS only case for μ = 0.5 road surface and the ABS phase flag for the Front Left wheel.

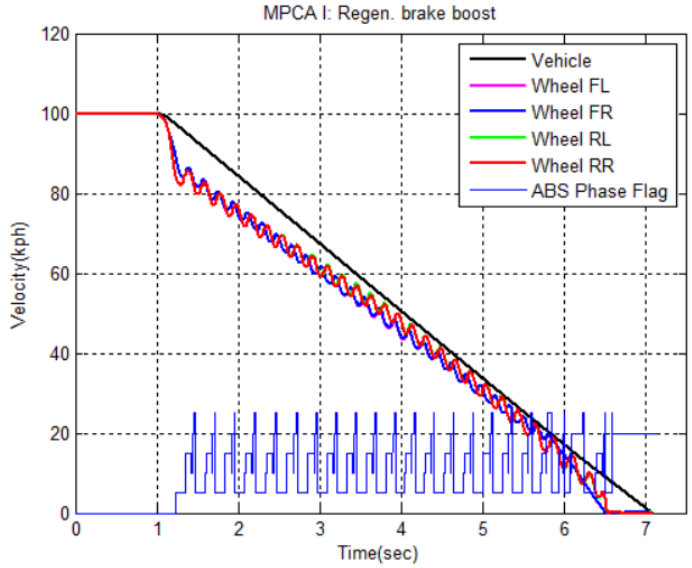

Figure 4.54: Vehicle and wheel velocities for the MPCA I case for μ = 0.5 road surface and the ABS phase flag for the Front Left wheel.

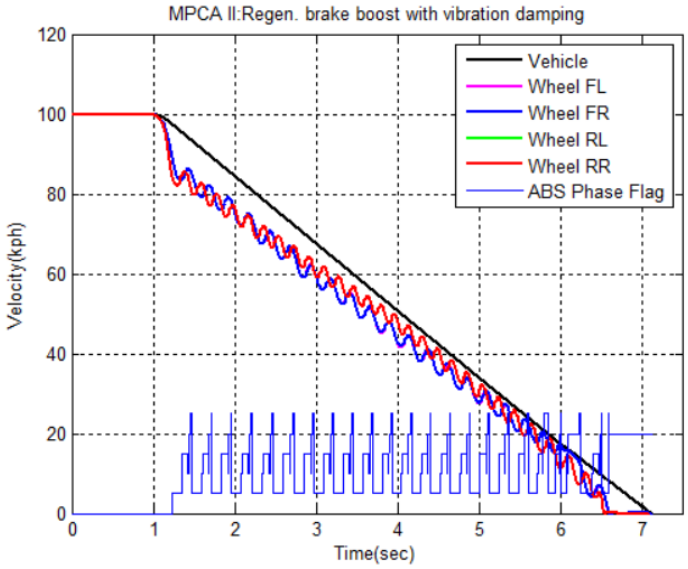

Figure 4.55: Vehicle and wheel velocities for the MPCA II case for μ = 0.5 road surface and the ABS phase flag for the Front Left wheel.

Figures 4.53, 4.54 and 4.55 show the vehicle and wheel velocity responses for the 3 cases. It can be observed from the figures that at t=1sec, when the brakes are applied, the vehicle velocity response starts to decrease, as expected. The wheel velocity response starts to "cycle" as per the brake torque applied at the wheel. These are the typical responses one would expect, when the

ABS is in action. It can further be observed from the plots that the wheel velocity starts to "cycle" around 1.3sec for all the 3 cases. This is the time at which the wheel slip first crosses the reference wheel slip, as can be confirmed from Figure 4.51. The ABS phase flag indicates the cycling of the ABS control, and also confirms the start of ABS control at about 1.3sec Also, the ABS is set to de-activate as the vehicle velocity falls below 10 kph in simulation, and can also be observed from the figures 4.51, 4.53, 4.54 and 4.55.

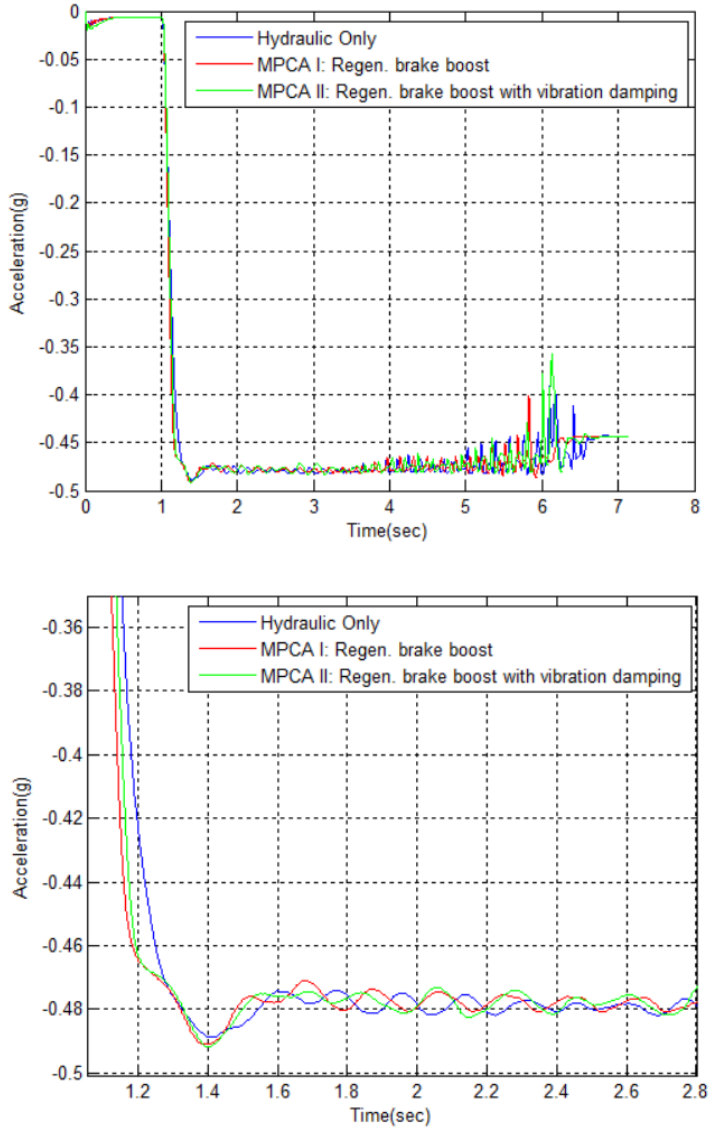

Figure 4.56: Comparison of the vehicle deceleration for the 3 strategies for μ = 0.5 road surface, for Carsim model

Figure 4.56 indicates the vehicle deceleration response for the 3 strategies. It can be observed that the vehicle deceleration for the MPCA cases is more concentrated towards the higher deceleration side. However, as compared to the single wheel model, one cannot conclude from this plot, the effectiveness of the MPCA strategies. This is because the Vehicle deceleration for a full vehicle model is influenced by the brake torques at all its wheels, but regenerative braking (and hence MPCA I and II) is available at only the front wheels as the vehicle in consideration is a front wheel drive.

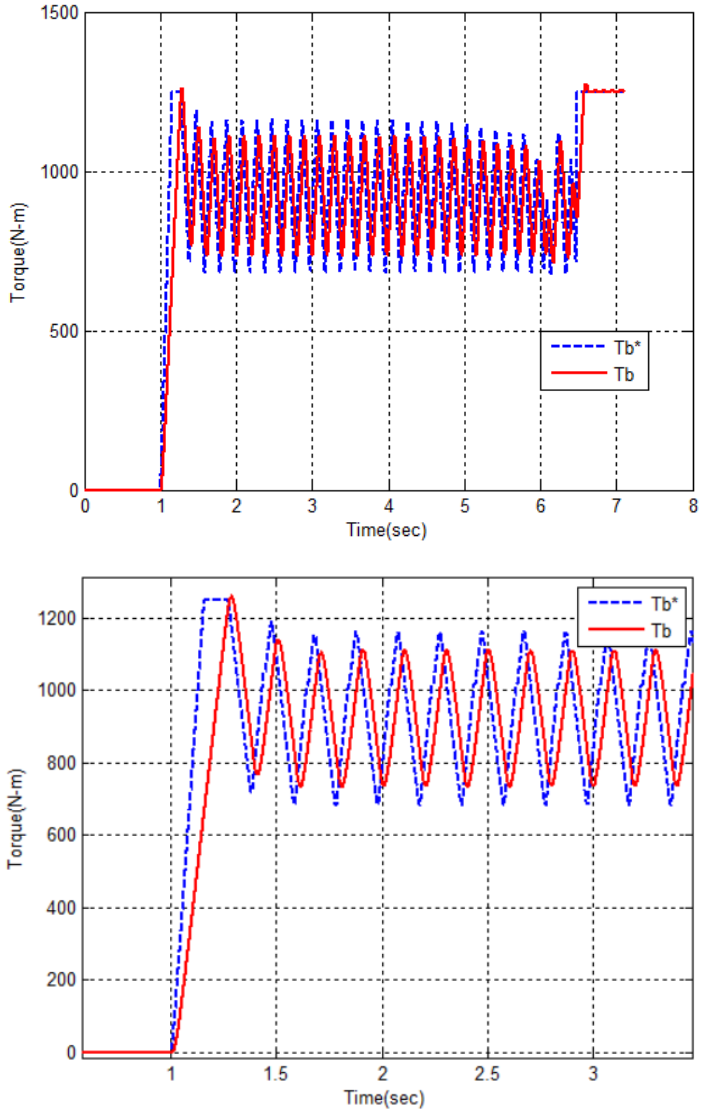

Figure 4.57: Comparison of Brake Torques for the Front left wheel for the hydraulic ABS only case for μ = 0.5 road surface: (Top) entire simulation, and (Bottom) Zoomed in view

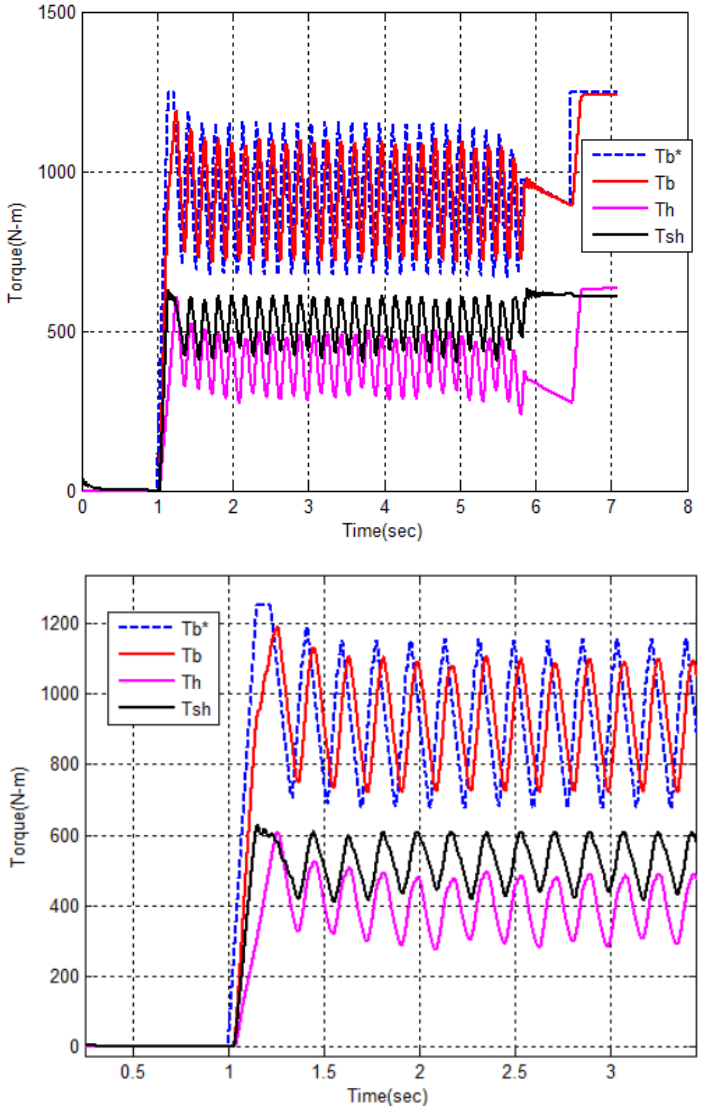

Figure 4.58: Comparison of Brake Torques for the Front left wheel for the MPCA I case for μ = 0.5 road surface: (Top) entire simulation, and (Bottom) Zoomed in view

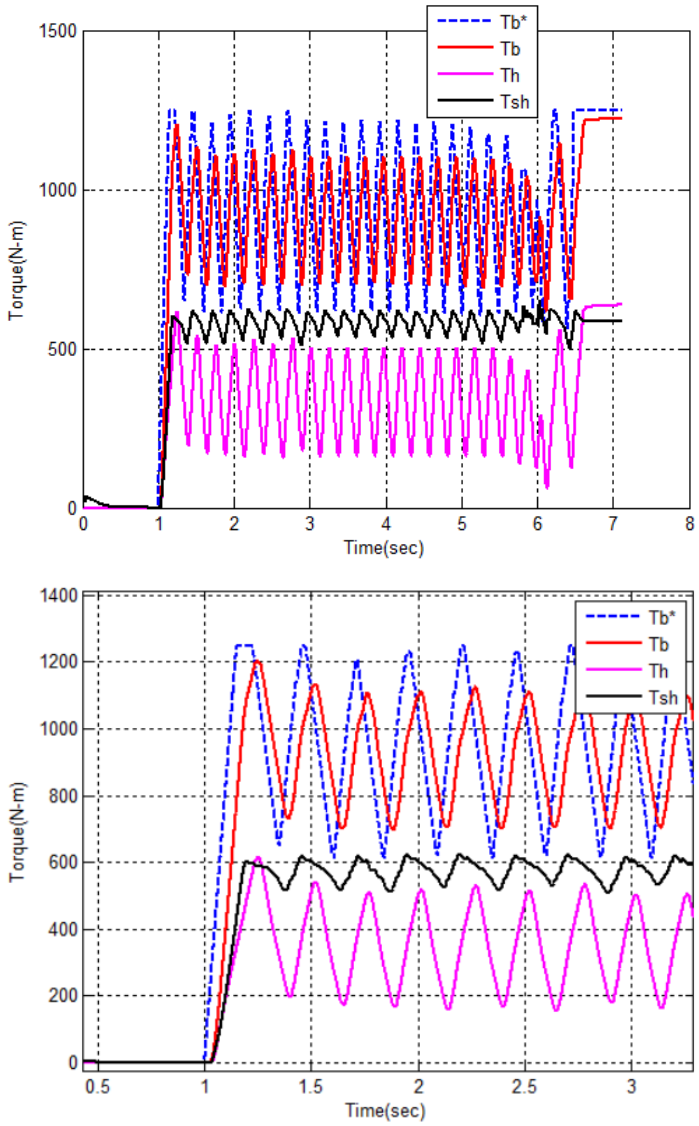

Figure 4.59: Comparison of Brake Torques for the Front left wheel for the MPCA II case for μ = 0.5 road surface: (Top) entire simulation, and (Bottom) Zoomed in view

Figures 4.57, 4.58, and 4.59 indicate the various actuator torques observed in the simulation for μ = 0.5 road condition. Firstly, it can be observed that the total actual torque in all the 3 cases, operate in the same torque range (750~1100 N-m), which imply that the 3 cases are indeed comparable. It can be observed that the total ABS torque modulates slightly faster for the MPCA I and II cases than the hydraulic only case. This is again because of the electric motor extending the bandwidth of the system. The modulation is however, only slightly faster as the addition of shaft dynamics also adds a delay to the regenerative brake torque applied to the wheel. The shaft

dynamics delay, however, does not affect the hydraulic only case, as the hydraulic torque is applied directly at the wheel, and not via the half shaft.

Figure 4.58 shows the brake torques during the ABS operation with MPCA I, where T_b* indicates the demanded brake torque and T_b represents total applied brake torque (sum of the hydraulic brake torque, T_h, and the electric motor torque, T_{sh}. As shown in Figure 4.58, MPCA I effectively allocates the demanded torque based on the bandwidth, in which the electric motor is allocated the high-frequency part of the torque signal and the hydraulic brakes are allocated the low-frequency part of the torque signal. In this case, the control effort is focused on tracking the demanded brake torque (T_b*) with the torque split without considering shaft vibration reduction. The MPC tuning parameters used in this case are: γ_b is set to 110000 and γ_{sh} is set to zero.
Figure 4.59 compares the brake torques during ABS operation with MPCA II. The torque split is not as effective compared to the earlier case since it also considers vibration control. A non-zero-value of γ_{sh} (120000) has been used in the cost function of the MPCA. With that, the hydraulic brakes modulate almost in phase with the regenerative brakes to reduce the shaft vibration, as shown in Figure 4.60. Although it vastly improves the shaft vibration damping, the frequency-based torque split performance has been degraded, and the motor torque is slightly delayed at the start of the simulation. It can be observed that the peak to peak vibrations at the natural frequency of the shaft (around 13 Hz) is reduced in the case of MPCA II.

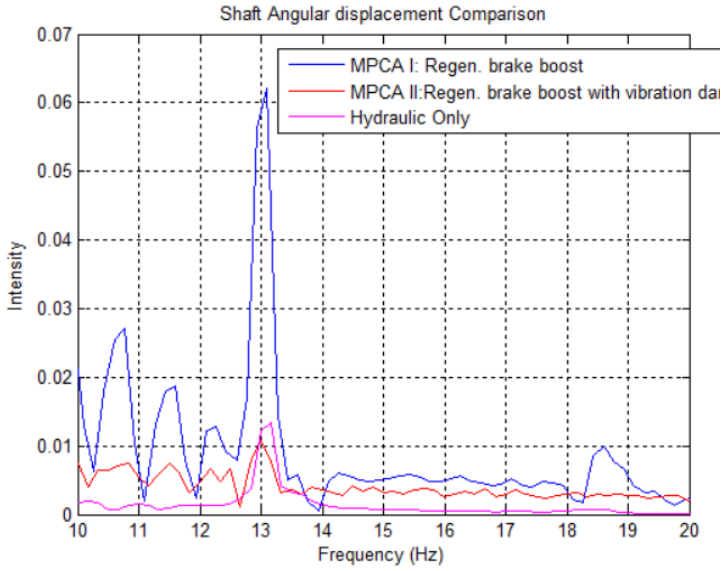

Figure 4.60: Comparison of the FFT of the shaft angular displacement for the Front left wheel for $\mu = 0.5$ road surface.

Hence to summarize, the tuning parameters used in the MPCA II case are: γ_b is set to 110000, and γ_{sh} is set to 120000.

Figures 4.61 and 4.62 show the Normal force response (for the front left wheel) and the vehicle pitch angle response respectively. Initial overshoot of both the responses is due to the forces in the Suspension model of Carsim not reaching steady state. Hence the braking is applied at 1 sec, so that the forces reach steady state and "settle down".

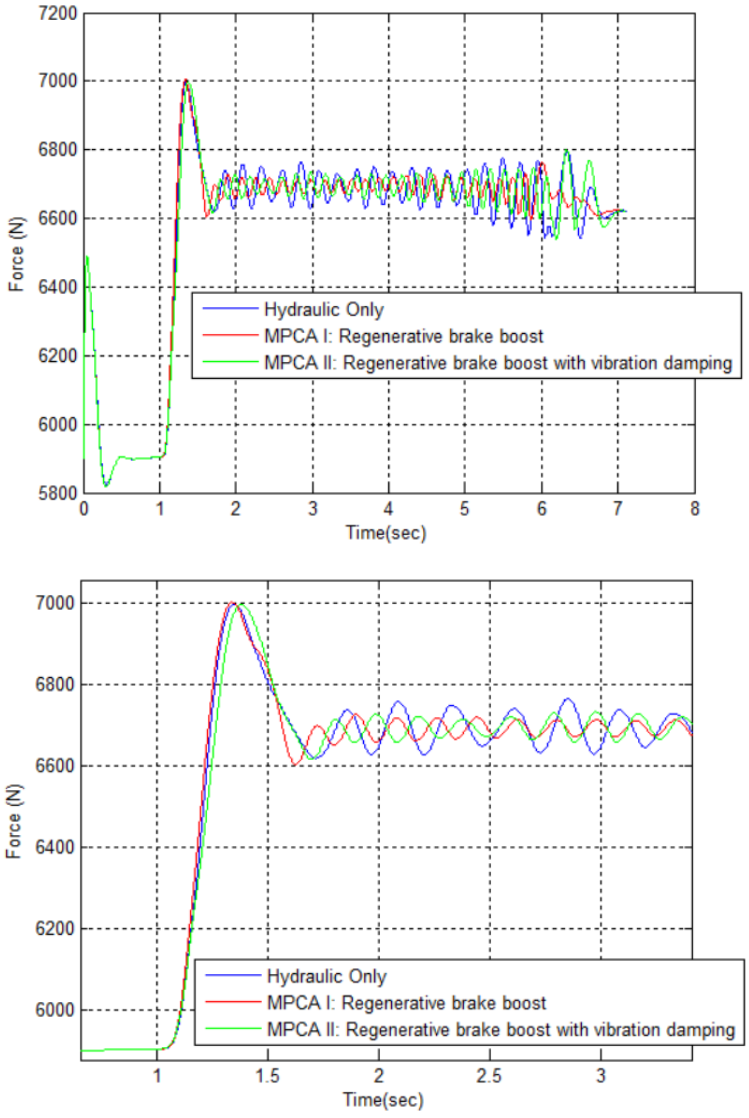

Figure 4.61: Comparison of Tire Normal Force response for the Front left wheel for the 3 strategies for $\mu = 0.5$ road surface: (Top) entire simulation, and (Bottom) Zoomed in view

It is observed that the Peak to Peak magnitude of the variation in Normal force, and pitch angle during ABS activation is least for MPCA II, followed by MPCA I and most for Hydraulic only

case, implying that the MPCA II strategy proposed in this work is successful. This can further be related to a more "comfortable" ride for the occupants in the vehicle, as the peak to peak magnitude of the Pitch angle is decreased in the MPCA II case.

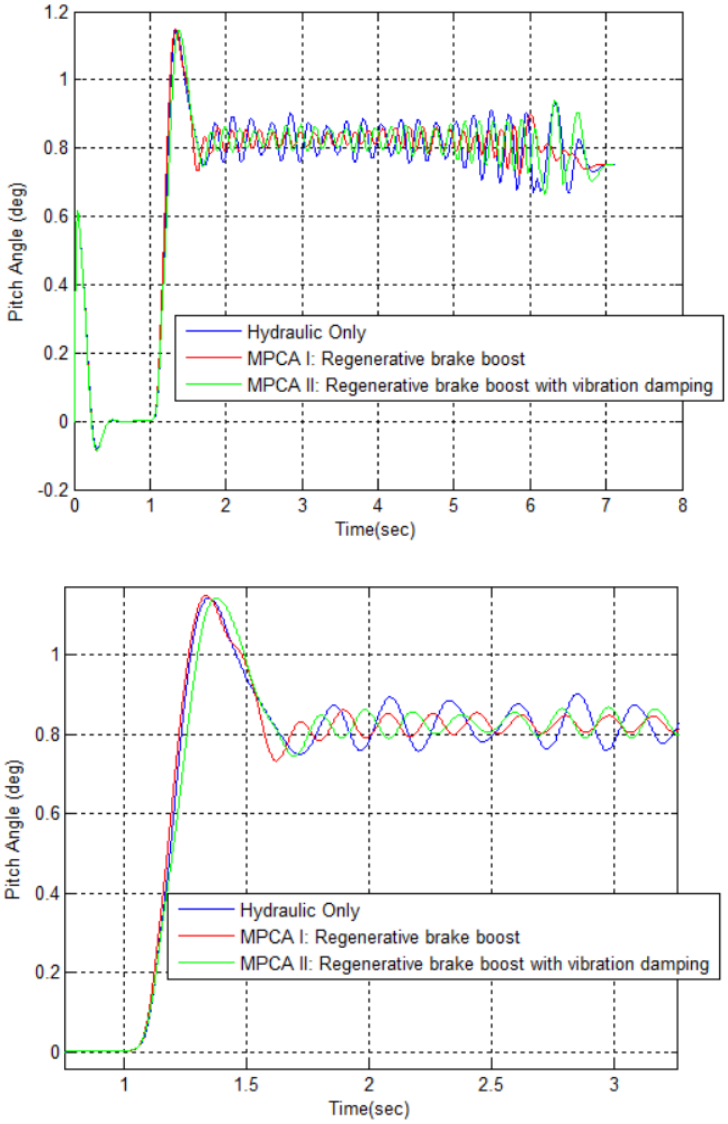

Figure 4.62: Comparison of Vehicle Pitch Angle for the 3 strategies for μ = 0.5 road surface: (Top) entire simulation, and (Bottom) Zoomed in view

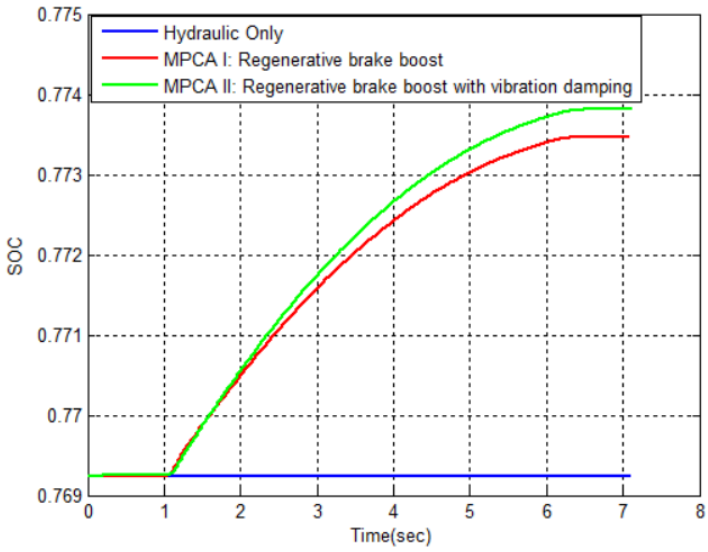

Figure 4.63: Comparison of the Battery SOC Response for μ = 0.5 road surface simulation, for Carsim vehicle model.

Table 4.10: Stopping distance summary for μ = 0.5 case, Carsim

Stopping Distance(m)	Hydraulic Only	MPCA I	MPCA II
During ABS	75.86	74.85	75.30
Overall	85.94	84.73	84.93

The effectiveness of the combined braking strategies over hydraulic strategies can be observed from the stopping distance comparison in Table 4.10. It is observed that due to faster torque modulation in the combined braking torques observed in figures 4.58 and 4.59, as compared to hydraulic only case in Figure 4.57. This leads to slightly faster slip control in Figure 4.51, which further leads to an improvement in stopping distance. Figure 4.63 indicates the comparison of the Battery SoC for the 3 strategies. It is observed that as expected, there is no energy recovered in the Hydraulic only case, while some amount of energy is recovered in the MPCA-I and II cases. This is hence a secondary advantage of implementing MPCA. However, one can argue that energy recovery cannot be a primary objective in the case of emergency braking for two reasons: first, this being a safety-critical control, one must prioritize safety instead of recovered energy, and second: one does not encounter emergency braking situations more often, in order to rely on ABS for energy recovery.

4.2.3 Low μ Test (μ=0.2)

The Single wheel model is simulated as per the simulation conditions described in section 4.1, for a tire-road friction coefficient (μ) of 0.2. In practice this may refer to a snow covered road

surface. In the five phase ABS Logic, the reference wheel deceleration (a_x*) for the low mu case (μ=0.2), is chosen as 1.96 m/s^2.

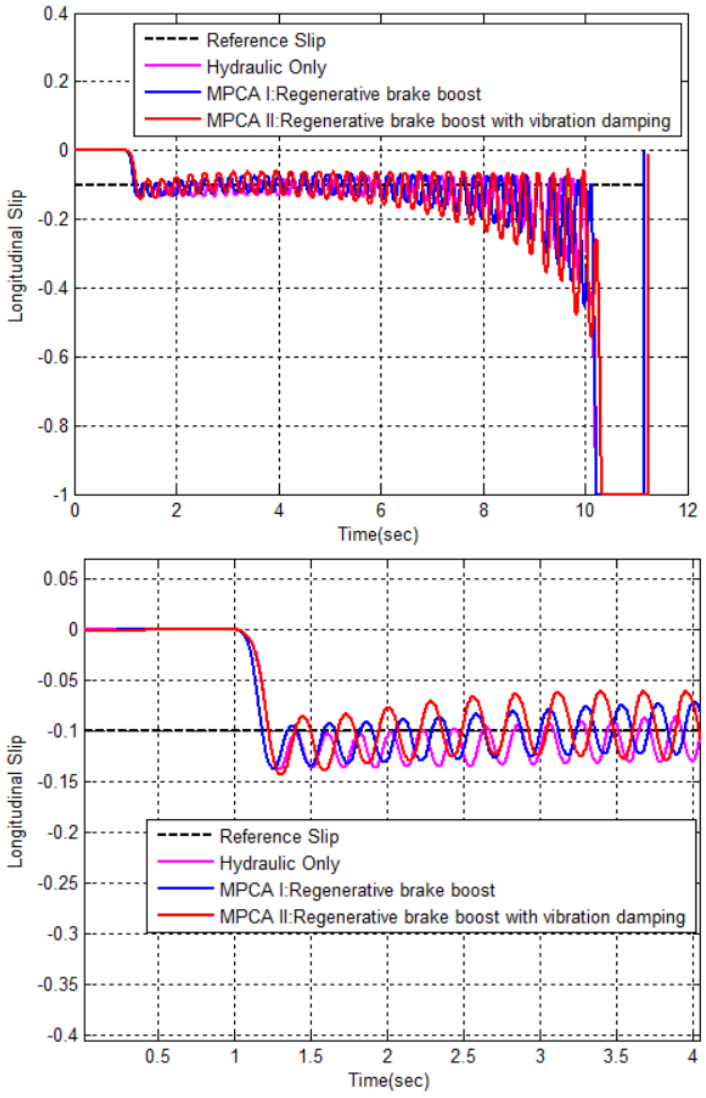

Figure 4.64: Comparison of the vehicle longitudinal slip for the Front left wheel for the 3 strategies for μ = 0.2 road surface: (Top) entire simulation, and (Bottom) Zoomed in view.

The comparison of longitudinal slip in this case is indicated in Figure 4.64. It can be observed that the ABS cycling, i.e. slip tracking is slightly faster for the MPCA I and II cases, as compared to the hydraulic only case. This is mainly because of using electric motor as an actuator during ABS cycling. The inclusion of the electric motor as an additional actuator, effectively extends the bandwidth of the system, and results in relatively faster slip tracking. In Figure 4.65, it can be observed that the range in which the limit cycle operates for the 3 cases is the same.

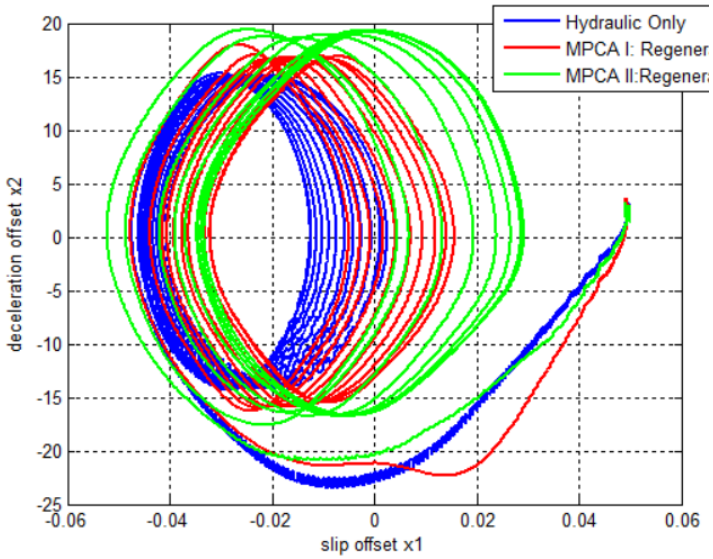

Figure 4.65: Comparison of the ABS limit cycles for the Front left wheel for the 3 strategies for μ = 0.2 road surface.

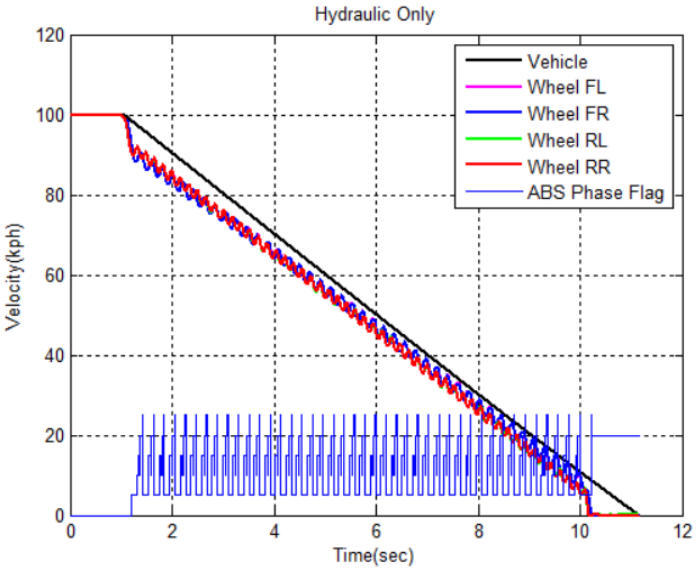

Figure 4.66: Vehicle and wheel velocities for the hydraulic ABS only case for μ = 0.2 road surface and the ABS phase flag for the Front Left wheel.

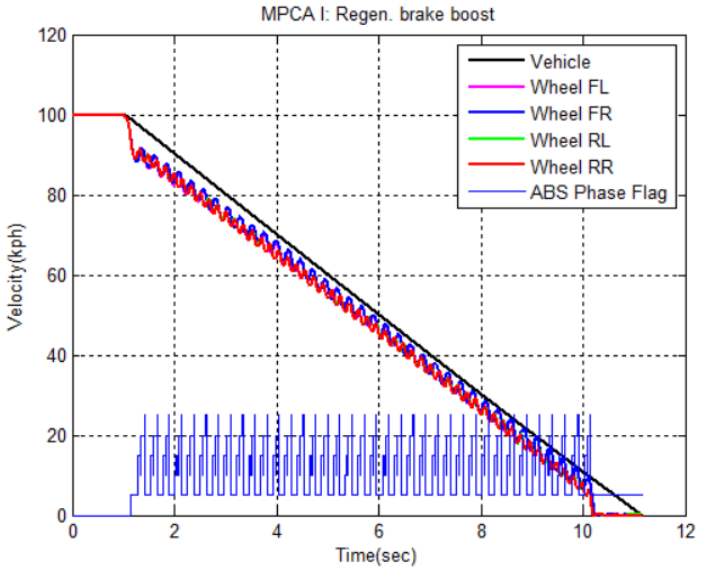

Figure 4.67: Vehicle and wheel velocities for the MPCA I case for μ = 0.2 road surface and the ABS phase flag for the Front Left wheel.

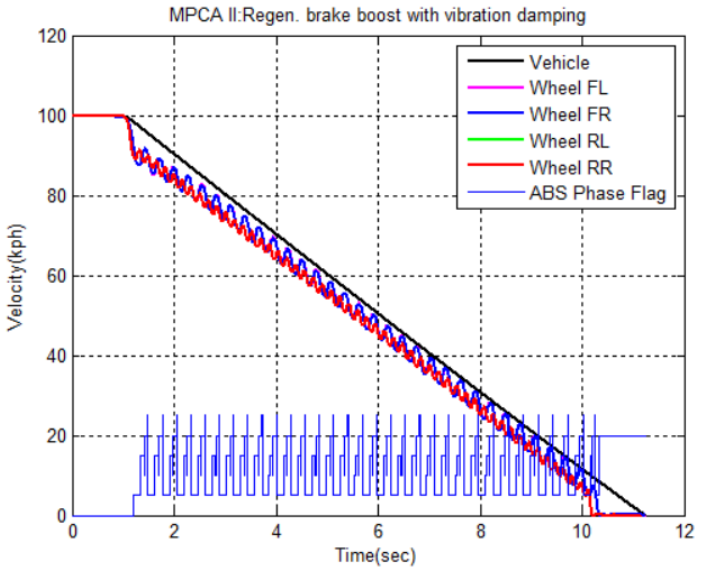

Figure 4.68: Vehicle and wheel velocities for the MPCA II case for μ = 0.2 road surface and the ABS phase flag for the Front Left wheel.

Figures 4.66, 4.67, and 4.68 show the vehicle and wheel velocity responses for the 3 cases. It can be observed from the figures that at t=1sec, when the brakes are applied, the vehicle velocity response starts to decrease, as expected. The wheel velocity response starts to "cycle" as per the brake torque applied at the wheel. These are the typical responses one would expect, when the ABS is in action. It can further be observed from the plots that the wheel velocity starts to "cycle" around 1.25sec for all the 3 cases. This is the time at which the wheel slip first crosses

the reference wheel slip, as can be confirmed from Figure 4.64. The ABS phase flag indicates the cycling of the ABS control, and also confirms the start of ABS control at about 1.25sec Also, the ABS is set to de-activate as the vehicle velocity falls below 10 kph in simulation, and can also be observed from the figures 4.64, 4.66, 4.67 and 4.68.

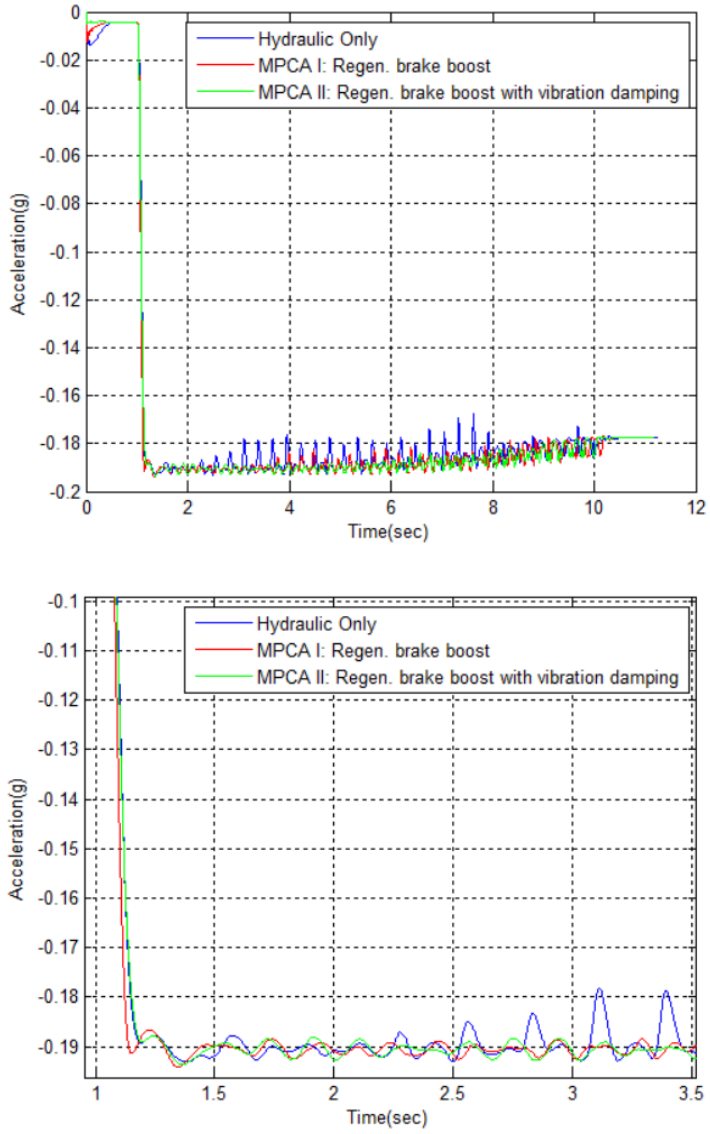

Figure 4.69: Comparison of the vehicle deceleration for the 3 strategies for μ = 0.2 road surface, for Carsim model

Figure 4.69 indicates the vehicle deceleration response for the 3 strategies. It can be observed that the vehicle deceleration for the MPCA cases is more concentrated towards the higher deceleration side. However, as compared to the single wheel model, one cannot conclude from

this plot, the effectiveness of the MPCA strategies. This is because the Vehicle deceleration for a full vehicle model is influenced by the brake torques at all its wheels, but regenerative braking (and hence MPCA I and II) is available at only the front wheels as the vehicle in consideration is a front wheel drive.

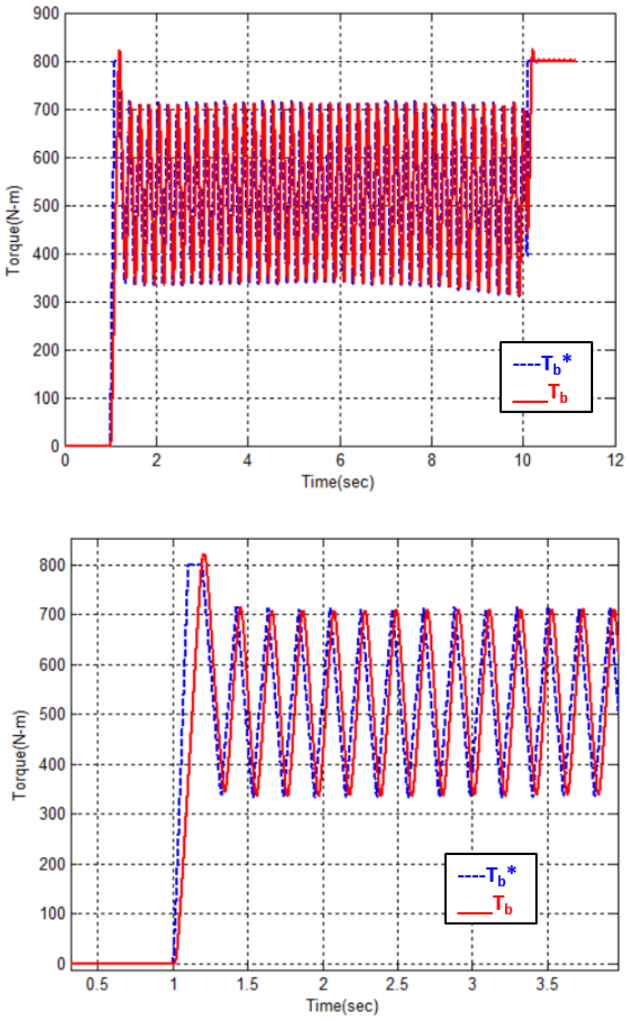

Figure 4.70: Comparison of Brake Torques for the hydraulic ABS only case for the Front left wheel for μ = 0.2 road surface: (Top) entire simulation, and (Bottom) Zoomed in view

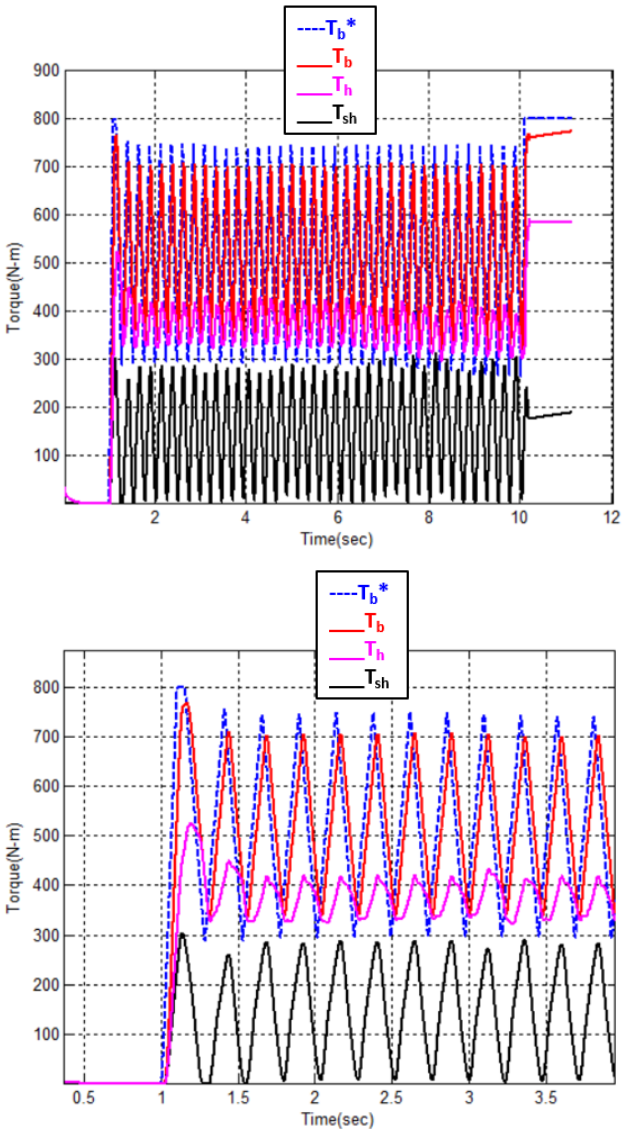

Figure 4.71: Comparison of Brake Torques for the Front left wheel for the MPCA I case for μ = 0.2 road surface: (Top) entire simulation, and (Bottom) Zoomed in view

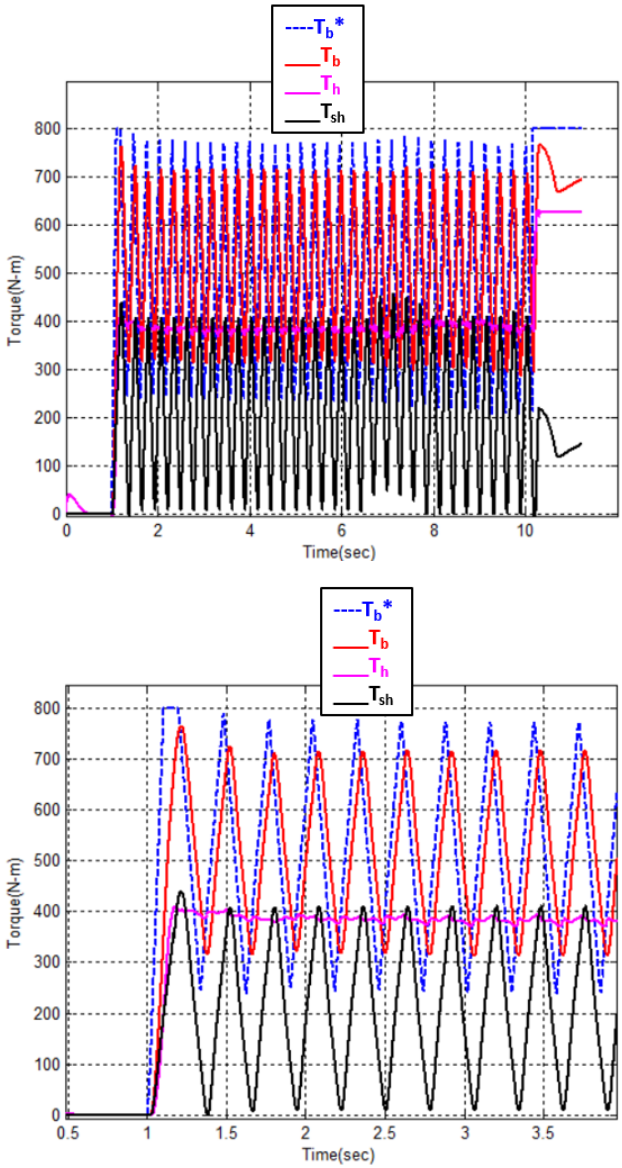

Figure 4.72: Comparison of Brake Torques for the Front left wheel for the MPCA II case for μ = 0.2 road surface: (Top) entire simulation, and (Bottom) Zoomed in view

Figures 4.70, 4.71, and 4.72 indicate the various actuator torques observed in the simulation for μ = 0.2 road condition. Firstly, it can be observed that the total actual torque in all the 3 cases, operate in the same torque range (300~700 N-m), which imply that the 3 cases are indeed comparable. It can be observed that the total ABS torque modulates slightly faster for the MPCA I and II cases than the hydraulic only case. This is again because of the electric motor extending the bandwidth of the system. The modulation is however, only slightly faster as the addition of shaft dynamics also adds a delay to the regenerative brake torque applied to the wheel. The shaft

dynamics delay, however, does not affect the hydraulic only case, as the hydraulic torque is applied directly at the wheel, and not via the half shaft.

Figure 4.71 shows the brake torques during the ABS operation with MPCA I, where T_b* indicates the demanded brake torque and T_b represents total applied brake torque (sum of the hydraulic brake torque, T_h, and the electric motor torque, T_{sh}. As shown in Figure 4.71, MPCA I effectively allocates the demanded torque based on the bandwidth, in which the electric motor is allocated the high-frequency part of the torque signal and the hydraulic brakes are allocated the low-frequency part of the torque signal. In this case, the control effort is focused on tracking the demanded brake torque (T_b *) with the torque split without considering shaft vibration reduction. The MPC tuning parameters used in this case are: γ_b is set to 130000 and γ_{sh} is set to zero.
Figure 4.72 compares the brake torques during ABS operation with MPCA II. The torque split is not as effective compared to the earlier case since it also considers vibration control. A non-zero-value of γ_{sh} (140000) has been used in the cost function of the MPCA. With that, the hydraulic brakes modulate almost in phase with the regenerative brakes to reduce the shaft vibration, as shown in Figure 4.73. Although it vastly improves the shaft vibration damping, the frequency-based torque split performance has been degraded, and the motor torque is slightly delayed at the start of the simulation. It can be observed that the peak to peak vibrations at the natural frequency of the shaft (around 13 Hz) is reduced in the case of MPCA II.

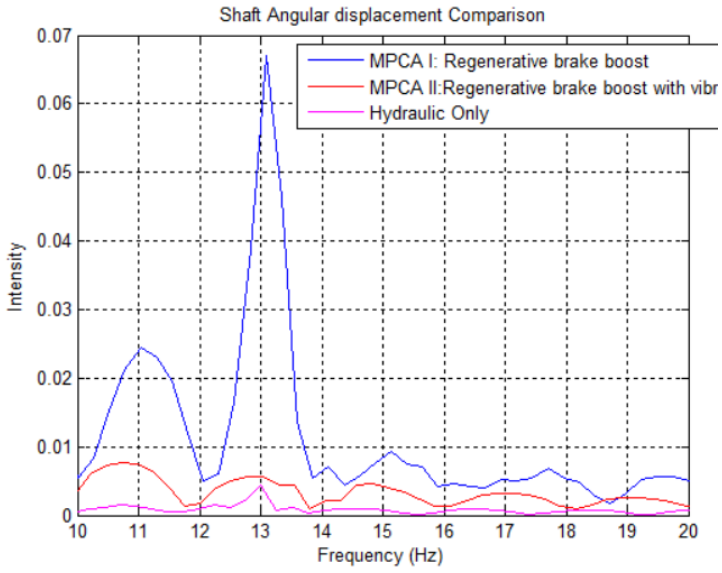

Figure 4.73: Comparison of the FFT of the shaft angular displacement for the Front left wheel for $\mu = 0.2$ road surface.

Hence to summarize, the tuning parameters used in the MPCA II case are: γ_b is set to 130000, and γ_{sh} is set to 140000.

Figures 4.74 and 4.75 show the Normal force response (for the front left wheel) and the vehicle pitch angle response respectively. Initial overshoot of both the responses is due to the forces in the Suspension model of Carsim not reaching steady state. Hence the braking is applied at 1 sec, so that the forces reach steady state and "settle down".

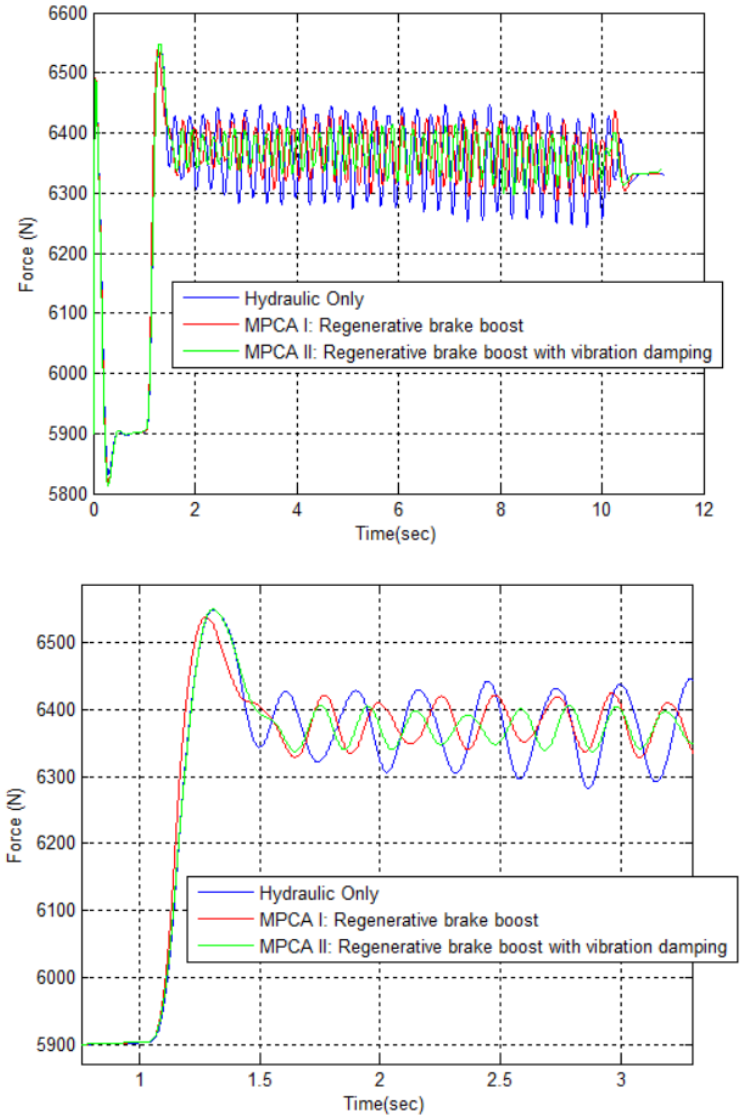

Figure 4.74: Comparison of Tire Normal Force response for the Front left wheel for the 3 strategies for $\mu = 0.2$ road surface: (Top) entire simulation, and (Bottom) Zoomed in view

It is observed that the Peak to Peak magnitude of the variation in Normal force, and pitch angle during ABS activation is least for MPCA II, followed by MPCA I and most for Hydraulic only

case, implying that the MPCA II strategy proposed in this work is successful. This can further be related to a more "comfortable" ride for the occupants in the vehicle, as the peak to peak magnitude of the Pitch angle is decreased in the MPCA II case.

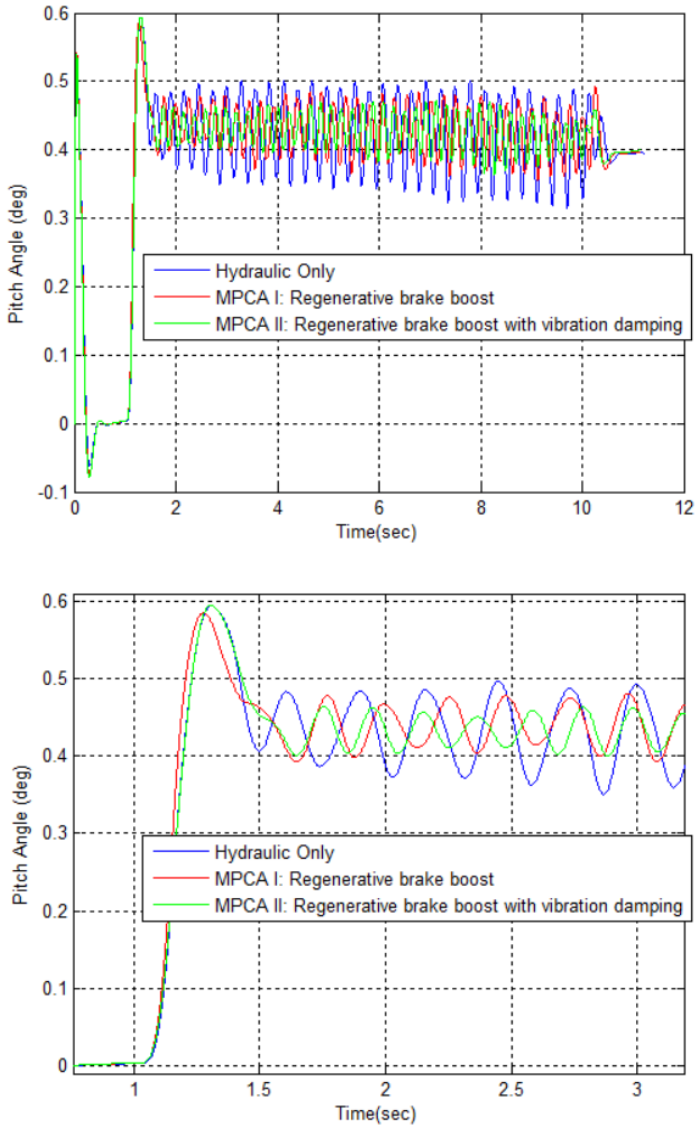

Figure 4.75: Comparison of Vehicle Pitch Angle for the 3 strategies for μ = 0.2 road surface: (Top) entire simulation, and (Bottom) Zoomed in view

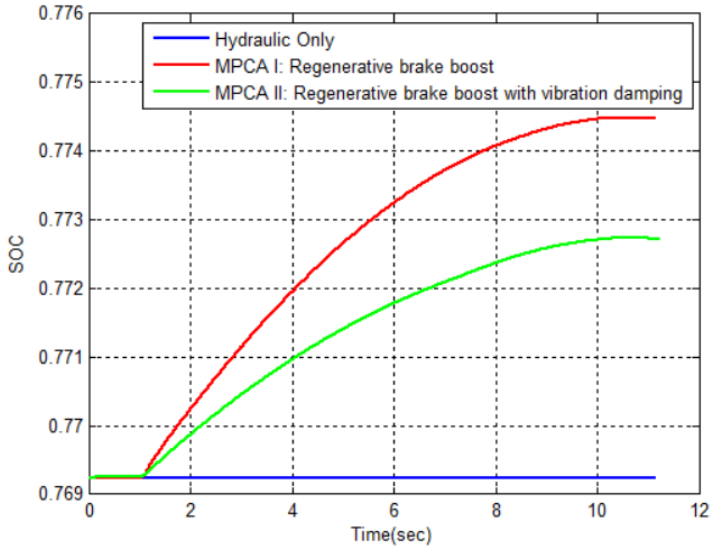

Figure 4.76: Comparison of the Battery SOC Response for μ = 0.2 road surface simulation, for Carsim vehicle model.

Table 4.11: Stopping distance summary for μ = 0.2 case, Carsim

Stopping Distance(m)	Hydraulic Only	MPCA I	MPCA II
During ABS	153.2	151.1	151.9
Overall	168.1	166.3	167.01

The effectiveness of the combined braking strategies over hydraulic strategies can be observed from the stopping distance comparison in Table 4.11. It is observed that due to faster torque modulation in the combined braking torques observed in figures 4.71 and 4.72, as compared to hydraulic only case in Figure 4.70. This leads to slightly faster slip control in Figure 4.64, which further leads to an improvement in stopping distance. Figure 4.76 indicates the comparison of the Battery SoC for the 3 strategies. It is observed that as expected, there is no energy recovered in the Hydraulic only case, while some amount of energy is recovered in the MPCA-I and II cases. This is hence a secondary advantage of implementing MPCA. However, one can argue that energy recovery cannot be a primary objective in the case of emergency braking for two reasons: first, this being a safety-critical control, one must prioritize safety instead of recovered energy, and second: one does not encounter emergency braking situations more often, in order to rely on ABS for energy recovery.

As indicated in Table 4.12, the stopping distance in the case of MPCA I is the lowest, followed by MPCA II and then hydraulic only case. This is majorly because of the fact that in the MPCA I

case, the control objective is to minimize the error in the total torque, based on the bandwidths of the actuators. The vibration damping gain in this case is zero.

Table 4.12: Stopping distance comparison: Summary of all cases

	Stopping Distance (m)	μ=0.9		μ=0.5		μ=0.2	
		During ABS	Overall	During ABS	Overall	During ABS	Overall
Single Wheel Model	Hydraulic Only	39.02	50.97	73.86	84.54	151.3	165.2
	MPCA I	37.95	49.77	72.96	83.53	147.4	162.3
	MPCA II	38.42	49.94	73.29	83.73	148.4	163.5
Carsim	Hydraulic Only	37.09	51.56	75.86	85.94	153.2	168.1
	MPCA I	35.77	50.00	74.85	84.73	151.1	166.3
	MPCA II	36.07	50.42	75.30	84.93	151.9	167.01

This results in tighter slip control as can be observed in Figures 4.4, 4.15, 4.26, 4.38, 4.51, and 4.64. However, in MPCA II, due to addition of the vibration control objective, the motor torque is slightly delayed, which results in a shorter stopping distance, but also effectively reduces the vibrations in the shaft, as indicated in the FFT plots in figures 4.13, 4.24, 4.35 4.48 4.61, and 4.73. Hence the proposed MPCA strategy in this work, not only reduces the half shaft vibrations, but also reduce the stopping distance, as compared to the MPCA I and hydraulic only cases respectively. It can be observed that there is close to a meter improvement in stopping distance using MPCA I in all cases, and 1.5 to 1.05 m improvement in stopping distance, and reduction in vibrations in the MPCA II case. The MPCA I performance for the 0.2 mu single wheel case is ideal, as compared to other simulations (high mu and mid mu cases). The reason for this is that the Desired Total ABS brake torque (T_b* in the previous slides) is below the maximum rated torque of the motor (T_b*~ 600 N-m and $T_{motormax}$=630 Nm). This allows the ABS to modulate faster, and hence results in a smaller limit cycle.

Chapter 5: Conclusion and Future Work

5.1 CONCLUSION

In this work, a model predictive control based brake torque allocation strategy for hydraulic and regenerative brakes during ABS operation, is proposed. The mathematical model of the system was described, which included: dynamic model of the hydraulic brakes, regenerative brakes, single wheel vehicle model, and Carsim vehicle model. The five phase ABS control strategy, and decoupled PMSM control were adopted in this work for literature. Model Predictive control system was then mathematically formulated, and applied in this work via the Matlab MPC toolbox. The plant model of MPCA: hydraulic and regenerative brakes were approximated with second order dynamics. The MPCA strategy proposed in this work is different from other strategies in literature, as it explicitly incorporates the half-shaft dynamics in to the plant model, and the cost function is subsequently modified, by including an additional weighted error, in order to reduce shaft vibrations. The effect of the additional weighted error was then discussed through simulation with a sample Pseudo Random Binary sequence. This work is applicable for HEVs, in which the motor torque is applied to the wheel via half-shafts. The developed control strategy is then simulated with an Anti-lock Brake System (ABS) module, and the system is co-simulated with a quarter car model and a full carsim model, for different road surfaces (μ=0.9, 0.5, 0.2) . The results show that the proposed MPCA scheme is effective in reducing the half shaft vibrations, and also reduces the stopping distance. The proposed strategy performs well in all road conditions, thus proving its robustness in different operating conditions.

5.2 FUTURE WORK AND RECOMMENDATIONS:

Model predictive control allocation has a wide variety of applications, especially in the aeronautical field, and has been a promising strategy in the automotive field as well, since the number of actuators/sensors in a vehicle has increased over the last decade. This section lists the specific application of model predictive control allocation in automobiles. The following are the possible methods of extending this work:

5.2.1 MPCA for ESC applications.

Almost all vehicles today are equipped with electronic stability control (ESC) which is responsible for maintaining the stability of the vehicle, in situations where there is a loss of steering-control. In general, the objective of ESC can be achieved in a number of way: differential braking, active steering, and using traction torque in the case of all-wheel drive vehicles [70]. This research work of MPCA of the brake torque during ABS activation can be directly extended for ESC applications involving differential braking.

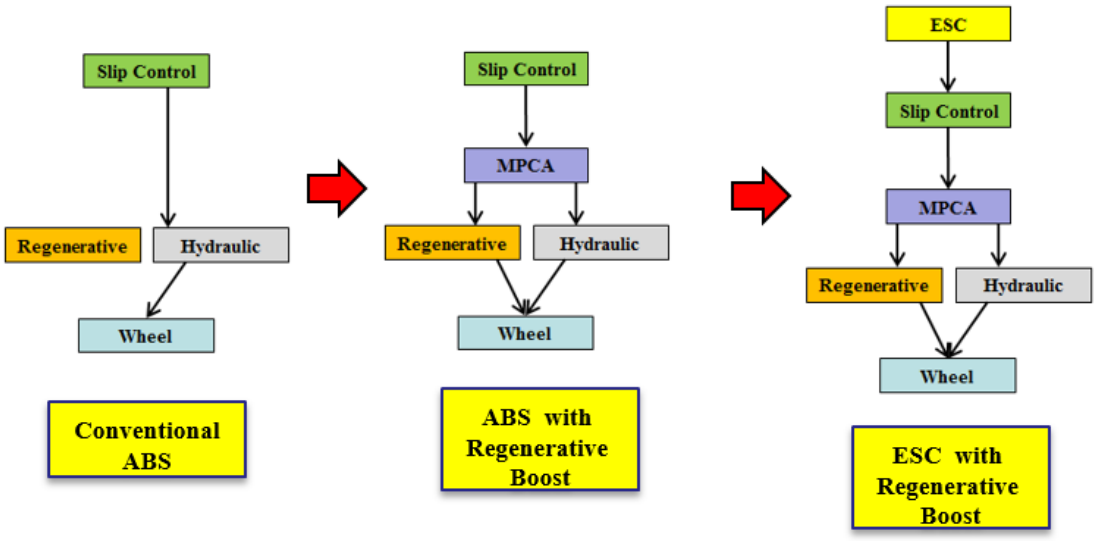

Figure 5.1: Future research trend for inclusion of ESC in MPCA application.

As indicated in Figure 5.1, conventional ABS only involved using the hydraulic brakes as the primary actuators, while in this work, ABS with regenerative brake boost was implemented. As discussed before, this work is limited to using MPCA with ABS for straight line maneuvers. In order to use slip control for maneuvers involving steering input, one must include an upper level control of ESC as shown in Figure 5.1. This aspect of MPCA extension is applicable to

EV/HEVs with electric motor fitted on all wheels, i.e. an all-wheel drive vehicle with in-wheel motors.

5.2.2 MPCA for traction control applications.

Anti-lock brake system and traction control system fall into the same category of vehicle dynamics control system called the slip control systems. Anti-lock brakes involve regulation of vehicle slip when the vehicle is decelerating (i.e. Brake is applied), whereas traction control systems involve regulation of wheel slip when the vehicle is accelerating.

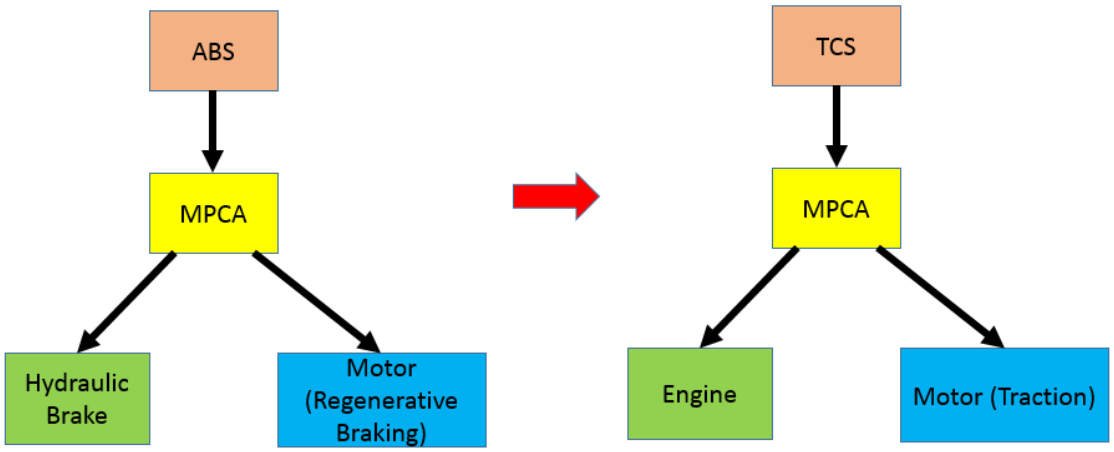

Figure 5.2: Extending the MPCA application for TCS

In the case of traction control for HEVs, we have two actuators which can be used: i.e. the motor and the Engine. The modulating acceleration torque for TCS can be achieved by allocating the high frequency part of the torque to the traction motor, and the low frequency part to the engine.

References

1. Rosenberger, M., Uhlig, R., Koch, T., and Lienkamp, M., "Combining Regenerative Braking and Anti-Lock Braking for Enhanced Braking Performance and Efficiency," SAE Technical Paper 2012-01-0234, 2012, doi: 10.4271/2012-01-0234.
2. Satzger, C.; de Castro, R.; Bunte, T., "A model predictive control allocation approach to hybrid braking of electric vehicles," Intelligent Vehicles Symposium Proceedings, 2014 IEEE , vol., no., pp.286,292, 8-11 June 2014.
3. Ricardo de Castro, Rui E. Araújo , Mara Tanelli , Sergio M. Savaresi & Diamantino Freitas (2012) "Torque blending and wheel slip control in EVs with in-wheel motors", Vehicle System Dynamics: International Journal of Vehicle Mechanics and Mobility, 50:sup1, 71-94.
4. Kim, D. H., et al. "Optimal brake torque distribution for a four-wheel drive hybrid electric vehicle stability enhancement." Proceedings of the Institution of Mechanical Engineers, Part D: Journal of Automobile Engineering 221.11 (2007): 1357-1366.
5. Zhang, Junzhi, et al. "Optimization of control strategy for regenerative braking of an electrified bus equipped with an anti-lock braking system." Proceedings of the Institution of Mechanical Engineers, Part D: Journal of Automobile Engineering (2011): 0954407011422463.
6. Luo, Yu, et al. "Model predictive dynamic control allocation with actuator dynamics." American Control Conference, 2004. Proceedings of the 2004. Vol. 2. IEEE, 2004.
7. Johansen, Tor A., and Thor I. Fossen. "Control allocation—A survey." Automatica 49.5 (2013): 1087-1103.
8. Härkegård, Ola. "Dynamic control allocation using constrained quadratic programming." Journal of Guidance, Control, and Dynamics 27.6 (2004): 1028-1034.
9. Härkegård, Ola. "Dynamic control allocation using constrained quadratic programming." Journal of Guidance, Control, and Dynamics 27.6 (2004): 1028-1034.
10. Knobel, Christian, Alfred Pruckner, and Tilman Bünte. "Optimized Force Allocation." Proceedings of the 4th IFAC Symposium on Mechatronic Systems. 2006.
11. Härkegård, Ola. "Backstepping and control allocation with applications to flight control." PhD Dissertation 2003 .
12. Plumlee, John H., David M. Bevly, and A. Scottedward Hodel. "Control allocation in ground vehicles." International journal of vehicle design 42.3 (2006): 215-243.

13. Hanger, M. B. (2011). Model Predictive Control Allocation. (Student paper). Norges teknisk-naturvitenskapelige universitet Institutt for teknisk kybernetikk.

14. Laine, Leo, and Jonas Fredriksson. "Traction and braking of hybrid electric vehicles using control allocation." International journal of vehicle design 48.3 (2008): 271-298.

15. Qin, Gang, et al. "Torque allocation strategy of 4WID in-wheel motor electric vehicle based on objective optimization." American Control Conference (ACC), 2014. IEEE, 2014.

16. Huang, Xiaoyu, and Junmin Wang. "Model predictive regenerative braking control for lightweight electric vehicles with in-wheel motors." Proceedings of the Institution of Mechanical Engineers, Part D: Journal of Automobile Engineering 226.9 (2012): 1220-1232.

17. Xiaoyu Huang; Junmin Wang, "Nonlinear model predictive control for improving energy recovery for electric vehicles during regenerative braking," Decision and Control and European Control Conference (CDC-ECC), 2011 50th IEEE Conference on , vol., no., pp.7458,7463, 12-15 Dec. 2011

18. Lu, Zijia, et al. "MPC-based torque distribution strategy for energy management of power-split hybrid electric vehicles." Control Conference (CCC), 2013 32nd Chinese. IEEE, 2013.

19. Fang-Chieh Chou; Kang Li; Lih-Wei Jeng; Cheng-Ho Li, "Model predictive control based optimal torque distribution strategy for a compound electric vehicle," Automatic Control Conference (CACS), 2013 CACS International , vol., no., pp.417,422, 2-4 Dec. 2013.

20. G. Le Solliec, A. Chasse, J. Van-Frank, D. Walser, "Dual Mode Vehicle with In-Wheel Motor: Regenerative Braking Optimization" Oil Gas Sci. Technol. – Rev. IFP Energies nouvelles 68 (1) 95-108 (2013).

21. Jihun Han, Youngjin Park, Youn-sik Park, "Co-operative regenerative braking control strategy considering nonlinear tire characteristic in front wheel drive hybrid electric vehicle", SAE 2011, 2011-39-7209.

22. Jan Fischer-Wolfarth, Gereon Meyer, "Advanced Microsystems for Automotive Applications 2013: Smart Systems for Safe and Green Vehicles" Springer Science & Business Media, 2013, ISBN: 331900476X, 9783319004761.

23. Wang, F., and B. Zhuo. "Regenerative braking strategy for hybrid electric vehicles based on regenerative torque optimization control." Proceedings of the Institution of Mechanical Engineers, Part D: Journal of Automobile Engineering 222.4 (2008): 499-513.

24. Jingming, Zhang, Song Baoyu, and Niu Xiaojing. "Optimization of parallel regenerative braking control strategy." Vehicle Power and Propulsion Conference, 2008. VPPC'08. IEEE. IEEE, 2008.

25. Xiaohua Zeng; Te Ba; Qingnian Wang; Xiaodong Qu; Dafeng Song, "A kind of accurately Optimized braking energy distribution strategy applied to switched Series-parallel Hybrid Electric Bus," Artificial Intelligence, Management Science and Electronic Commerce (AIMSEC), 2011 2nd International Conference on , vol., no., pp.3634,3637, 8-10 Aug. 2011

26. Jingang Guo; Junping Wang; Binggang Cao, "Study on Braking Force Distribution of Electric Vehicles," Power and Energy Engineering Conference, 2009. APPEEC 2009. Asia-Pacific , vol., no., pp.1,4, 27-31 March 2009.

27. Bottiglione, Francesco, Aldo Sorniotti, and Leo Shead. "The effect of half-shaft torsion dynamics on the performance of a traction control system for electric vehicles." Proceedings of the Institution of Mechanical Engineers, Part D: Journal of Automobile Engineering (2012): 0954407012440526.

28. Kou, Y. and Weslati, F., "Development of a Hybrid Powertrain Active Damping Control System via Sliding Mode Control Scheme," SAE Technical Paper 2013-01-0486, 2013, doi:10.4271/2013-01-0486.

29. Couderc, P., Callenaere, J., Der Hagopian, J., Ferraris, G., Kassai, A., Borjesson, Y., & Gaimard, S. (1998). Vehicle driveline dynamic behaviour: experimentation and simulation. Journal of sound and vibration, 218(1), 133-157.

30. Yongsoon Yoon; Youngse An; Youngjoo Park; Kim, H.J., "Model predictive control for drivability enhancement with input dead-segment," Control Automation and Systems (ICCAS), 2010 International Conference on , vol., no., pp.916,921, 27-30 Oct. 2010

31. Cychowski, M. T., and Krzysztof Szabat. "Efficient real-time model predictive control of the drive system with elastic transmission." IET control theory & applications 4.1 (2010): 37-49.

32. Baumann, J., Torkzadeh, D. D., Ramstein, A., Kiencke, U., & Schlegl, T. (2006). Model-based predictive anti-jerk control. Control engineering practice, 14(3), 259-266.

33. BUDACIU C., LAZĂR C., "Predictive control strategy in delta domain for damping oscillations in driveline system" , Buletinul Institutului Politehnic din Iaşi, Secţia Automatică şi Calculatoare, 2011, LVII (LXI), 4, 33–42.

34. Caruntu, Constantin Florin, et al. "A predictive control solution for driveline oscillations damping." Proceedings of the 14th international conference on Hybrid systems: computation and control. ACM, 2011.

35. G. Tak´acs and B. Rohal'-Ilkiv, "Model predictive control algorithms for active vibration control: a study on timing, performance and implementation properties," Journal of Vibration and Control, 2013.

36. L. Webersinke, D. Feth, M. Hertweck, A. von Vietinghoff, U. Kiencke, "Optimization of heavy truck's driveline performance via model predictive control rated by a comfort evaluation algorithm," IFAC World Congress, Seoul, Korea, June, 2008.

37. Cychowski, M.; Cuong Do; Serkies, P.; Szabat, K., "Position tracking in electrical drives with elastic coupling using model predictive control," IECON 2010 - 36th Annual Conference on IEEE Industrial Electronics Society , vol., no., pp.956,961, 7-10 Nov. 2010

38. Szabat, K.; Serkies, P.; Cychowski, M., "Application of the MPC to the robust control of the two-mass drive system," Industrial Electronics (ISIE), 2011 IEEE International Symposium on , vol., no., pp.1901,1906, 27-30 June 2011

39. Serkies, Piotr J., and Krzysztof Szabat. "Application of the MPC to the position control of the two-mass drive system." Industrial Electronics, IEEE Transactions on 60.9 (2013): 3679-3688.

40. Serkies, P.; Orlowska-Kowalska, T.; Cychowski, M.; Szabat, K., "Robust model predictive speed control of the drive system with an elastic joint," EUROCON - International Conference on Computer as a Tool (EUROCON), 2011 IEEE , vol., no., pp.1,4, 27-29 April 2011

41. Szabat, K.; Serkies, P.; Nalepa, R.; Cychowski, M., "Predictive position control of elastic dual-mass drives under torque and speed constraints," Power Electronics and Motion Control Conference (EPE/PEMC), 2010 14th International , vol., no., pp.T5-79,T5-83, 6-8 Sept. 2010

42. Cychowski, M.; Jaskiewicz, R.; Szabat, K., "Model Predictive Control of an elastic three-mass drive system with torque constraints," Industrial Technology (ICIT), 2010 IEEE International Conference on , vol., no., pp.379,385, 14-17 March 2010

43. Cychowski, M.; Szabat, K.; Orlowska-Kowalska, T., "Constrained Model Predictive Control of the Drive System With Mechanical Elasticity," Industrial Electronics, IEEE Transactions on , vol.56, no.6, pp.1963,1973, June 2009

44. Cychowski, M.; Serkies, P.; Nalepa, R.; Szabat, K., "Model predictive speed and vibration control of dual-inertia PMSM Drives," Industrial Electronics (ISIE), 2011 IEEE International Symposium on , vol., no., pp.1919,1924, 27-30 June 2011

45. Lu Xiaohui; Chen Hong; Zhang Huayu; Wang Ping; Gao Bingzhao, "Design of model predictive controller for anti-jerk during tip-in/out process of vehicles," Control Conference (CCC), 2011 30th Chinese , vol., no., pp.3395,3400, 22-24 July 2011

46. Amann, Notker, J. Bocker, and Franz Prenner. "Active damping of drive train oscillations for an electrically driven vehicle." Mechatronics, IEEE/ASME Transactions on 9.4 (2004): 697-700.

47. J.B¨ocker, N.Amann, B.Schulz,"Active Suppression of Torsional Oscillations", 3rd IFAC Symposium on Mechatronic Systems, Sydney, Sept. 2004.

48. Cychowski, M.; Szabat, K., "Model predictive speed control with optimal torque constraints handling of drive systems with elastic transmission," Electric Machines and Drives Conference, 2009. IEMDC '09. IEEE International , vol., no., pp.251,258, 3-6 May 2009

49. Kim, Yong Seok, et al. "Anti-jerk controller design with a cooperative control strategy in hybrid electric vehicle." Power Electronics and ECCE Asia (ICPE & ECCE), 2011 IEEE 8th International Conference on. IEEE, 2011.

50. Rosenberger, M.; Kirschneck, M.; Koch, T.; Lienkamp, M.: Hybrid-ABS. Integration der elektrischen Antriebsmotoren in die ABS-Regelung. In: 2. Automobiltechnisches Kolloquium (CD-Rom) 2011

51. Vandenplas, B., Gotoh, K., and Dutre, S., "Predictive Analysis for Engine/Driveline Torsional Vibration in Vehicle Conditions using Large Scale Multi Body Model," SAE Technical Paper 2003-01-1726, 2003, doi:10.4271/2003-01-1726.

52. Caruntu, C.F.; Onu, D.; Lazar, C., "Real-time simulation of a vehicle drivetrain controlled through CAN using a robust MPC strategy," System Theory, Control, and Computing (ICSTCC), 2011 15th International Conference on , vol., no., pp.1,7, 14-16 Oct. 2011

53. Rodriguez, J. M., Rubén Meneses, and Javier Orus. "Active vibration control for electric vehicle compliant drivetrains." Industrial Electronics Society, IECON 2013-39th Annual Conference of the IEEE. IEEE, 2013.

54. Gerard, M., Pasillas-Lépine, W., De Vries, E., & Verhaegen, M. (2012). "Improvements to a five-phase ABS algorithm for experimental validation." *Vehicle System Dynamics*, *50*(10), 1585-1611.

55. Pasillas-Lépine, W. (2006). "Hybrid modeling and limit cycle analysis for a class of five-phase anti-lock brake algorithms." *Vehicle System Dynamics*, *44*(2), 173-188.

56. W. Li, "ABS Control on Modern Vehicle Equipped with Regenerative Braking", Master Thesis, Delft University of Technology, 2010.

57. Tremblay, O. et al., "A Generic Battery Model for the Dynamic Simulation of Hybrid Electric Vehicles," Vehicle Power and Propulsion Conference, 2007. VPPC 2007. IEEE, vol., no., pp.284-289, 9-12 Sept. 2007.

58. Chuan Yu, T. Shim, "Modelling of Comprehensive Electric Drive System For study of Regenerative brake system", 2013 American Control Conference, Washington DC, USA.

59. Shoudao Huang; Ziqiang Chen; Keyuan Huang; Jian Gao; , "Maximum torque per ampere and flux-weakening control for PMSM based on curve fitting," Vehicle Power and Propulsion Conference (VPPC), 2010 IEEE , vol., no., pp.1-5, 1-3 Sept. 2010.

60. Ivanov, V.; Savitski, D.; Shyrokau, B., "A Survey of Traction Control and Antilock Braking Systems of Full Electric Vehicles With Individually Controlled Electric Motors," in *Vehicular Technology, IEEE Transactions on* , vol.64, no.9, pp.3878-3896, Sept. 2015 doi: 10.1109/TVT.2014.2361860.

61. Wen-Po Chiang, Dejun Yin, Manabu Omae, Hiroshi Shimizu, "Integrated Slip-Based Torque Control of Antilock Braking System for In-Wheel Motor Electric Vehicle" IEEJ Journal of Industry Applications Vol. 3 (2014) No. 4 p. 318-327.

62. Bin Wang; Xiaoyu Huang; Junmin Wang; Xuexun Guo; Xiaoyuan Zhu, "A robust wheel slip control design for in-wheel-motor-driven electric vehicles with hydraulic and regenerative braking systems," in American Control Conference (ACC), 2014 , vol., no., pp.3225-3230, 4-6 June 2014 doi: 10.1109/ACC.2014.6858977.

63. Jingang Guo, Junping Wang, Binggang Cao, "Study on Braking Force Distribution of Electric Vehicles", 978-1-4244-2487-0/09/$25.00 ©2009 IEEE.

64. Zhang jingming, Song baoyu, Niu xiaojing, "Optimization of Parallel Regenerative Braking Control Strategy", IEEE Vehicle Power and Propulsion Conference (VPPC), September 3-5, 2008, Harbin, China 978-1-4244-1849-7/08/$25.00○C 2008 IEEE.

65. Hongwei Liu, Xiaoyin He, Liang Chu, Junhui Tian, “Study on Control Strategy of Regenerative Braking for Electric Bus based on Braking Comfort.” 2011 International Conference on Electronic & Mechanical Engineering and Information Technology.

66. Zhang, Junzhi, et al. "Cooperative control of regenerative braking and hydraulic braking of an electrified passenger car." Proceedings of the Institution of Mechanical Engineers, Part D: Journal of Automobile Engineering (2012): 0954407012441884.

67. G. Adireddy, “MPC Based Integrated Chassis controller to enhance vehicle handling with roll stability” Masters’ Thesis, University of Michigan – Dearborn 2011.

68. Daniel Simon, “Model Predictive Control in Flight Control Design: Stability and Reference tracking” Linköping studies in science and technology. Licentiate Thesis. No. 1642

69. A. Bemporad, M. Morari, N. Lawrence Ricker, “Model Predictive Control Toolbox For Use with Matlab User Guide” © COPYRIGHT 1995-2005 by The MathWorks, Inc.

70. Uwe Kiencke, Lars Nielsen, “Automotive Control Systems For Engine, Driveline, and Vehicle”, Springer Berlin Heidelberg New York, ISBN 3-540-23139-0.

71. S. Savaresi, M. Tanelli, “Active Braking Control Systems Design for Vehicles”, Springer London Dordrecht Heidelberg New York, ISBN 978-1-84996-349-7.

72. Andrew J. Day, Hon Ping Ho and Khalid Hussain, “Brake System Simulation to Predict Brake Pedal Feel in a Passenger Car”, SAE paper, 2009-01-3043

Appendix 1: Nomenclature

PMSM UNIT

u_d ,u_q	d and q-axis component of stator voltage (V)
i_d ,i_q	d and q-axis component of stator current (Amps)
L_d, L_q	d and q-axis component of stator inductance (Henry)
R_s, ω	Stator resistance (ohms) and motor angular speed (rad/s)
λ_f, P	Flux linkage (Weber) and Number of pole pairs
J_{mot}	mass moment of inertia (kg-m^2) of the motor
B_{mot}	bearing friction coefficient (Nms/rad) of the motor
T_e, T_l	Motor Torque (N-m) and Load Torque (N-m)

BATTERY UNIT:

i, q	Battery charging /discharging current (Amps) & charge
Q, $Q_{initial}$	Total charge capacity and initial charge of the battery
E, Eo	Battery no load and constant voltage (V)
A_i, B_i	exponentiel zone amplitude and amplitude zone time constant inverse
K	Polarization voltage (V)
V_{batt}, R_b	Battery voltage (V) and internal resistance (Ohms)

DRIVESHAFT UNIT

T_b, T_m	Friction brake torque and equivalent motor brake torque (N-m)
k_s, d_s	Drive shaft torsional stiffness (Nm/rad) and damping (Nms/rad)
J_m, J_w	Equivalent motor inertia reflected at final drive(kgm^2) and wheel inertia($kg\text{-}m^2$)
F_x, R	Longitudinal tire force (N) and tire rolling radius (m)
T_{shaft}	Shaft torque (N-m)
$\dot{\theta}_m, \dot{\theta}_w$	Angular velocities of the equivalent motor (Jm), wheel (Jw) (rad/sec)
λ, β	Longitudinal slip and side-slip angle (deg)
F_z, ω	Normal force (N), wheel speed (rad/s)
MPCA	
T_r , T_{rdem}	Actual and demanded regenerative brake torque (Nm)
T_h, T_{hdem}	Actual and demanded hydraulic brake torque (Nm)
ω_{nr}, ζ_r	Natural frequency (rad/s) and damping of Regen. Brake
ω_{nh}, ζ_h	Natural frequency (rad/s) and damping of Hydraulic brake
ω_{ns}, ζ_s	Natural frequency (rad/s) and damping of shaft
A, B	Continuous state and input matrix
A_k, B_k	Discretized state and input matrix
T_b, T_b^*	Actual and reference total brake torque (Nm)
T_{sh}, T_{sh}^*	Actual and reference shaft torque (Nm)
T_{rmin}, T_{rmax}	Min. and max. regenerative brake torque (Nm)
T_{hmin},T_{hmax}	Min. and max. hydraulic brake torque (Nm)
$\dot{T}_{rmin}, \dot{T}_{rmax}$	Min. and max. regenerative brake torque rate (Nm/s)

$\dot{T}_{hmin}, \dot{T}_{hmax}$	Min. and max. hydraulic brake torque rate (Nm/s)
N_p, N_c	Prediction and control horizon
Q_y, Q_u	Output and input weight matrix
γ_b	Total torque error penalty
γ_{sh}	Shaft torque error penalty
α_r, α_h	Regenerative and hydraulic input weight

Appendix 2: Matlab Code for Fast Fourier Transform (FFT) Evaluation

This section describes the Code used to generate the FFT's of the signals used in chapter 4. The code is written in a Matlab script and is applied to the generated data, after the simulation has finished. The following is the code used for FFT:

```
%% Main FFT parameters
fs=5000*2; % Sampling frequency [Hz]
nop=60000; % Number of points for fft
iny=nop/2+1; %Nyquist index
df=fs/nop;    % frequency resolution
fa=[0:iny-1]*df; % Frequency Axis Values

%% FFT
specu=fft(sd(1:60000)); % fft of the shaft deflection
spec1u=specu(1:iny);
spec2u=spec1u/nop;
magu=abs(spec2u);
```

In this code, the main parameter is the number of points (nop). The sampling time of the Simulink model is 1e-4 sec. Hence the sampling frequency 'fs' is selected accordingly. In this analysis, the parameter 'nop', is chosen such that it equals to the sampling instant at which, the ABS is switched off in the simulation. This is chosen so that the end-effects, i.e. when the ABS is switched OFF is neglected. If the 'nop' is chosen as the sample at the end of simulation, then the FFT will show additional peaks, mainly due to the vibrations when the wheel speed and vehicle speeds reach zero.

Appendix 3: Carsim-Simulink co-simulation model